Fluorinated Photoproduct Formation from Photolysis of Fluorinated Pharmaceuticals and Phenols

A Thesis SUBMITTED TO THE FACULTY OF THE UNIVERSITY OF MINNESOTA
BY

Quinn Thomas Whiting

IN PARTIAL FULFILLMENT OF THE REQUIREMENTS FOR THE DEGREE OF
MASTER OF SCIENCE

William A. Arnold

August 2020

Acknowledgments

I would like to thank my advisor, Dr. William Arnold for his patience, support, and advice throughout my master's program. I grew in countless ways both as a scientist and as a person with the time I spent in the Arnold Research Group. Also, thank you to Dr. William Pomerantz, whose insight with NMR instrumentation and fluorine chemistry helped broaden my knowledge of both subjects, which improved the work presented in this thesis.

Classmates and lab-mates alike were inspirational for both my coursework and my research. In particular, the Arnold Group, Dr. Priya Hoya, Matthew Berens, Dr. Meghan O'Connor, Adel Soroush, and Lara Frankson.

Thank you to my family for providing the opportunity to follow my passions and interests. And for the many "vacations" I took back home; filled with strong coffee, adventures, and a warm bed to sleep in.

Finally, a heart-felt thank you to my friends for the constant support, laughter, food, and good times.

Dedication

To my teachers.

Abstract

Use of fluorine has increased since its first use in 1957 due to its ability to change the physiochemical properties of compounds, including lipophilicity, solubility, conformation, pK_a, and metabolic stability. Common fluorine motifs include: -CF_3, -CF_2, and -CF groups bonded directly onto an aromatic (Ar-CF_3 and Ar-F) or pyrazole rings (Py-CF_3). Photolysis of these compounds is a potential source of new fluorinated compounds into the environment. With potential toxicity of organofluorine products, such as fluoroacetic acid, monitoring of product formation during photolysis of various fluorinated motifs is needed. To determine fluorinated products, selected pharmaceuticals with the Ar-CF_3, Ar-F, and Py-CF_3 motifs were subjected to photolysis in four aqueous conditions: pH 7, pH 10, 1 mM H_2O_2 at pH 7 to form •OH, and 0.5 mM SO_3^{2-} at pH 10 to form e_{aq}^-. Additionally, 2-, 3-, and 4-trifuoromethylphenol (TFMP) and fluorophenol (FP) were used as Ar-CF_3 and Ar-F model compounds, respectively. These model compounds were subjected to photolysis to further study product formation from these fluorine motifs, as well as determine if ring placement influences product formation. Product identification and fluorine quantification by ^{19}F-NMR on a 600 MHz magnet equipped with a 5 mm cryoprobe were conducted. Rate constants of parent compound loss were monitored on an HPLC. All Ar-F model compounds only produced fluoride. The three Ar-CF_3 model compounds led to different organofluorine products based on motif placement as well as reaction conditions. Trifluoroacetic acid (TFA) was only produced by 4-TFMP, suggesting ring placement is important for TFA formation. TFA was also found to form from fluoxetine, matching the 4-TFMP model compound. Sitagliptin formed fluoride and followed the trend of the Ar-F model compounds except when the pH was above the pK_a of the molecule.

Table of Contents

List of Figures

List of Tables

Chapter 1 Introduction and Literature Review

1.1 Naturally Occurring Fluorinated Compounds

Fluorinated compounds derived from natural processes are rare in the environment, despite fluorine being the thirteenth most abundant element in the Earth's crust. Most of the fluorine is in the mineral form of fluorite and not bioavailable to any organisms.[1,2] Roughly 3700 organohalides naturally occur in the environment, of which only 30 contain fluorine, possibly due to the lack of bioavailability of fluorine.[3] Both abiotic and biotic processes form organofluorides, with volcanic ash being the largest contributor of hydrogen fluoride in the atmosphere.[4] In addition to hydrogen fluoride, other small fluorinated molecules such as alkanes are found in volcanic gas.[5] During eruptions, these fluorinated compounds are released into the environment.

Biotically derived organic fluorine molecules, however, do exist. Plant species have been found to produce fluoroacetate as a defense mechanism against grazing. In 1943, *Dichapetalum cymosum* was found to produce fluoroacetate.[6] This plant was known to be toxic to cattle and sheep in South Africa before understanding that fluoroacetate was the reason. Less than a half of an ounce of the plant is fatal to sheep, proving that fluoroacetate production is an effective mechanism for defense against grazing.[7] This mechanism, however, is not common. Other fluorinated organic compounds have been found to be synthesized in plants and bacteria including: (2R,3R)-fluorocitrate, fluorooleic acid, fluoroacetone, nucleocidin, and 4-fluorothreonine.[8] It suggests that nature has found a way to incorporate fluorine, the most electronegative element, into synthetic pathways that benefit the organism. Interestingly, no biotically derived fluorinated compound has more than one fluorine atom while multiple fluorine

atoms can be present in abiotically derived compounds, including tetrafluoroethylene, hexafluoropropene, and chlorodifluoromethane.[3]

1.2 Use of Fluorine in Pharmaceuticals and Agrochemicals

Contrary to naturally derived molecules, the presence of fluorine is widespread in anthropogenic compounds, and its use is becoming more common. In 2018, 17 new pharmaceuticals that contained fluorine were approved by the U.S. Food and Drug Administration (FDA), which was the most ever to date.[9] Since the first fluorinated drug, fludrocortisone, came to market in 1955, over 150 other fluorinated drugs have followed. In 2010, 20% of administered drugs contained fluorine, with an increasing trend.[10] Some of the most common drugs, fluoxetine (Prozac), atorvastatin (Lipitor), and ciprofloxacin (Ciprobay) contain fluorine and generate billions of dollars in revenue.[11–13] Thus, the increasing popularity of fluorine in the pharmaceutical industry is not to be ignored.

Fluorine is even more abundant in the agrochemical industry, with 50% of fungicides, herbicides, and insecticides containing fluorine.[14] If not fluorine, many agrochemicals contain another halogen, chlorine, or in some cases both fluorine and chlorine. In fact, between 2010 and 2016, 96% of new agrochemicals contained at least one halogen atom, and the presence of fluorine in pesticides increased 52% over this time period.[14,15] Agrochemicals can be broken down to three categories: insecticides, fungicides, and herbicides. All three categories have an increasing trend of fluorine use. Between 1990 and 2002, 41% of insecticides, 36% of herbicides, and 23% of fungicides contained at least one fluorine atom.[16] The increase in fluorine use is attributed to the fact that agrochemicals that contained fluorine were found to have an increased potency compared to non-fluorinated agrochemicals.[16] Thus, the dose of the agrochemicals is

decreased, which is cost beneficial to the farmer. Many factors are considered when developing agrochemicals, including environmental safety, economic viability, efficacy, and user friendliness. Agrochemicals that are approved for use should degrade into a benign product, have rapid mode of action, be sold at a price that farmers can afford, and should be safe to apply and have a low acute toxicity.[15] Similar guidelines are used for the pharmaceutical industry.

1.3 Appeal of Fluorine

The application of fluorine to pharmaceuticals and agrochemicals changes the physiochemical properties such that they become more appealing and useful to these industries.[9,16] The addition of fluorine onto a molecule yields desirable effects including metabolic stability, thermal stability, change in pK_a values, increased lipophilicity and polarity, and increased membrane permeability.[14] Substituting a hydrogen for a fluorine atom in drug development is being done at a faster rate than ever before, because substituting one atom for fluorine can change the biological function of the entire molecule.[9,17] Additionally, substituting hydrogen for fluorine does not change the steric and geometric structure relative to the entire molecule.[18] One reason for this is that fluorine is a small atom (van der Waals radius of 1.35Å) that lies between hydrogen (1.2Å) and oxygen (1.4Å). .[17] The substitution of fluorine, however, does change the electronegativity, bond strength, and molecular weight of the molecule.[17,19]

Fluorine is the most electronegative atom, and, it also has one of the strongest bonds to carbon at 116 kcal/mol.[17] The strong bond energy leads to high resistance to oxidative and thermal stresses.[20] The resistance to these stresses is appealing to drug developers because it is a simple way to create stability while not changing the

conformation of the molecule. This allows for a longer half-life within the body and an increased time over which the drug is effective.[21] In an aromatic system, fluorine reduces oxidation mainly through its high inductive effect (Figure 1-1). The inductive effect pulls electron density away from the aromatic structure and towards the electron withdrawing group, decreasing the ability of nucleophilic attack. Conversely, resonance adds electron density to the aromatic structure, and these two effects compete. With fluorine being the most electronegative atom, its inductive effect is large and outcompetes the resonance effect, resulting in a deactivation of oxidation. With enzymatic and biochemical processes, the fluorine atom reduces oxidation sterically. This is because enzymes are particular in the shape of their active sites and slight changes in molecular shape can cause the enzyme to no longer work. One of the main chemical oxidation pathways is the abstraction of a hydrogen atom followed by oxidation to an alcohol group. With the addition of fluorine, that abstraction is halted, stopping the oxidative process. This is because of the strong bond energy between carbon and fluorine (Figure 1-2).[21]

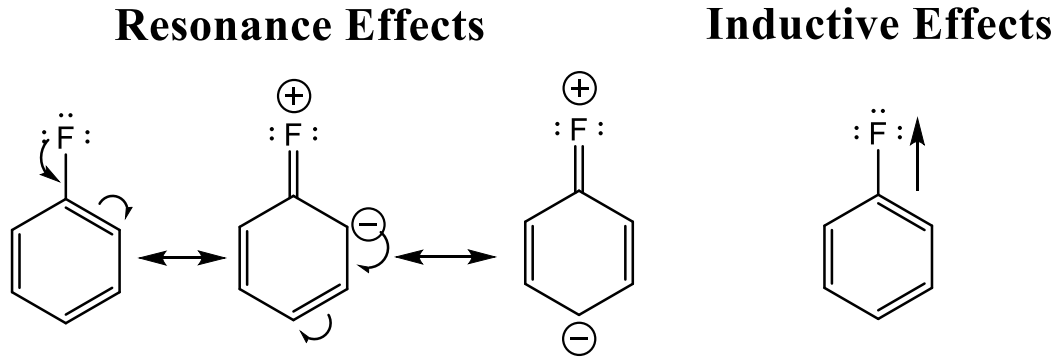

Figure 1-1. Diagram of the resonance effect with fluorine on a benzene ring, showing the electron density moving throughout the molecule, and the inductive effect of fluorine, showing that the electrons will not be moving throughout the molecule due to the large electronegative effect of fluorine.

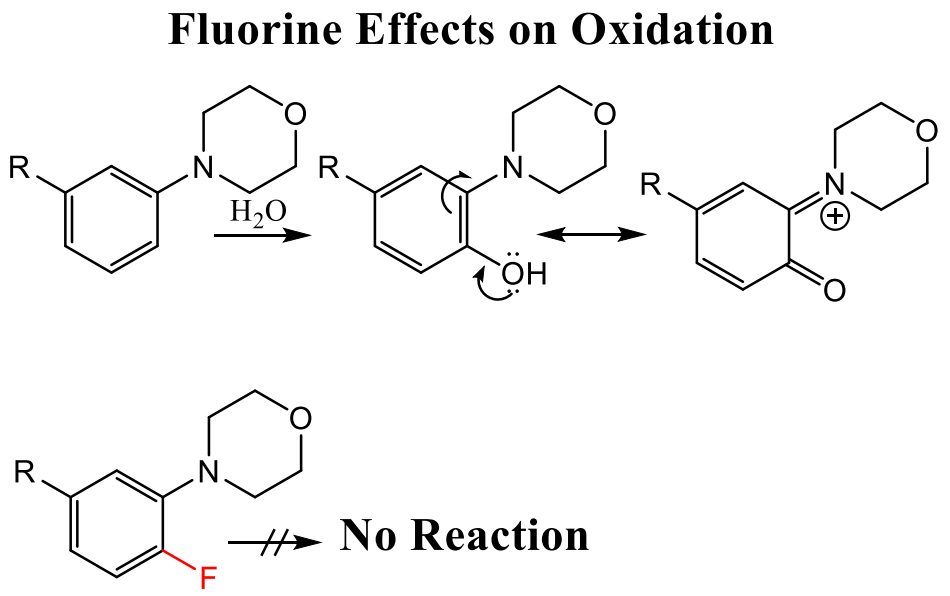

Figure 1-2. A part of a drug in development for migraines showing the addition of fluorine to inhibit the oxidation of the molecule. The top reaction shows the oxidation without fluorine and the bottom shows it with the addition of fluorine.[21]

Changing the lipophilicity of a molecule with the addition of fluorine is complex. Typically, it increases the lipophilicity, but in certain molecular environments it can decrease.[21] When the addition of fluorine decreases the lipophilicity, there is an oxygen atom at most 3.1 Å away from the fluorine.[22] Using log D values to measure lipophilicity, where D is the partition coefficient between octanol and water (also known as K_{ow}). A database containing 293 compounds showed a Gaussian distribution with an average increase in lipophilicity by 0.25 log units by substituting one hydrogen atom for a fluorine.[22] These changes in lipophilicity aid permeation of molecules through the cell membrane.

The addition of fluorine has strong effects on the acidity or basicity of functional groups. In some cases, it changes the pK_a by multiple log units. For acetic acid and trifluoroacetic acid, the pK_a values are 4.76 and 0.23, respectively.[23] The pK_a value

changes with every addition of a fluorine atom, such that the pK_a of a compound can be optimized to a certain degree by adding single or multiple fluorines.[23] This fact is used when dealing with the two competing variables of binding affinity and cell permeation through the membrane.[24] The changes in pK_a values can be attributed to the high electronegativity of fluorine. It is effective at pulling the electron density towards itself, resulting in lower electron densities elsewhere in the molecule. These lower electron densities could be where a hydrogen lies, and so it becomes more acidic and likely to leave the molecule altogether, reducing its pK_a value.

There are varying functional groups to which fluorine is added to a molecule, herein called motifs. These motifs can be split into broad categories e.g., aromatic, aliphatic, pyrazole ring, and other (Table 1-1). A common fluorine environment of the "other" motif is a trifluoromethyl group bound to sulfur. In any of these motifs, the fluorine addition can range from a single fluorine to multiple, often three via the addition of the trifluoromethyl group.

Table 1-1. Examples of fluorinated motifs that can be found in common pharmaceuticals and agrochemicals.

Motif	Example
Aromatic	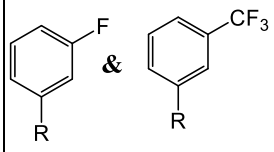
Pyrazole Ring	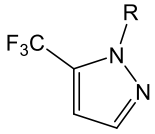
Aliphatic	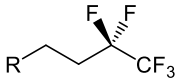
Other	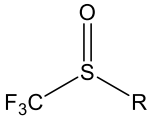
Trifluoro-amide	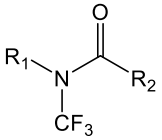

The trifluoromethyl group is commonly used in the pharmaceutical and agrochemical industry. Additionally, the aryl fluorine is one of the more common aromatic fluorine motifs.[10,19] The trifluoroamide group may soon come to market because synthesis has become economically feasible. Amide groups are already widely used for their ability to interact with biological and enzymatic receptors. The fluorine addition allows for metabolic stability. One of the bestselling pharmaceuticals, atorvastatin, has both fluorine and an amide group albeit not bonded to each other. This motif allows for

the advantages of both fluorine and amides to be utilized together in drug development.[25] This motif is also shown in Table 1-1.

1.4 Anthropogenic Fluorine in the Environment

Poly- and perfluoroalkyl substances (PFAS) are highly fluorinated manmade chemicals used throughout industry. There are thousands of variations of PFAS molecules, and they persist in the environment with no known biotic or abiotic route of degradation.[26] These compounds are so persistent in the environment that they were found at ng/g levels in the tissues of arctic animals, far from human civilization.[26] Within the sediments of Lake Ontario, detection of these perfluoroinated compounds was ubiquitous among the samples, ranging from about 0.5 ng/g to 30 ng/g dry weight. These samples were also radiometric dated and found to range from 1952 to 2005. No detection of these perfluoroinated compounds were found before 1952, roughly a decade after they started to be widely used.[27] PFAS have received substantial attention for their persistence and impact on the environment. Many other compounds, including pharmaceuticals and agrochemicals, also have fluorine in their structures and contribute to the total fluorine in the environment.

Wastewater treatment plants (WWTP) are a large point source of pharmaceuticals in the environment.[28] WWTPs are currently not designed to fully degrade or remove the pharmaceuticals. Pharmaceuticals can be active in the ng/L and µg/L range, while WWTPs were designed for degrading higher concentrations of organic carbon.[29] Hospital effluent is another source that is rich in pharmaceuticals and provides a pathway to the environment. A study in Japan showed detection of 41 pharmaceuticals, antiseptics, and

other healthcare drugs in a hospital effluent. They also tested the WWTP to which the hospital waste flows, and they found 8 compounds to the hospital waste.[30]

In rural areas, where WWTPs and hospitals are not present or small, agriculture, animal husbandry, and aquaculture are the main sources of anthropogenic compounds into the environment.[31] Fungicides, both fluorinated and not, have been found in agricultural catchments. In a screening for 24 different fungicides, 17 were detected. With 63% of water samples having detection, 44% of passive samplers had a detection, and 42% of sediment samples had detection of fungicides. Water samples had the largest variety of fungicides, at 14. Only two of the 24 fungicides were fluorinated, tetraconazole ($R\text{-}CF_2\text{-}CHF_2$) and trifluoxystrobin ($Ar\text{-}CF_3$), both of which were the 14 detected compounds in surface water. Trifluoxystobin had a higher frequency of detection and concentration than tetraconazole, and it was also detected in sediment, while tetraconazole was not.[32]

Organic fluorine found in surface water, sediment, and groundwater is most likely due to human activity because few organic fluorine molecules naturally occur.[1] Detection of agrochemicals in the environment is not surprising, because most agrochemicals are applied directly onto fields, where runoff can occur, and in cases where the plants are aquatic, the agrochemicals are applied directly into the water.[33] Furthermore, pharmaceutical residues have been detected in almost all environmental matrices, including ground water and surface water. They have even been detected in polar regions, where the human population is scarce.[29] The release of pharmaceuticals and agrochemicals into the environment is no longer of question. The increased use of fluorine in these compounds will increase the total amount of organic fluorine released

into the environment. These fluorinated compounds are of concern because the fluorine addition alters the microbial degradation, resulting in a more persistent contaminant.[34]

Increase in production and use of fluorinated compounds increases the chances of fluorine containing compounds being released into the environment, through wastewater and industrial plants or agricultural sources. The nature of these compounds makes it so that they persist within the environment and degrade slowly, causing concern. Although the fluorine atom can alter susceptibility to microbial degradation, there are still pathways of degradation within the environment. The identities and impacts of fluorinated breakdown products of these compounds are unknown.

1.5 Photolysis

While biotic degradation can occur, many routes of abiotic degradation are important, such as hydrolysis, acid-base reactions, thermal degradation, and photolysis.[35] Because pharmaceuticals are designed to be stable in aqueous solutions and biological systems, photolysis is an important degradation pathway. Simply put, photolysis is the degradation of a compound by light. Light can be emitted from the sun, or by lamps, usually set to emit UV light, in an engineered environment. Wastewater treatment plants use UV light as part of advanced oxidation processes to degrade compounds before discharging effluent into the environment.[36] There are two main pathways of photolysis, direct and indirect. Direct photolysis occurs when the compound of interest is capable of absorbing the wavelengths emitted by the light source, whether it be the sun or UV lamps, and chemical transformation occurs due to the energy absorbed. Indirect photolysis occurs when the compound of interest cannot absorb the wavelengths emitted, but other species in the solution can and they become excited and react with the

compound of interest, leading to transformation. Both processes are shown in Figure 1-3.[37] Common species involved in indirect photolysis include triplet state dissolved organic matter (^{3}DOM*), hydroxyl radicals (•OH), and singlet oxygen ($^1O_2$).[37]

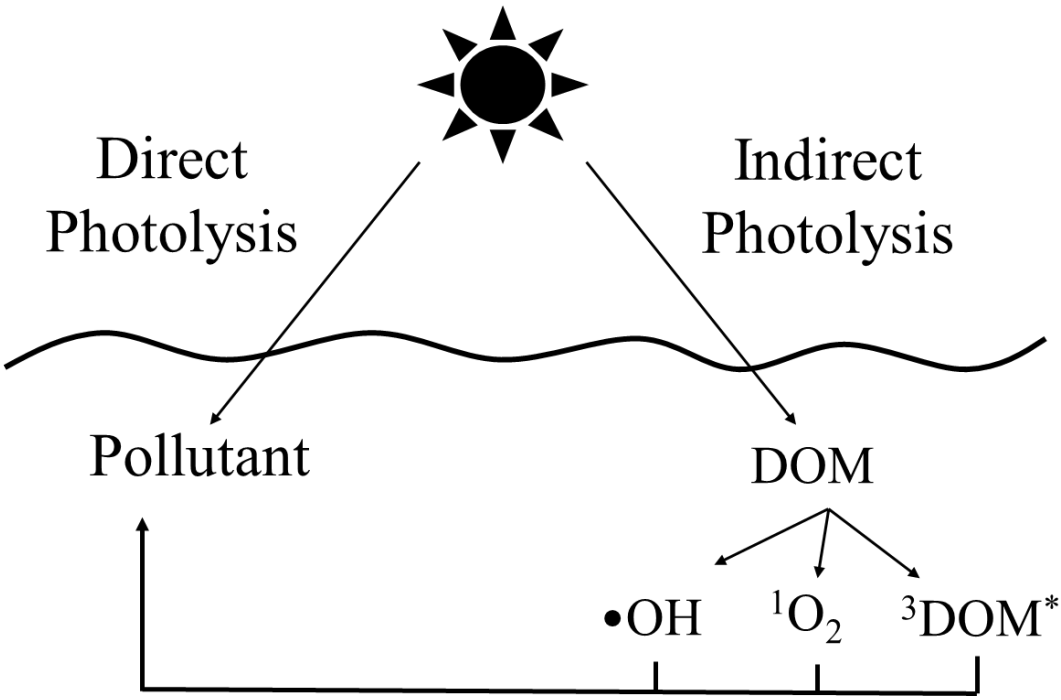

Figure 1-3. Diagram of direct photolysis and indirect photolysis through photochemically produced reactive intermediates (PPRIs) from dissolved organic matter (DOM).

Ground state dissolved organic matter (DOM) is capable of excitation to the singlet-state by the absorption of light. It then undergoes nonradiative relaxation through intersystem crossing or vibrational relaxation.[37,38] This relaxation produces the triplet-state which is longer lasting and capable of facilitating indirect photolysis. ^{3}DOM* is also capable of producing other reactive intermediates. In the presence of oxygen, ^{3}DOM* transfers energy to ground state oxygen ($^3O_2$), producing singlet oxygen ($^1O_2$).[39]

Singlet oxygen is an important environmental oxidant. It can be produced in from many pathways in varying media. It is produced from ^{3}DOM*, but it can also be formed

through the particulate matter stirred up from road dust that reacts with oxygen in the atmosphere.[40] Another formation pathway is with common active ingredients in sunscreen, such as *p*-aminobenzoic acid (PABA).[41] This suggests that it is ubiquitous in the environment, being produced from multiple pathways in both aquatic and atmospheric environments. One obvious limiting factor is that the environment must be oxic, such that it has a sufficient concentration of oxygen molecules to create $^1O_2$.[42]

Another oxidant found in the environment is the hydroxyl radical (•OH). This reactive oxygen species is unselective and will react with organic pollutants with rate constants typically near diffusion limits (10^9 to 10^{10} M^{-1} s^{-1}).[43] Hydroxyl radicals are formed via multiple pathways. The photo-Fenton reaction creates •OH in the presence of ferric iron (Fe(III)) and light.[44] Other formation pathways of •OH are the photolysis of H_2O_2, which splits into two •OH species (Figure 1-4), and the photolysis of the nitrate ion, which will also create •OH in water.[45] Wastewater treatment facilities have used these formation mechanisms in advanced oxidation processes (AOPs) to remove organic pollutants.[46]

Another species that can be produced during photolysis is the hydrated electron (e_{aq}^-). This is a highly reactive and short-lived species, but it is important in the degradation of highly oxidized species. While oxidative reactants are important in degrading many compounds, e_{aq}^- is capable of reducing highly oxidized species, such as PFAS.[47,48] Like •OH, e_{aq}^- can have reaction rates near diffusion limits. Due to the high selectivity of e_{aq}^-, however, the rate constants may be much slower for some compounds. It was found that in general, rate constants range from 10^6 to 10^{10} M^{-1} s^{-1}.[49] Hydrated electrons are created by photolysis of sulfite (SO_3^{2-}) at basic pH conditions, as shown in

Figure 1-5.[50–56] It has been proposed to use this reaction as an advanced reduction process (ARP) for destruction of PFAS.[48,57]

$$H_2O_2 + h\nu \rightarrow 2 \bullet OH$$

Figure 1-4. Reaction mechanism for •OH production form H_2O_2.

$$SO_3^{2-} + h\nu \rightarrow SO_3^{-} + e_{aq}^{-}$$

Figure 1-5. Reaction mechanism for e_{aq}^- production from sulfite.

Wastewater treatment facilities have adopted photolysis as a method of disinfection, with the knowledge that reactive intermediates, both oxidative and reductive, will also degrade organic pollutants that do not absorb in the wavelengths emitted by the UV lamps as an added benefit. UV is used to disinfect the effluent and obtain coliform levels below the legal requirement.[5859] As knowledge increased in the photochemistry field, AOPs were adapted into WWTP operations.[60] These could be as simple as adding ozone or hydrogen peroxide to the wastewater and irradiating it with UV light. These processes are meant to degrade organic pollutants to benign products. If a contaminant is already highly oxidized, AOPs may not be effective. ARPs were first proposed a decade after AOPs were implemented in wastewater treatment.[57] Although these are not as popular as AOPs, ARPs can reduce highly oxidative and persistent

pollutants, and for this reason the addition of ARPs to water treatment is being considered.[57]

The discharge of WWTPs into surface waters provides a source of organic pollutants.[28] Photolysis occurs in the photic zone of surface waters and degrades pollutants discharged from WWTPs. Another source of organic pollutants is from agricultural runoff. Again, photolysis is capable of degrading these agricultural compounds.[31,61] It should be noted that even though photolysis occurs in surface waters, the process is often not fast enough to prevent pseudo-persistence of organic pollutants that are continually released into the environment.

1.6 Environmental Impact of Anthropogenic Compounds

It has been proven that pharmaceuticals and agrochemicals are present in surface waters. The occurrence of these compounds in surface waters may be of concern, especially if the compounds or their metabolites impact the environment, the organisms within the environment, or drinking water sources. The addition of fluorine as a single fluorine or as a trifluoromethyl group has been proven to increase the antimicrobial activity of compounds.[34] One environmental concern is the antimicrobial resistance of microorganisms due to the release of antimicrobial drugs into the environment. Even though they are found in much lower doses than what is deemed effective treatment, selective pressure on microorganisms to develop or retain resistance to antimicrobial drugs may still occur.[62] With the use of polymerase chain reactions (PCR), antimicrobial resistance genes from microbes in surface waters were found, providing evidence that microorganisms within the environment have resistance to antimicrobial drugs important

to human and animal treatment.[63] One type of antimicrobial drug is the fluoroquinolone, which contains a single aryl fluorine.[64]

Bioaccumulation is another concern with pharmaceutical release into the environment. To estimate the bioaccumulation potential of compounds, the octanol-water partition coefficient (K_{ow}) is determined, the log-value must be greater than 3 to be considered to bioaccumulate, according to the Organization for Economic Co-operation and Development (OECD) guidelines. A dataset was created from the U.S. Food and Drug Administration (FDA) and top selling commercial pharmaceuticals from RxLists, this database contains 3193 compounds. It was found that 275 of these compounds have already been detected in the environment. Based on K_{ow} calculations, 92 out of the 275 compounds have the potential to bioaccumulate, some of which contain fluorine.[65]

In rivers where pharmaceuticals were detected in the surface water, fish tissues were also found to have bioaccumulated these persistent compounds including venlafaxine, fluoxetine, and sulfamethazine, all common pharmacuticals.[66] Hand-in-hand with bioaccumulation is trophic magnification –organisms higher on the food chain will have higher concentrations of bioaccumulative compounds. This is not the case for many pharmaceuticals found in surface waters. In fact, for pharmaceuticals, trophic dilution often occurs. This phenomenon is not fully understood but some hypothesize that larger organisms may be able to metabolize the drugs and excrete them from their system.[67]

Bioaccumulation of non-pharmaceutical anthropogenic compounds also occurs. As previously mentioned, PFAS are being found in animal tissues across the world.[26] Additionally, pesticides such as fipronil, a fluorine containing compound used mostly for flea treatment in pets, was detected in rainbow trout. It was noted that the

bioaccumulation seemed to not have any health effects on the trout.[68] Earthworms in agricultural fields were studied for bioaccumulation of pharmaceuticals, personal care products, sterols, and other anthropogenically sourced compounds. The presence of these compounds was derived from either biosolid or swine manure application to the soil. The concentrations of the targeted compounds were below the limits of detection in the soil, but within the worms, they were higher and detectable. By definition, bioaccumulation of anthropogenic compounds is occurring in earthworms.[69] Another study looked at duckweed's ability to bioconcentrate fluorinated compounds as a removal method from surface waters. It was found to be effective, but the duckweed has to be removed before it decomposes to prevent re-release into the water.[70]

Transformations of anthropogenic compounds can be either be advantageous or not, depending on the identity and toxicity of the transformation products. Some transformations lead to benign products, while other transformation products may be more harmful than the parent. This is the case for tonalide and galaxolide, two common musk compounds used in fragrances of personal care products. The parent compounds are not toxic, but transformations in WWTPs create products, that, at low concentrations, are toxic.[71] It has been proven that trifluoroacetic acid (TFA) is formed from certain fluorinated pharmaceuticals during the UV/ozonation process at WWTPs. It was noticed that the concentration of TFA in rivers in Germany was higher than expected, (>100 µg/L). It was found that in WWTPs, the highest percentage of TFA formation on a molar basis were from pharmaceuticals with a trifluoromethyl group attached to a benzene ring (Ar-CF_3). This small and polar transformation product passes though most WWTPs and flows into surface waters.[72] This was thought to be the reason for the high concentration

of TFA in German rivers. TFA was not found to be a large concern in an environmental risk assessment, with little concern for human health at the concentrations being detected in surface waters.[73] It should, however, be noted that TFA has little to no degradation pathways in the environment and can accumulate.[74]

1.7 Common Fluorinated Pharmaceuticals and MRI Agents

Fluoxetine, better known as Prozac, is one of the best-selling drugs on the market.[11] It contains a trifluoromethyl group bound to a benzene ring. The photolysis of this compound has been well studied, but the degradation pathway is still unclear. Until recently, the formation of TFA from the photolysis of fluoxetine was not known. New studies are showing the formation of TFA and proposing mechanisms for its formation (Figure 1-6).[75] Other photoproducts contain the original motif, while mineralization of fluorine also occurs, generating fluoride.[76] Exact mechanisms of fluorinated photoproduct formation are unclear.

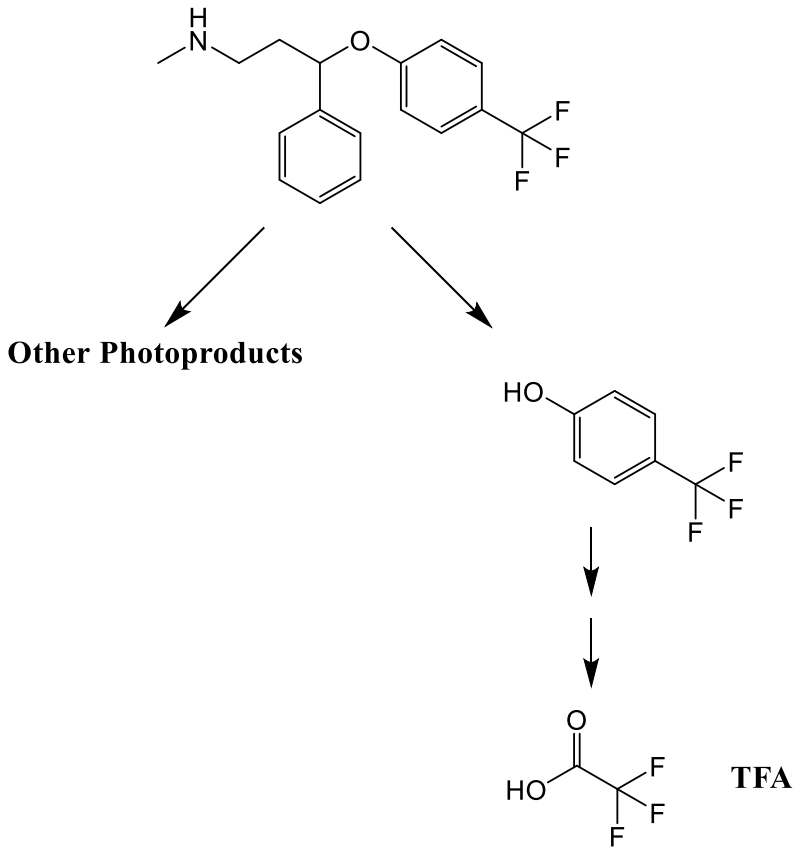

Figure 1-6. Proposed mechanism from Tilser et al. of the photochemical formation of trifluoroacetic acid (TFA) from the parent compound, fluoxetine.[75]

Atorvastatin, commonly known as Lipitor, is another one of the best-selling pharmaceuticals on the market.[11] It also has a fluorine motif, a single fluorine bound to a benzene ring. Due to only having a single fluorine, TFA formation from photolysis is not possible. This compound is not as well studied as fluoxetine, but the rate constants for reaction with •OH, $^1O_2$, and ^{3}DOM* have been calculated. Direct photodegradation does not happen at a relevant rate due to atorvastatin not absorbing wavelengths present in

sunlight. It was found that ^{3}DOM* and $^{1}O_2$ are capable of facilitating indirect photodegradation.[77]

Ciprofloxacin, commonly known as Ciprobay, is another of the top selling pharmaceuticals.[11] Ciprofloxacin is part of the fluoroquinolone class of drugs, used for their antibiotic properties.[78] The fluorine motif of this drug is similar to that of atorvastatin, a single aryl fluorine on a benzene ring. Direct and indirect photolysis of ciprofloxacin has been studied, and direct photolysis occurs rapidly. Addition of H_2O_2 to study the indirect photolysis with •OH does not increase the rate of photolysis.[79] Many of the photoproducts resemble the parent compound and maintain the aryl fluorine, but fluoride was detected, suggesting that mineralization pathways do exist. It was found that the main pathway of fluoride formation was by replacing the fluorine atom with an alcohol group.[80,81] Due to the widespread use and stability of fluoroquinolones, release into the environment is inevitable but different wastewater practices could lead to lower concentration.[82]

^{19}F-MRI is a relatively new technique used in medicine, first applied in the 1970s.[83] Highly fluorinated compounds are given to patients, which eventually reside in targeted tissues. Two common ^{19}F-MRI agents are perfluoroctyl bromide and perfluoro-15-crown-5-ether.[84] The many fluorine atoms on these agents are necessary to obtain a strong signal resonance. The use of fluorine is appealing to MRI operators due to the low background noise. The concentration of fluorine within the human body is relatively negligible, allowing for little to no background signal. Thus, the only signal detected by the MRI is from the agents injected into the patient. Nanoemulsions of these highly fluorinated MRI agents are made so that the hydrophobic MRI agent has a hydrophilic

barrier surrounding it, allowing for it to move throughout human tissues. The main pathway of removal from the body is through exhalation.[85,86] These compounds are highly oxidized and resistant to degradation within the body. ARPs, however, could prove useful in degrading these compounds.

1.8 Nuclear Magnetic Resonance

Study of product formation from fluorinated pharmaceutical and agrochemicals in aqueous environments of is of importance because fluorine used in these industries is relatively new, and pathways of organic fluorine removal in the environment are not well studied. Thus, fluorinated products formed via degradation of these compounds may pose unforeseen consequences. To better understand these fluorinated compounds in the environment, reliable detection methods must first be established. Nuclear magnetic resonance (NMR) is a tool which chemists use to help identify chemical structures of compounds. It can only detect one nucleus at a time. For example, ^{1}H-NMR can only detect all the hydrogen atoms on a compound. By applying a magnetic pulse, all the magnetically active nuclei align in the same pattern. Then when the magnetic pulse stops the nuclei relax into ground state. During this relaxation the NMR picks up the frequencies emitted from the nuclei, which vary based on each nuclei's surrounding chemical environment.[87] One limitation of NMR is that it can only detect NMR active nuclei and to be NMR active, nuclei must have an odd number of neutrons, protons, or both. The use of isotopes with odd numbers of neutrons are used to synthesize compounds so that they can be analyzed by NMR. The most common being 13-carbon. Hydrogen (or proton) NMR detects the hydrogen atoms on molecules because hydrogen contains only one proton.

Advanced NMR analysis provides greater detail of a compound's conformation and structure. Advanced NMR techniques include correlating the magnetization of two if the same (homonuclear) or two different (heteronuclear) NMR active nuclei on the same compound (2-D NMR). A correlation between these signals is made in such a way that allows for identification of bonds and interactions between specific atoms in the molecule.[88] Two of the more common 2-D NMR experiments are ^{1}H-^{1}H and ^{1}H-^{13}C. ^{1}H-^{13}C and ^{1}H-^{1}H 2-D NMR experiments were used to obtain the exact structure of unknown polycyclic aromatic hydrocarbons (PAHs),[89] demonstrating that NMR can be used to identify unknown compounds.

The use of fluorine in NMR is possible because the ^{19}F isotope has 9 protons. It is also 100% abundant, which is critically important and gives fluorine NMR a large advantage over NMR analyses of other nuclei. Any compound containing fluorine will be detected in an ^{19}F-NMR spectrum. The spectra also have a larger spectral range than ^{1}H-NMR, and due to the fact that fluorine has 9 electrons, the sensitivity to the chemical environment is higher than that of hydrogen, which only has one electron. Compounds with similar local fluorine environments will have similar shifts in the NMR spectra. Effects on the fluorine spectra, however, can be felt from 7 bonds away.[90] This long-range effect on fluorine means that overlap in spectra will only occur if the compounds are extremely similar.

Signal optimization for NMR is done on a molecule to molecule basis. Every molecule takes time (T_1) to relax back to its original state after being aligned by the magnetic pulse. Using the delay time (D1) function, the operator can ensure that there is enough time between scans for the molecules to completely relax, thus giving the best

signal to noise ratio (S/N).[91] The T_1 time of a molecule is found using a single-scan inversion recovery (SSIR) method. This method magnetically inverts the sample with a 180-degree pulse, then after varying delay time, will pulse again at 90 degrees and acquire the data. Performing these multiple times will give a spectrum with signals that are inverted and upright, with varying S/N. When the signal is upright and has the highest S/N, the T_1 time has been found.[92] The D1 and T_1 times do not always have to match. For instance, if quantification and S/N are not an issue and only detection of a compound is needed, the D1 time can be smaller such that the spectra will still show the compound but not with the highest S/N possible. This reduces analysis time. Additionally, the T_1 and D1 time do not need to match and can be optimized for efficiency with the use of the acquisition time (AT). Once the magnetic pulse is stopped, the molecules start to relax, in order to be quantitative, enough time must be given for the nucleus to completely relax. The AT is how long the NMR acquires data for after the pulse stops and is counted towards T_1. By adding the AT and the D1 to equal the T_1, optimization for analysis time is accomplished.[93]

Quantification of chemical concentrations using NMR is possible though the use of standards with known concentration. There are, however, issues with the use of standards. They dilute the sample creating smaller signals, they may react with the matrix of the sample creating different products and signals, and the standard chosen may potentially be a product of a reaction and so any chance of monitoring that product is no longer available. These issues are overcome using a capillary tube containing the standard and a careful selection of the standard. The use of a capillary tube for a standard has been adopted and is a viable way to obtain quantitative information from NMR

spectra.[94,95] Analogous to the Beer-Lambert law, the signal is proportional to the pathlength. Thus, the ratio between the smaller capillary tube containing the standard to the larger NMR tube must be known.[94] The use of this ratio on the signal of the standard will allow for an accurate reference peak and an accurate quantification. Generating quantifiable NMR spectra adds complexity to the NMR process but provides useful information from the analysis.

1.9 Application of NMR to Environmental Samples

Measurement of chemicals in the environment encompasses a broad range of compounds in various matrices, including groundwater, wastewater, soils, sediments, and air. Accurately analyzing these compounds is of utmost importance. Many types of instrumentation and are able to isolate compounds of interest in the various media. Sample preparation for analysis can be complex and may only select for certain compounds. In many cases, knowledge of what compounds are in the sample is necessary to select the correct type of sample preparation. NMR is an instrument that requires little to no sample preparation to study environmental samples across all types of media.[96] This in turn eliminates sample preparation bias found in other types of instrumental analysis. NMR techniques are applicable to all NMR active nuclei, which include ^{1}H, ^{13}C, ^{19}F, ^{31}P, ^{14}N, ^{111}Cd, ^{195}Pt, ^{199}Hg, and many more. Due to the large number of active nuclei, NMR is able to detect organic contaminants, organic matter, inorganic contaminants, and heavy metals, providing a powerful technique in environmental analysis. NMR analysis already has a strong presence in industrial settings. From 1980 to 2016, the number of publications using ^{19}F-NMR increased from roughly 5,000 to 35,000, following the same

trend of the use of fluorine in synthetic commercial compounds.[97] This technique, however, has seen limited use in environmental applications.[98]

Perhaps the most popular uses of NMR with environmental samples is the study of organic matter. Although the use of ^{19}F-NMR is not common in organic matter analysis, the same technique applies if it were to be used. The use of NMR on soil organic matter is done so that scientists can better understand its structure and environmental processes.[99,100] Soil has previously been described as "the most complex biomaterial on earth." With the use of NMR techniques, critical information about this complex material can be studied.[101] Organic matter samples have varying amounts of hydration. Ranging from solid sediment cores to dissolved water matrixes. The hydrogen from water can create an unwanted peak in the spectra. Due to advances in the water suppression technique during NMR acquisition, no additional drying is required for analysis. This parameter suppresses the proton signal from the water which the sample is often dissolved in. Allowing for accurate analysis with ^{1}H-NMR without having to dry the sample.[102] The simplicity of the sample preparation for NMR analysis is a great appeal for use of the instrument. At most, sample preparation consists of addition of hydrofluoric acid to dissolve and reduce paramagnetic elements that may decrease the resolution of the spectra.[96,99]

Other studies have used ^{19}F-NMR to study sorption of fluorine-containing pollutants to organic matter and other minerals. Focusing on the contaminant rather than the organic matter. With the increase used of fluorine in anthropogenically derived compounds, the fluorine probe on the NMR has become a simple way for detection of these compounds.[14,16] Environmental samples are complex, with organic matter,

metabolites, biomolecules, and microbes present. Organic fluorine is not abundant in these environmental samples, and thus the background noise when using ^{19}F-NMR is minimal.[3,103]

An example is the study of the herbicide trifluralin. Using ^{19}F-NMR instead of ^{13}C or ^{15}N- NMR enables tracking of trifluralin in a matrix containing organic matter.[103] This study took various soil organic matter samples and was able to determine if and how sorption of trifluralin happens. Ultimately, it was found that trifluralin covalently bonds to the soil, and that the soil type is important for the sorption efficiency and formation of metabolites. By using NMR, it was determined that some soils did not degrade the parent compound at all while other soil types completely transformed the parent into various metabolites. Line broadening in NMR spectra is a sign that the corresponding compound is covalently bonded to something in the matrix.[104] In the study with trifluralin, the ^{19}F peak was broadened after being exposed to the soil organic matter, suggesting that covalent bonding was the mechanism of sorption to the tested soils.[103]

Other studies have investigated the sorption of the fluoride ion to clay minerals. Using solid state ^{19}F-NMR, it was determined that a small portion of fluoride was substituted for hydroxyl groups on kaolinite while most of the fluoride was adsorbed to the aluminum on the surface of the mineral. Specific shift ranges were found for silicon-fluorine bonds, none of which were present in the sorption experiments, indicating that fluoride and silicon do not interact with each other in the sorption process.[105] Shifts in the NMR spectra, although sometimes small, provide useful information on changes in chemical environments. Hydrogen-bond interactions have large effects on ^{19}F-NMR spectra, which provides structural information about fluorinated substances.[106]

^{19}F-NMR is a useful tool to quickly analyze samples for detection of compounds that contain the fluorine atom. Even though the simplicity of the NMR is appealing for environmental analysis, few peer-reviewed experiments have used this technology. One study looked at two different and independent methods for detection of perfluorinated compounds in surface water after a spill of these compounds occurred and released them into the environment. Liquid chromatography mass spectrometry (LC-MS) and ^{19}F-NMR methods were made for detection and quantification. Comparison of results between the two methods showed that ^{19}F-NMR was a viable technique for environmental sampling for fluorinated compounds. It was noted that the detection limit for the NMR was much higher (10 μg/L) than the LC-MS, giving the LC-MS an advantage over the NMR technique. The advantage of the NMR was that it was less expensive, easier to use, had well resolved peaks for quantification, and there were no matrix effects due to the lack of other sources fluorine in the water sample. It should be noted that in the water samples taken near agricultural fields, there were other organic fluorine sources found in the NMR spectra. These fluorinated compounds did not affect the spectra of the contaminant of interest because the sharp and well resolved peaks did not overlap. Another advantage of the NMR is not needing chromatography to separate molecules for analysis, which can sometimes prove difficult.[107]

The use of ^{19}F-NMR was also used for the detection and quantification of fluorinated acids in rainwater, including trifluoroacetic acid. Gas chromatography-mass spectroscopy (GS-MS) was used to verify the NMR analysis. The ^{19}F-NMR analysis of the environmental samples matched the concentrations found with the GC-MS, further

proving that ^{19}F-NMR can be used to both identify and quantify compounds in environmental samples.[108]

1.10 Goals and Outline of Thesis

The primary goal of this thesis is to detect a variety of fluorinated photoproducts produced upon direct photolysis of pharmaceuticals and reactions of these pharmaceuticals with ·OH and e_{aq}^-. The aromatic motif was studied in detail with six model compounds. Three fluorophenols with the aryl fluorine at the ortho, meta, or para positions as well as three trifluoromethylphenol with the trifluoromethyl group bonded at the ortho, meta, or para position were studied. This was done to determine if the motif type and position influences photoproduct formation. Along with the six model compounds, two pharmaceuticals were studied, fluoxetine (Prozac) and sitagliptin phosphate (Januvia), both of which contain aromatic fluorine motifs. Fluoxetine contains an aromatic trifluoromethyl group (Ar-CF_3) while sitagliptin contains a trifluoromethyl group on a pyrazole ring (Py-CF_3) as well as three aryl fluorine atoms (Ar-F). All eight compounds were studied in various aqueous conditions, including pH values at circa 5, 7, and 10. Additionally, the pharmaceuticals and trifluoromethylphenols were studied in conditions with hydrogen peroxide and with sulfite, to mimic the AOPs and ARPs that water treatment facilities use. A secondary goal of this thesis is to create a robust ^{19}F-NMR method so that quantification of both the parent compound as well as any unknown fluorinated products can be accurately made.

Reaction rate constants under the tested conditions are measured. Additionally, the ^{19}F-NMR spectra of each compound of interest is shown both pre and post reaction to quantify the amount of fluorine in the photoproducts. Comparisons between the model

compounds are made to better understand the fluorinated photoproduct formation as it relates to motif and position of fluorine on the molecule. Comparisons between pH, AOP and ARP experiments are made to determine if differences in the matrix affect fluorinated photoproduct formation. Additionally, the use of LC-HRMS is used to determine the structure of fluorinated products, because the ^{19}F-NMR is not capable of determining chemical structure from fluorine resonances alone.

Chapter 2 Photolysis of Fluorinated Model Compounds and Pharmaceuticals

2.1 Introduction

Since the first fluorinated drug was approved for use in 1955, the application of fluorine in the pharmaceutical industry has consistently increased.[10] In 2018, 17 new fluorine-containing drugs were approved by the FDA, the highest number ever.[9] Agrochemicals have also experienced an increase in fluorine application. As of 2010, 50% of fungicides, herbicides, and pesticides contain the fluorine atom.[14] Fluorine incorporation changes the physiochemical properties of the molecules to which it is attached to. These properties include thermal and metabolic stability, change in pK_a, change in lipophilicity and polarity, and increase in cell permeability.[14] Fluorine can be attached to molecules with various chemical motifs. Some of the most common motifs include the aromatic trifluoromethyl group (Ar-CF_3), aryl fluorine (Ar-F), pyrazole ring trifluoromethyl group (Py-CF_3), and aliphatic fluorine (R-F). These motifs vary in their number of total fluorine atoms. Typically, there is either a single fluorine or a group of three in the form of a trifluoromethyl group.

The physiochemical properties drug developers seek using fluorine result in a more persistent environmental pollutant. Fluorination adds thermal, metabolic, and oxidative stability to the molecule, making it more persistent than its non-fluorinated counterparts.[14,21] Due to the limited occurrence of natural organic fluorine, pathways for biotic degradation are minimal.[1,2] Abiotic degradation pathways do exist. Direct and indirect photolysis can occur depending on the light absorbance of the molecule and the composition of the aqueous matrix. Water treatment facilities have adopted ultraviolet radiation coupled with advanced oxidation practices (AOPs) for disinfection, and

advanced reduction practices (ARPs) have been proposed to degrade oxidized contaminants.[57,58,60] These same practices can degrade various fluorinated compounds.[46] Although the parent molecule may degrade in these processes, organic fluorinated photoproducts may form and could be cause for concern.

Trifluoroacetic acid is produced from the photolysis of fluoxetine, a common fluorinated pharmacutial.[75] Due to the large variety of fluorinated pharmaceuticals and agrochemicals, identifying every fluorinated photoproduct is difficult. Model compounds representing different fluorine motifs can be studied as a proxy to compounds with the same motif. Determining fluorinated photoproducts from various fluorinated motifs allows better prediction of the photochemical fate of fluorinated compounds. The Ar-F and Ar-CF_3 motifs were studied with fluorinated phenol model compounds. The fluorine motif was either positioned at the ortho, meta, or para position on the phenol (Figure 2-1). Photodegradation occurred and fluorinated photoproducts were analyzed. Fluoxetine, with the Ar-CF_3 motif and sitagliptin, with the Ar-F and Py-CF_3 motifs, were also photolyzed. The fluorinated photoproducts from these compounds were analyzed and compared to the model compound photoproducts. Photolysis experiments were conducted at pH 5, 7, and 10. To mimic AOPs and ARPs, H_2O_2 was used at pH 7 to produce •OH and SO_3^{-2} was used at pH 10 to produce e_{aq}^-.

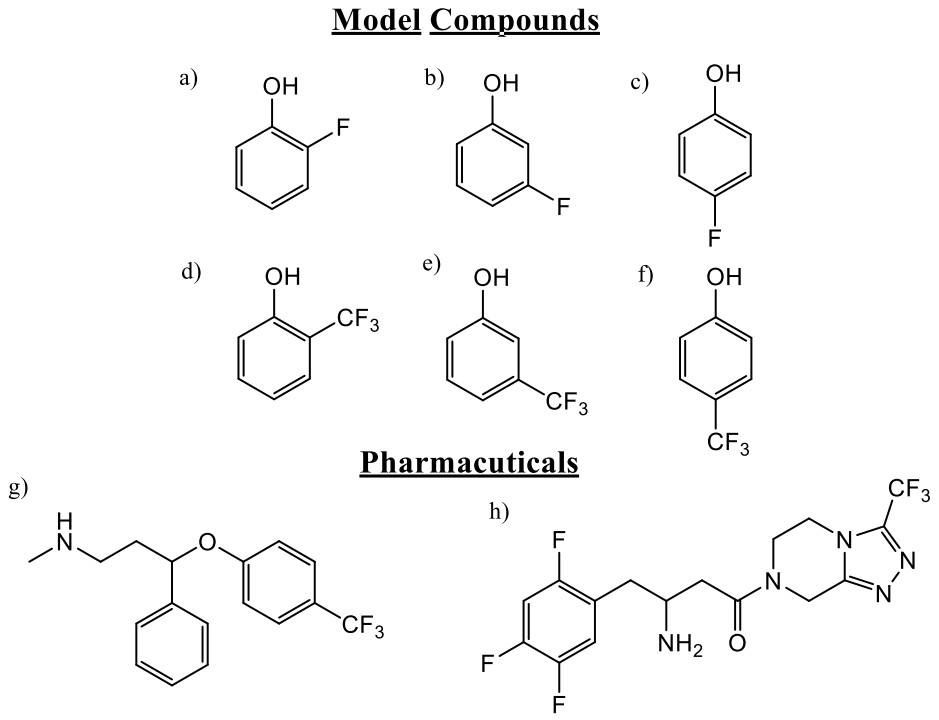

Figure 2-1. Structure of model compounds (a-f) and pharmaceutical compounds (g and h) used in this study. Model compounds vary in the position of the fluorine motif. Fluoxetine (g) has an Ar-CF_3 motif and sitagliptin (h) has three Ar-F motifs as well as a Py-CF_3 motif.

^{19}Fluorine-nuclear magnetic resonance (^{19}F-NMR) techniques for quantification are accurate and useful for dealing with similar fluorinated compounds in a single sample when compared to GC-MS and LC-MS.[107,108] Use of ^{19}F-NMR allowed for fluorinated photoproducts to be quantified without chromatography methods. Structural information was also obtained from the ^{19}F-NMR analysis by studying the shift and geometry of the photoproduct peaks. Trifluoroacetic acid and fluoride had unique NMR shifts and peak geometry and were able to be identified as photoproducts. LC-HRMS was also used to verify fluorinated photoproducts that match the motifs of the ^{19}F-NMR spectra.

2.2 Experimental Methods

2.2.1 Chemicals and Reagents

Fluoxetine HCl (pharmaceutical secondary standard), sitagliptin phosphate (pharmaceutical secondary standard), 2-fluorophenol (98%), 3-fluorophenol (98%), 4-fluorophenol (99%), 2-hydroxybenzotrifluoride (97%), 3-(trifluoromethyl)phenol (99%), 4-trifluoromethyl(phenol) (97%), trifluoroacetic acid (99%),and methanol (>99.9%) were purchased from Sigma-Aldrich. Hexafluorobenzene (HFB; >99.0%) was purchased from Tokyo Chemical Industry. Sodium sulfite anhydrous (99.2%) and boric acid (analytical reagent grade) were purchased from Mallinckrodt. Sodium phosphate monobasic monohydrate (certified ACS grade), ortho-phosphoric acid 85% (HPLC grade), sodium hydroxide (50% w/w), and 2-propanol (HPLC grade) were purchased from Fischer Chemical. Sodium phosphate dibasic anhydrous (ACS grade) and acetonitrile (HPLC grade) were purchased from J.T. Baker. Deuterium oxide (99.9%) was purchased from Cambridge Isotope Laboratories Inc. Hydrochloric acid was purchased from BDH Aristar. Ultrapure water (18.2 MΩ•cm) was produced by a Milli-Q Academic system (Millipore).

2.2.2 Sample Preparation

Stock solutions of fluoxetine, sitagliptin, 2-fluorophenol, 3-fluorophenol, 4-fluorophenol, 2-hydroxybenzotrifluoride, 3-(trifluoromethyl)phenol, 4-(trifluoromethyl)phenol were made at or near 1 mM concentration in either MilliQ water or methanol, depending on the solubility limits of each compound, and stored at 4 °C. A 0.5 M stock solution of sodium sulfite in pH 10 boric acid buffer was prepared and stored in the dark.

Acetate (pH 5), phosphate (pH 7) and borate (pH 10) buffers, each at 10 mM, were prepared and used in direct photolysis experiments. The compound of interest was diluted into the buffer matrix for a final concentration of 10 µM. To study the degradation due to hydroxyl radicals (•OH), 1 mM hydrogen peroxide was added into the pH 7 buffer matrix. Sodium sulfite (0.5 mM) was added into the pH 10 buffer matrix to study the degradation due to hydrated electrons (e_{aq}^-).[50–55]

2.2.3 Photolysis Experiments

Irradiation was performed using a mercury vapor lamp apparatus consisting of a 450-Watt UV immersion lamp, a quartz immersion well with cooling water circulating through it, and a Pyrex 7740 absorption sleeve with a cutoff value of 280 nm (Ace Glass). A carousel was placed around the lamp such that vials were rotated around the lamp in the center to ensure similar light exposure for all the vials.

The compounds of interest at a concentration of 10 µM in a pH 5 acetate buffer, pH 7 phosphate buffer, pH 10 boric acid buffer, pH 7 phosphate buffer with 1 mM hydrogen peroxide, or pH 10 boric acid buffer with 0.5 mM sodium sulfite were poured into two quartz test tubes, one of which was wrapped in aluminum foil and used as a dark control. Samples were capped with rubber stoppers and placed in the carousel. Each experiment was performed in triplicate, for a total of three irradiated samples and three dark control samples.

2.2.4 High Pressure Liquid Chromatography (HPLC)

A minimum of 5 timepoints including a zero timepoint were taken for analysis using HPLC. Before irradiation, an aliquot was taken from each of the quartz test tubes and placed into amber HPLC vials for the initial unphotolyzed sample. Additional

aliquots were subsequently taken at later timepoints and placed into amber HPLC vials for analysis. The volume of each aliquot was 330 µL, enough for the injection needle to pull up 50 µL of sample. To quench the hydrolysis of the trifluoromethylphenols and fluorophenols in the pH 10 boric acid buffer, 4.0 µL of 1 M HCl was added into the HPLC vial with the sample aliquot. The minimum exposure for degradation of each compound of interest was set at two half-lives.

An Agilent 1100 series HPLC with a variable wavelength detector was used for analysis. An ultraviolet absorbance spectrum of each compound of interest was taken on a spectrophotometer to best choose a detection wavelength (Appendix A). Some compounds had products that were detectable at the same wavelength as that monitored for parent compound. Methods were optimized to separate any products from the parent peak. The conditions for each method are shown in Table 2-1.

Table 2-1. Agilent 1100 series HPLC conditions for each compound of interest. The pH 3 phosphate buffer is at a concentration of 10 mM and has a ratio of 9:1 of buffer to ACN.

Compound	Mobile Phase	Detection Wavelength (nm)	Column	Flow Rate (mL/min)
Fluorophenols	ACN: pH 3 phosphate buffer	210	Eclipse XDB-C18 3.5 μm 4.6 × 150 mm	1.0
Trifluoromethyl-phenols	ACN: pH 3 phosphate buffer	220	Eclipse XDB-C18 3.5 μm 4.6 × 150 mm	1.5
Fluoxetine HCl	ACN: pH 3 phosphate buffer	230	Eclipse XDB-C18 3.5 μm 4.6 × 150 mm	1.0
Sitagliptin Phosphate	ACN: pH 3 phosphate buffer	210	Eclipse XDB-C18 3.5 μm 4.6 × 150 mm	1.0

2.2.5 ^{19}F-Nuclear Magnetic Resonance (NMR)

Wilmad 7-inch class A glass 500 MHz NMR tubes were used for analysis. All aqueous NMR samples contained 9% D_2O (v/v) by injecting 50 μL of deuterium dioxide into the NMR tube. To prepare the final NMR samples (535 μL total volume), 485 μL aliquots were taken from the quartz test tubes at desired time points and pipetted into the NMR tube. In the case for the trifluoromethylphenols and fluorophenols in the pH 10 matrix, an additional 6 μL of 1 M HCl was added to the NMR tube to prevent hydrolysis, for a total volume of 541 μL. Samples included, a time-zero unphotolyzed sample and a

sample at the completion of photolysis. HFB, enclosed in a sealed melting-point capillary tube, was used as an internal standard, and placed inside the NMR tube.

A 600 MHz Avance Neo NMR equipped with a 5 mM three channel TCI inverse cryoprobe for ^{19}F NMR spectral acquisition was used to determine and quantify the fluorinated parent compound and any fluorinated products from the photolysis experiments. Experimental parameters were determined to maintain a sufficient signal to noise ratio for accurate and reproducible quantitative measurements. Parameters included number of scans, pulse angle, and optimized delay and acquisition times. Additional parameters are shown in Table 2-2. For further explanation of these parameters, see Appendix B. Spectra were obtained without ^{1}H decoupling.

HFB was used to calibrate the axis of the NMR spectra and quantify the fluorine in each sample. HFB was chosen due to the presence of 6 magnetically equivalent fluorine atoms, yielding a sharp singlet peak in the NMR spectra. It was also assumed that HFB would not be a product of any of the compounds of interest, meaning there would be no overlap in the spectra. The ^{19}F-NMR resonance corresponding to HFB is at -164.9 ppm.[97] By setting the HFB peak to this value, the axis for all the fluorine products in the sample was calibrated to the correct value.

Table 2-2. Parameters of NMR analysis, some values are rounded due to the relationship between the parameters.

Parameter	Value	Unit
Pulse Angle	90	[degrees]
Size of FID (TD)	68180	[ ]
Number of Dummy Scans (DS)	4	[ ]
Loop Count (TD0)	1	[ ]
Number of Scans (NS)	1024	[ ]
Sweep Width (SW)	201	$[ppm]$
Acquisition Time (AQ)	0.3	$[seconds]$
FID Resolution (FIDRES)	0.33	[Hz]
Filter Width (FW)	2.4×10^{8}	[Hz]
Delay (D1)	4.0	$[seconds]$
Receiver Gain (RG)	101	[ ]
Dwell Time	4.40	[μ $seconds$]

The HFB standard was prepared at a concentration of 100 μM in 2-propanol and pipetted into melting-point tubes to a height that would fit the window of the NMR tube for data acquisition. This technique was used in previous NMR studies.[95,97] To seal the end of the melting-point tube, it was placed over a Bunsen burner flame and the open tip was pulled until it came off the tube, sealing it. This allowed for the standard to be taken out of the NMR tubes and reused. To account for the concentration of HFB in the smaller diameter melting point tube, a ratio between the fluorine atoms in the melting-point tube versus the fluorine atoms in the NMR tube was found, allowing for comparison between the standard and the sample.[94] For this, 500 μL of 100 μM trifluoroacetic acid (TFA) in a

ratio of 9:1 MilliQ water to deuterium oxide was pipetted into the NMR tube and the melting-point tube containing the HFB standard was placed in the NMR tube, bringing the total volume to roughly the equivalent of 550 µL. The ratio between single fluorine atoms was found by solving for IS_{ratio} in Equation 2-1. With TFA and HFB having the same concentration of 100 µM, the [TFA] and [HFB] variables cancel out. TFA has three fluorine atoms and HFB has six, which further simplifies the equation for the IS_{ratio}, shown in Equation 2-2. The TFA sample with the HFB standard was run three times, taking an average for the final ratio.

$$\frac{Area_{TFA}}{[TFA]*TFA_{\#F}} = \frac{Area_{HFB}*IS_{ratio}}{[HFB]*HFB_{\#F}} \quad \text{Equation 2-1}$$

$$IS_{ratio} = \frac{2*Area_{TFA}}{Area_{HFB}} \quad \text{Equation 2-2}$$

Each HFB standard ratio was different as shown in Table 2-3, because each melting point tube had a slightly different inner diameters, leading to a different cross-sectional area for NMR analysis. This difference led to variable IS_{ratio} values. Each standard was individually labeled and stored at room temperature. A standard was placed in the NMR tube as described in Appendix B. After every use, both melting-point and NMR tubes were rinsed with methanol so that no residual fluorine remained on the tubes.

Table 2-3. NMR HFB internal standard ratios and errors.

HFB Standard	IS_{ratio}	% ERROR
I	10.89	0.64
II	8.14	1.15
III	11.98	0.44
IV	8.10	0.70
V	10.12	0.73
VI	8.96	0.33
VII	11.63	0.80
IIX	12.19	0.74
IX	10.56	0.83

Bruker Topspin 4.0.7 was used to analyze the NMR spectra. A spectral window of 201 ppm with offset of -100 (O1P) was set in the acquisition parameters to capture the broad range of fluorine resonances. First, the spectrum with the HFB standard resonance was phased, and the baseline corrected. Next, the spectrum was referenced according to the HFB resonance and set to -164.9 ppm. The HFB resonance was then integrated. Every additional experimental resonance in the spectrum was then individually brought into phase, baseline adjusted, and integrated. The integration values with their corresponding shifts were copied into Microsoft Excel for analysis.

Each integration value was converted into moles of fluorine by the HFB internal standard with Equation 2-3 and solving for the unknown amount of fluorine using Equation 2-4. All other variables are known constants with [HFB] being 100 µM, $HFB_{\#F}$ being 6, and the areas of HFB and the peak being the integration values, the IS_{ratio} for a given melting point tube was previously found with Equation 2-2.

$$\left(\frac{Area_{peak}}{[F_{unknown}]}\right) = \frac{Area_{HFB*IS_{ratio}}}{[HFB]*HFB_{\#F}} \quad \text{Equation 2-3}$$

$$[F_{unknown}] = Area_{peak} * \left(\frac{[HFB]}{\frac{Area_{HFB*IS_{ratio}}}{HFB_{\#F}}}\right) \quad \text{Equation 2-4}$$

After all peaks were integrated and converted into moles of fluorine, an additional calculation was made to correct for the dilution factor of the D_2O. Equations 2-5 and 2-6 show the simple calculation made, with M_1 being the concentration calculated from the total volume, V_1 being the total volume of 535 µL, V_2 being the 485 µL of sample added in the NMR tube, and M_2 being the unknown. For the case of trifluoromethylphenol and fluorophenol in the pH 10 matrix, V_1 was 541 µL, accounting for the additional 6 µL of 1 M HCl added to the time-zero NMR tubes, V_2 remained the same.

$$M_1V_1 = M_2V_2 \quad \text{Equation 2-5}$$

$$\frac{M_1V_1}{V_2} = M_2 \quad \text{Equation 2-6}$$

A fluorine mass balance was conducted on the unphotolyzed and photolyzed samples after Equations 2-3 through 2-6 were applied to the spectra. Fluoride was sometimes present in the unphotolyzed sample (at -121.5 ppm). When this was the case, the amount of fluoride in the unphotolyzed sample was subtracted from both the photolyzed and unphotolyzed samples. Error in the mass balance was sometimes observed at roughly 20%, possibly because the photoproducts created were electromagnetically different from the parent compounds, such that different delay and acquisition times are required. Although these parameters were acceptable for the parent compounds, they may be either too long or too short for some of the photoproducts. Other factors include low signal to noise, especially on products that showed low

concentrations and were multiplets. Low S/N ratios lead to inaccurate quantification, it was demonstrated that a S/N ratio must be 150:1 or greater to obtain < 1% error.[109] It was also shown that S/N ratios are directly related to concentration.[110] Thus, if a parent molecule produces many fluorinated photoproducts, they may be at too low of concentration to obtain a large enough S/N ratio to perform accurate quantification.

2.2.6 Liquid Chromatography-High Resolution Mass Spectrometry (LC-HRMS)

For analysis on the LC-HRMS, sample preparation was similar to the HPLC samples. Using the HPLC amber vials, an initial unphotolyzed sample, a final photolyzed sample were taken. Samples from intermediate timepoints were taken if products were formed and degraded by the time photolysis was completed. Each vial had a total volume of 330 μL, enough for the 4 μL injection of the instrument. A blank sample consisted of only the aqueous matrix of the photolysis experiments.

A Velos HRAM LC MS Orbitrap system equipped with a Luna C18 nano-column was used for mass spectrometry analysis. The mobile phase was a mixture of HPLC grade water and acetonitrile, both with 0.1% formic acid. The starting ratio was 98:2, water to acetonitrile, which switched to 2:98 water to volume was acetonitrile over the course of 33 minutes. The flow rate was constant at 0.1 mL/min. Injection volume was set to 4.0 μL and the typical detection rage was from a molecular weight of 100 to 800 m/z. A smaller range was used for smaller molecules (e.g., phenols) which had a detection range of 65 to 300 m/z. The blank sample containing only the unspiked photolysis aqueous matrix was injected to obtain a baseline. Then the unphotolyzed and photolyzed samples were run on the instrument. Retention times, areas, and the most abundant ion masses of peaks were recorded. To be considered for analysis, the peak

must have an area greater than 15,000, and the peak must be 5 times greater than any corresponding peak in the blank and unphotolyzed sample. MS/MS fragmentation data was obtained for the most abundant ion masses of each peak that met these criteria. An online chemical formula calculator was used to generate possible chemical formulas of fragments and products and isotopic patterns were calculated from enviPat. Chemical structures matching these formulas were made in ChemDraw. Structures were made by using the parent compound as a starting point, then breaking bonds and adding atoms to obtain viable structures. Oxygen was the only atom allowed to be added to the structure. Levels of product identification are summarized in Table 2-4.

Table 2-4. Levels of product identification with mass spectrometry.[56]

Level	Description
1	Peak mass and retention are matched to a reference standard
2a	Matched peak mass to a spectrum in a library
2b	Matched largest mass and at least one fragment
3	Exact mass match and matches MassFrontier
4	Exact mass match
5	No mass match, but a clear peak

2.2.7 Reaction Kinetics

Concentrations measured by HPLC were used to asses reaction kinetics. The unphotolyzed sample was taken as the initial value, C_0 and first-order kinetics were applied by integrating Equation 2-7 with respect to time, *t* and solving for *-kt.*[111]

$$-\frac{d[C]}{dt} = k[C] \qquad \text{Equation 2-7}$$

$$\ln[C] = \ln[C_0] - kt \qquad \text{Equation 2-8}$$

$$\ln\frac{[C]}{[C_0]} = -kt \qquad \text{Equation 2-9}$$

To calculate rate constants and 95% confidence intervals, regression of $\ln(C/C_o)$ versus time was performed in Microsoft Excel. The upper 95% confidence interval was subtracted from the rate constant, yielding the total 95% confidence interval. A weighted average of the 95% confidence intervals from the replicates was taken for the final error, while the rate constants were averaged. Photolysis rate constants were found by subtracting the dark control hydrolysis rate constant from the total rate constant of the photolyzed sample. $\ln(C/C_0)$ versus time plots were prepared in Orgin, error bars on the timepoints were calculated from the standard deviation of triplicate samples (Appendix A).

2.3 Results and Discussion

2.3.1 Photolysis of Trifluoromethylphenol Model Compounds

Photolysis and fluorinated photoproduct formation of the aromatic trifluoromethyl motif ($Ar\text{-}CF_3$) were studied with ortho-, meta-, and para-trifluoromethylphenol model compounds. 2-TFMP photolysis was pH dependent, with the rate constant at pH 7 an order of magnitude faster than at pH 5 and the rate constant at pH 10 an order of magnitude faster than at pH 7 (Figure 2-2; Table 2-5). 3-TFMP had a 100-fold increase in rate constant at pH 10 compared to 5 and 7. The 4-TFMP rate constant increased with increasing pH. The addition of H_2O_2 increased the photolysis rate constants for each model compound while the addition of SO_3^{-2} did not dramatically affect the photolysis rate. Thus, AOPs are effective at increasing the degradation of $Ar\text{-}CF_3$ motifs, while ARPs are not (Table 2-5). All other kinetic plots are shown in Appendix A.

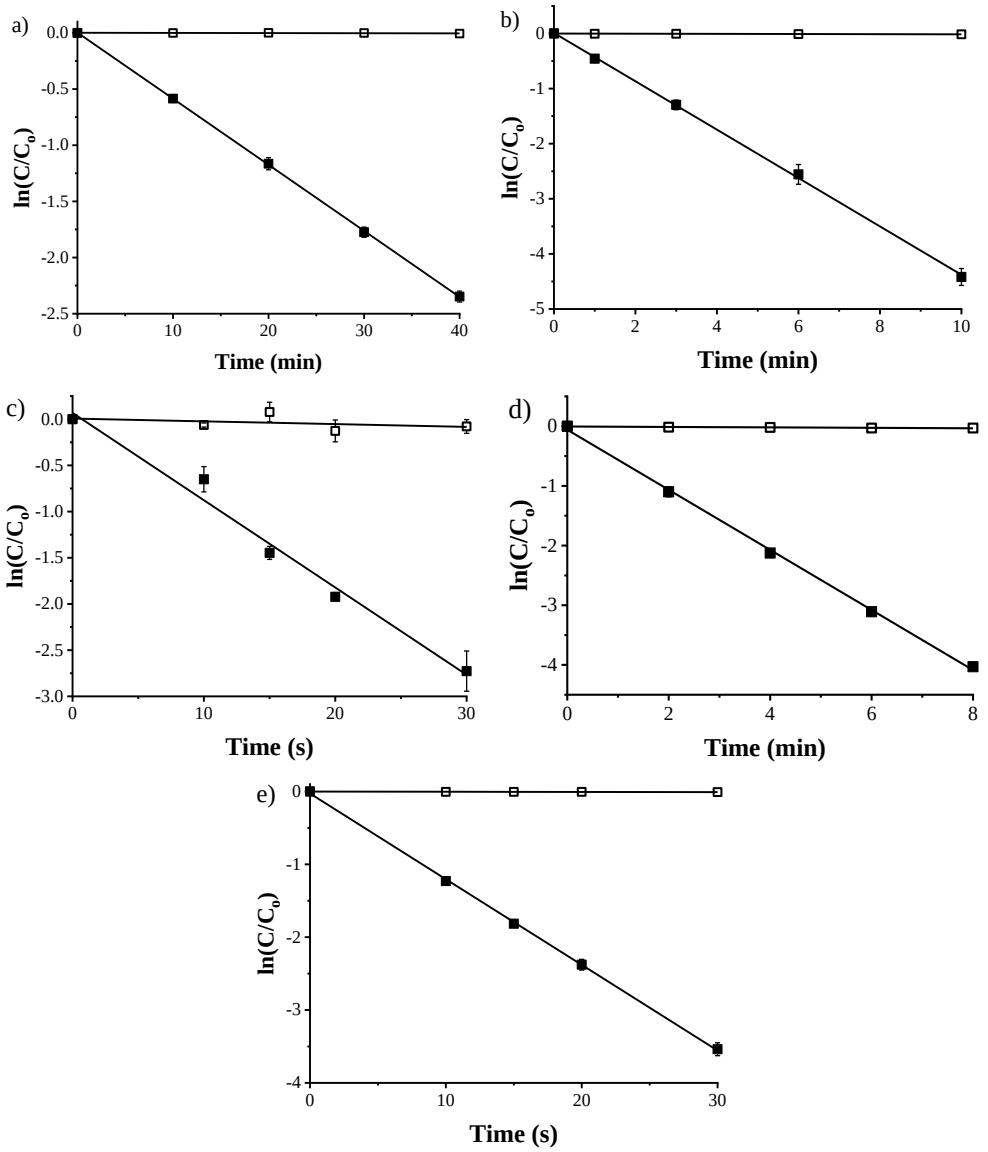

Figure 2-2. Photochemical degradation plots of ortho-trifluoromethylphenol (2-TFMP) with hydrolysis (□) and photolysis (■) rate constants of 0.01 ± 0.01 h^{-1} and 3.52 ± 0.07 h^{-1} in a 10 mM pH 5 acetate buffer (a), 0.08 ± 0.03 h^{-1} and 26.37 ± 0.64 h^{-1} in a 10 mM pH 7 phosphate buffer (b), 10.78 ± 28.57 h^{-1} and 334.09 ± 93.45 h^{-1} in a 10 mM pH 10 borate buffer (c), 0.22 ± 0.10 h^{-1} and 29.99 ± 1.47 h^{-1} in a 10 mM pH 7 phosphate buffer with 1 mM H_2O_2 (d), and 0.99 ± 1.62 h^{-1} and 422.43 ± 9.38 h^{-1} in a 10 mM pH 10 borate buffer with 0.5 mM SO_3^{-2} (e). Error bars represent the standard deviation between triplicate samples taken on HPLC. Reported rate constant errors represent the average 95% confidence interval determined by regression statistics. Note the change in units along the x-axis.

Table 2-5. Photolysis rate constants for 2-,3-, and 4-trifluoromethylphenols (TFMP) using a 450-Watt UV immersion lamp with a 280 nm cutoff value and the corresponding hydrolysis rate constants found with dark control experiments in various aqueous matrices. The pH values were set by acetate, phosphate, and borate for pH 5, 7, and 10, respectively, and the pH for H_2O_2 and SO_3^{-2} were 7 and 10, respectively.

Compound	Matrix	Photolysis k (h^{-1})	Hydrolysis k (h^{-1})
2-TFMP	pH 5	3.52 ± 0.07[a]	0.01 ± 0.01
	pH 7	26.37 ± 0.64	0.08 ± 0.03
	pH 10	334.09 ± 93.45	10.78 ± 28.57
	1 mM H_2O_2	29.99 ± 1.47	0.22 ± 0.10
	0.5 mM SO_3^{-2}	422.43 ± 9.38	0.99 ± 1.62
3-TFMP	pH 5	2.72 ± 0.06	0.01 ± 0.01
	pH 7	3.27 ± 0.63	0.04 ± 0.04
	pH 10	207.9 ± 7.51	2.84 ± 2.08
	1 mM H_2O_2	7.80 ± 0.20	0.08 ± 0.08
	0.5 mM SO_3^{-2}	225.83 ± 13.60	0.72 ± 0.41
4-TFMP	pH 5	$0.02 \pm 5.5\times10^{-4}$	$4.1\times10^{-3} \pm 3.6\times10^{-4}$
	pH 7	0.10 ± 0.02	0.25 ± 0.01
	pH 10	1.58 ± 0.71	3.93 ± 0.57
	1 mM H_2O_2	6.85 ± 0.93	0.52 ± 0.18
	0.5 mM SO_3^{-2}	2.38 ± 0.45	2.85 ± 0.39

[a] Reported errors are 95% confidence intervals determined by a weighted average of triplicate samples.

Fluorinated photoproduct formation from the Ar-CF_3 model compounds varied with pH and position of the Ar-CF_3 motif on the phenol, all fluorinated products formed are listed with shifts (ppm) and peak geometry in Table 2-6. 2-TFMP had one organic fluorinated product near the parent NMR shift (Product E), that occurred at pH 10 with and without the addition of SO_3^{2-}. At pH 5, one organofluorine product was detected downfield (Product F). The only other fluorinated photoproduct formed was fluoride (Figure 2-3 and 2-4). The single organic fluorine product at pH 10 and with the addition of SO_3^{-2} suggest that different mechanisms may occur under basic conditions. Some of

the fluoride peaks are broad and have two peaks, this could be due to the shimming of the NMR instrument or overlap with an organofluorine photoproduct.

Table 2-6. ^{19}F-NMR shifts of fluorinated products identified from photolysis of 2-, 3-, and 4-TFMP in pH 7, pH 10, 1 mM H_2O_2, or 0.5 mM sulfite. Peaks were either singlets (s) or complex multiplets (cm), as defined by an indistinguishable number of peaks.

Product Name	Shift [ppm]	Peak Geometry
A	-63.0	s
B	-63.8	s
C	-66.4	s
D	-69.5	s
E	-82.0	s
TFA	-77.3	s
Fluoride	-121.5	s
F	-157.9	cm

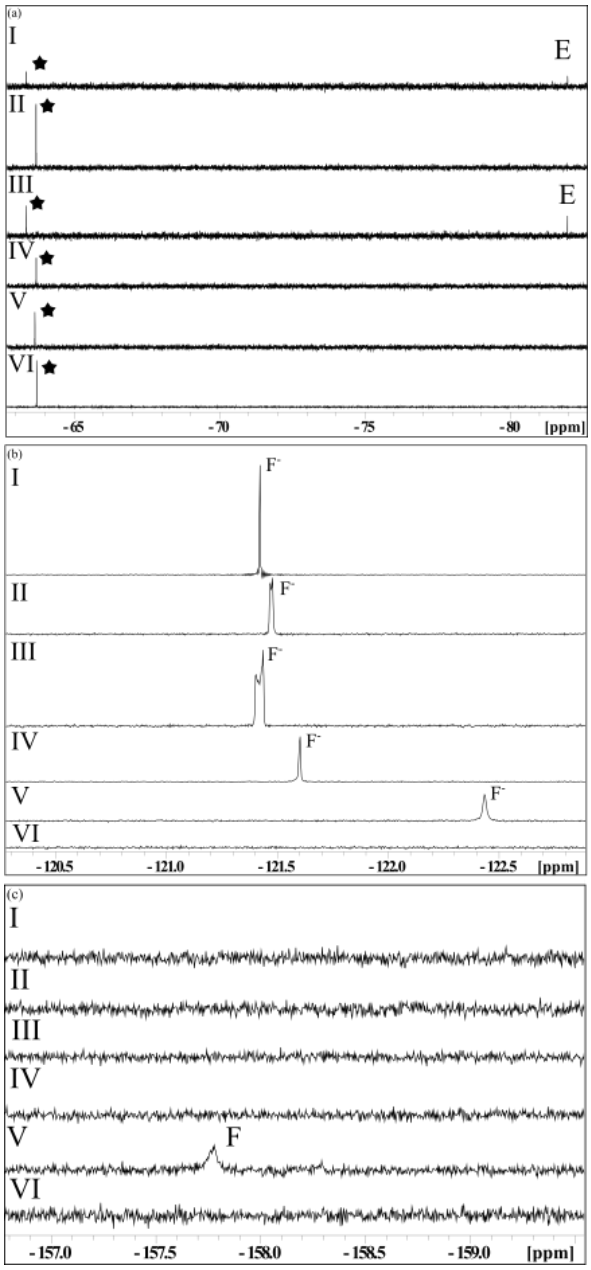

Figure 2-3. ^{19}F-NMR spectra of ortho-trifluoromethylphenol (2-TFMP) before photolysis (VI) and after photolysis in pH 5 acetate buffer (V), pH 7 phosphate buffer (IV), pH 10 borate buffer (III), pH 7 buffer with 1 mM H_2O_2 (II), and pH 10 with 0.5 mM SO_3^{2-} (I). The parent, 2-TFMP (★) is shown in (a), the peaks of the unphotolyzed sample was scaled by a factor of 8. Fluoride (F^-) production is shown in (b), the I and IV samples were scaled by a factor of 4 and 2, respectively. The single organofluorine product (F) is shown in (c). Shift in ppm is resultant of pH change.

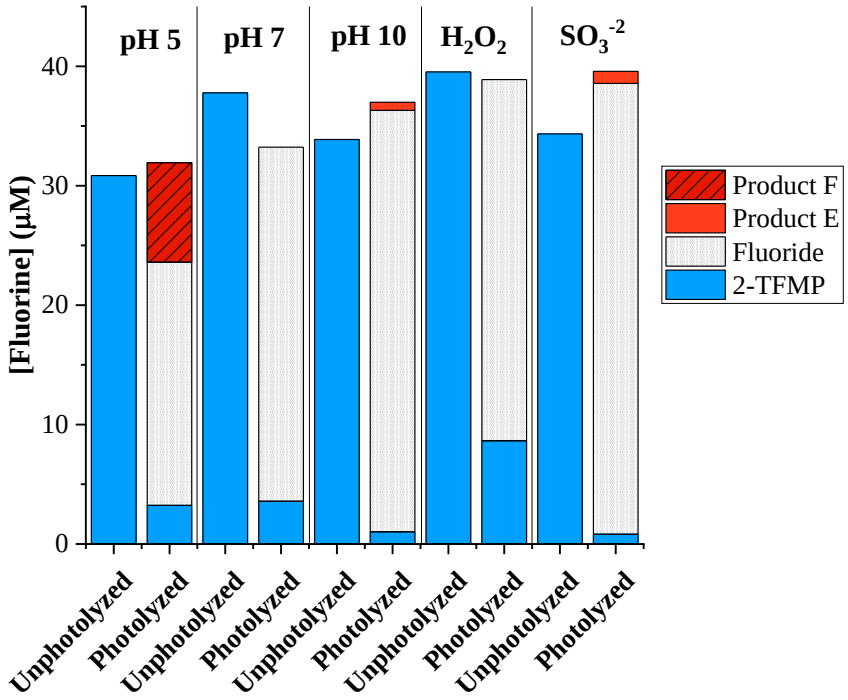

Figure 2-4. Fluorine mass balance as moles of total fluorine for the photolysis of ortho-trifluoromethylphenol (2-TFMP) at 40 minutes for pH 5, 6 minutes for pH 7, 0.5 minutes for pH 10, 4 minutes for 1 mM H_2O_2, & 0.5 minutes for 0.5 mM SO_3^{2-}.

Fluoride was the only fluorinated photoproduct formed from 3-TFMP in all reaction conditions (Figure 2-5 and 2-6).

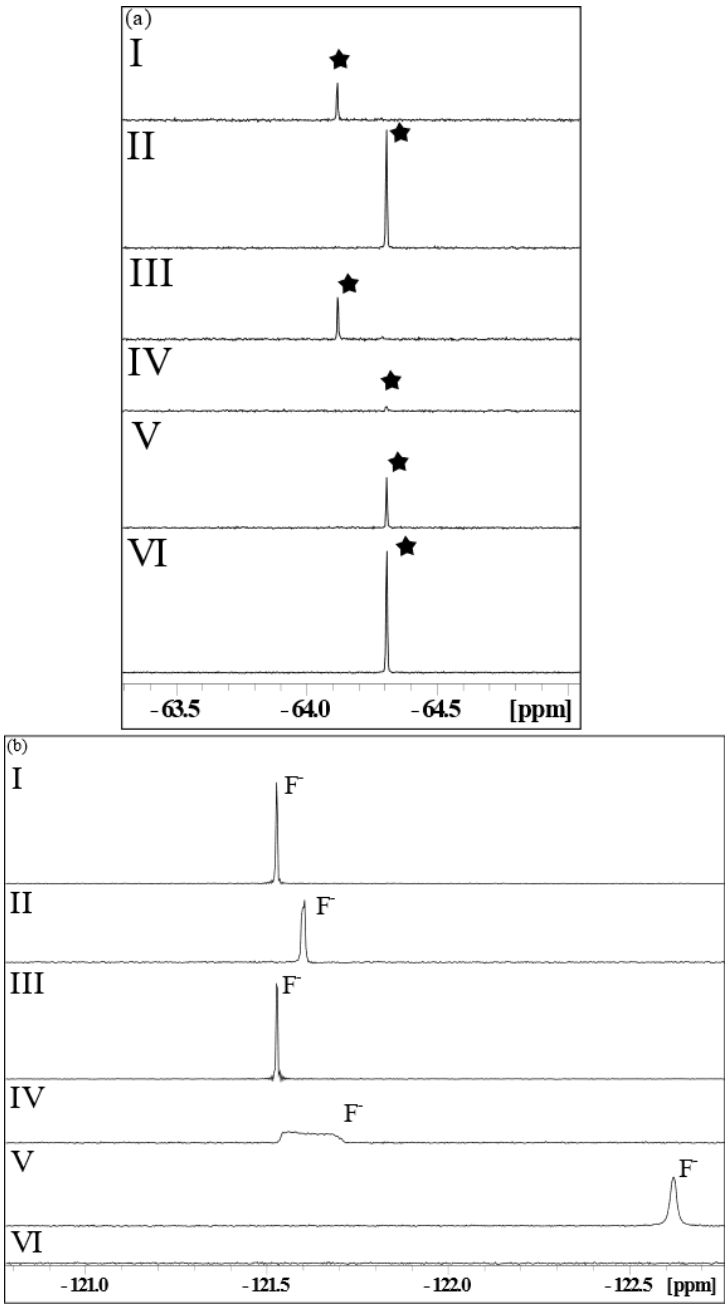

Figure 2-5. ^{19}F-NMR spectra of meta-trifluoromethylphenol (3-TFMP) before photolysis (VI) and after photolysis in pH 5 acetate buffer (V), pH 7 phosphate buffer (IV), pH 10 borate buffer (III), pH 7 buffer with 1 mM H_2O_2 (II), and pH 10 with 0.5 mM SO_3^{2-} (I). The parent, 3-TFMP, (★) is shown in (a), the unphotolyzed sample was scaled by a factor of 4. Fluoride (F^-) production is shown in (b), the broad peak in sample IV could be due to the shimming of the NMR instrument. Samples III and I were scaled by a factor of 4. Shift in ppm is resultant upon pH change.

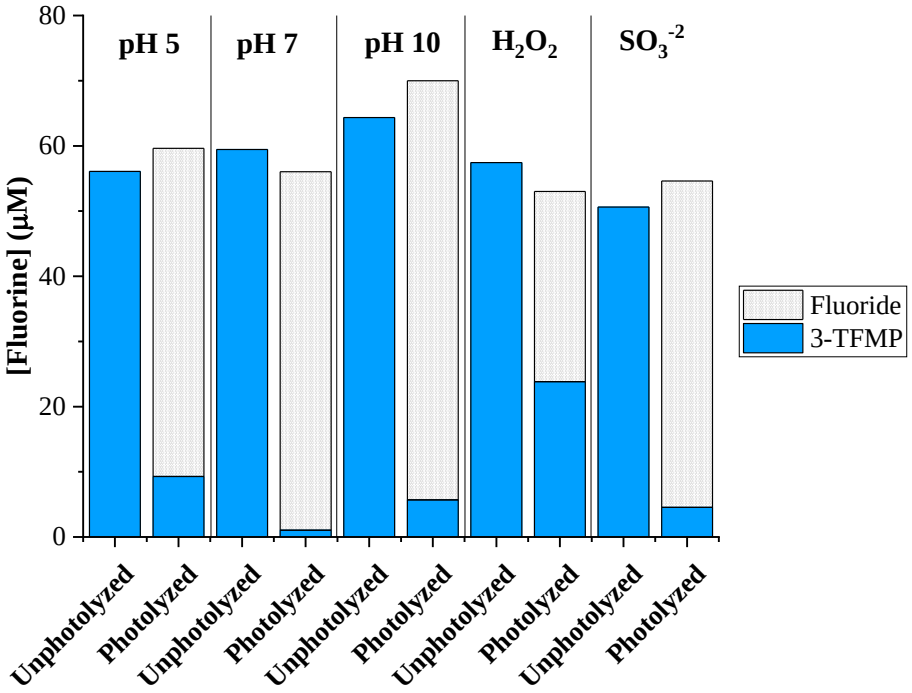

Figure 2-6. Fluorine mass balance as moles of total fluorine for the photolysis of meta-trifluoromethylphenol (3-TFMP) at 40 minutes for pH 5, 40 minutes for pH7, 1 minute for pH 10, 6 minutes for 1 mM H_2O_2, and 1 minute for 0.5 mM SO_3^{2-}.

Fluoride was the main fluorinated photoproduct for 4-TFMP at all reaction conditions. Organofluorine products were consistently detected and near the parent NMR shift, including TFA. Unique products were formed based on reaction conditions, product A is observed with the addition of H_2O_2, product C is observed at pH 5, and product D is observed at pH 10 with and without the addition of SO_3^{2-} (Figures 2-7 and 2-8). This suggests that different mechanisms of degradation may be occurring with varying reaction conditions.

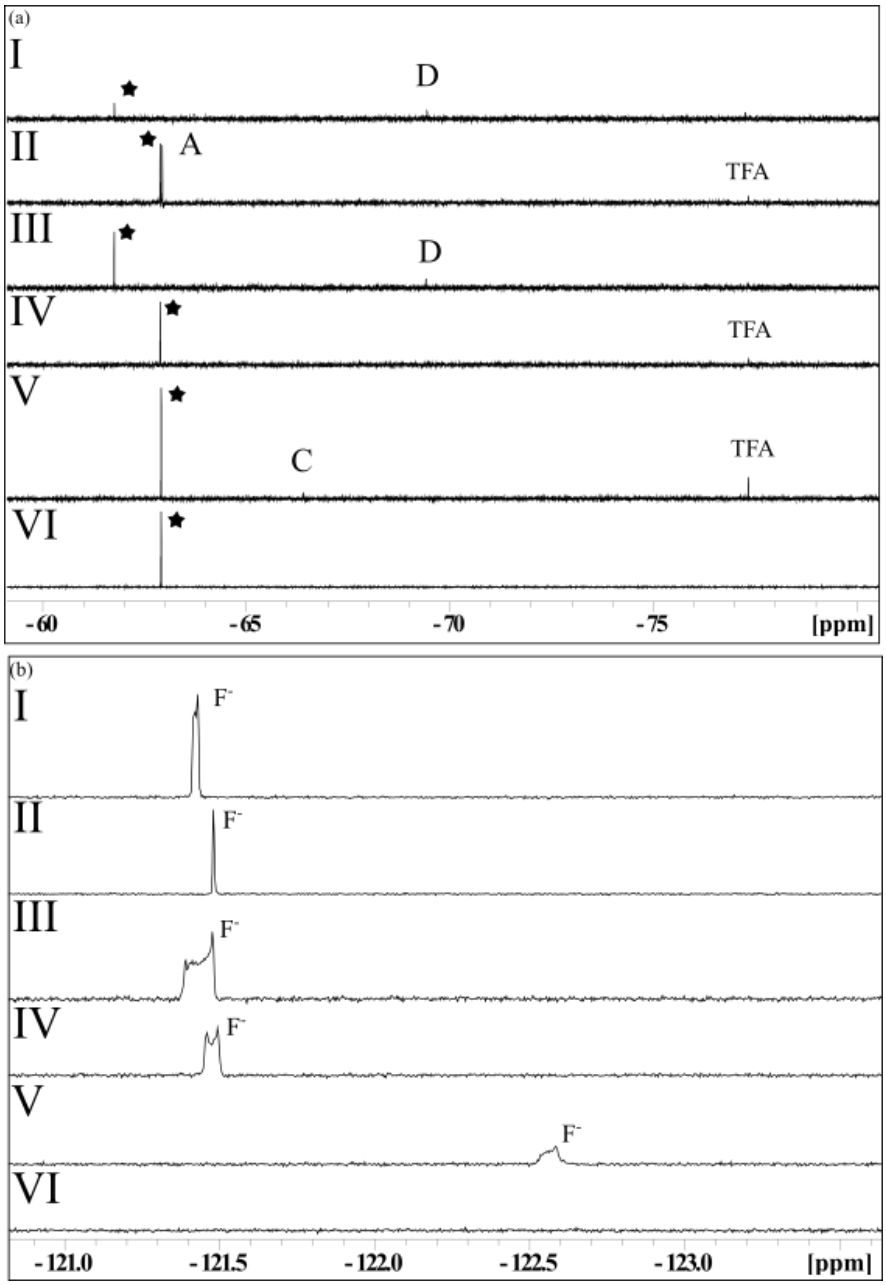

Figure 2-7. ^{19}F-NMR spectra of para-trifluoromethylphenol (4-TFMP) before photolysis (VI) and after photolysis in pH 5 acetate buffer (V), pH 7 phosphate buffer (IV), pH 10 borate buffer (III), pH 7 buffer with 1 mM H_2O_2 (II), and pH 10 with 0.5 mM SO_3^{2-} (I). The parent, 4-TFMP, (★) and fluorinated photoproducts with similar NMR shifts (A,C,D) including trifluoroacetic acid (TFA) are shown in (a), the unphotolyzed sample was scaled by a factor of 4. Fluoride (F^-) production is shown in (b) and samples I and II were scaled by a factor of 2.

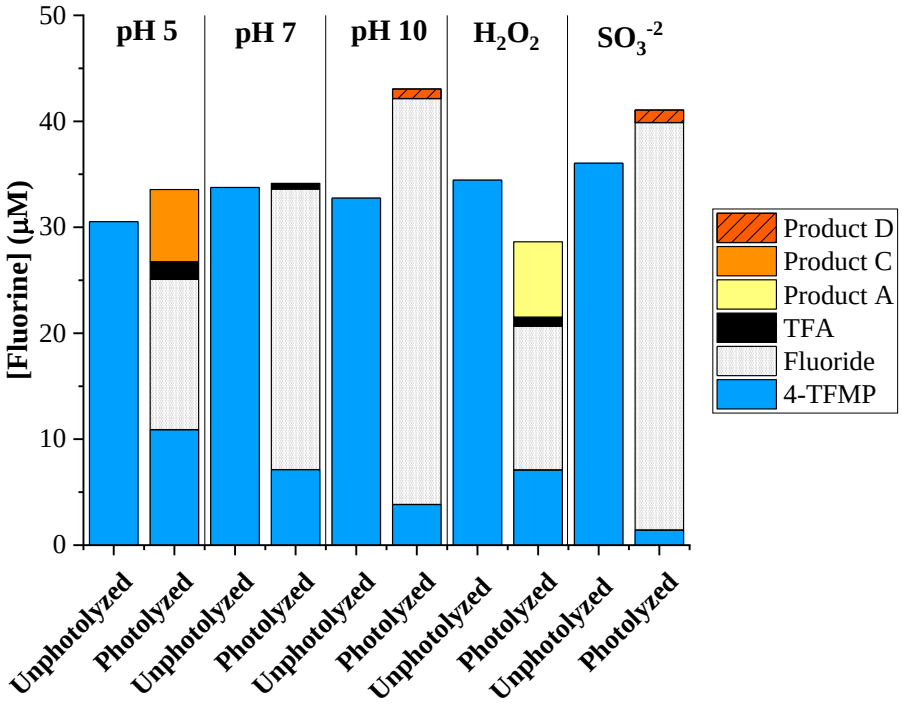

Figure 2-8. Fluorine mass balance as moles of total fluorine for the photolysis of meta-trifluoromethylphenol (4-TFMP) at 40 hours for pH 5, 6 hours for pH 7, 25 minutes for pH 10, 20 minutes for 1 mM H_2O_2, & 20 minutes for 0.5 mM SO_3^{2-}.

4-TFMP had relatively rapid degradation in the dark controls compared to the other model compounds. ^{19}F-NMR was conducted on the dark controls in all the reaction conditions except for pH 5, where the dark control rate was much slower. Fluoride was the major fluorinated photoproduct in all reaction conditions. At pH 10 and with the addition of sulfite, an organofluorine product was formed near the parent NMR shift (Product B). Suggesting that under basic conditions, hydrolysis forms different products than when under neutral conditions. With the addition of H_2O_2, a different organofluorine NMR shift was observed near the parent NMR shift (Product A). Suggesting that in the presence of •OH, a different hydrolysis mechanism may be occurring than with buffered water (Figures 2-9 and 2-10).

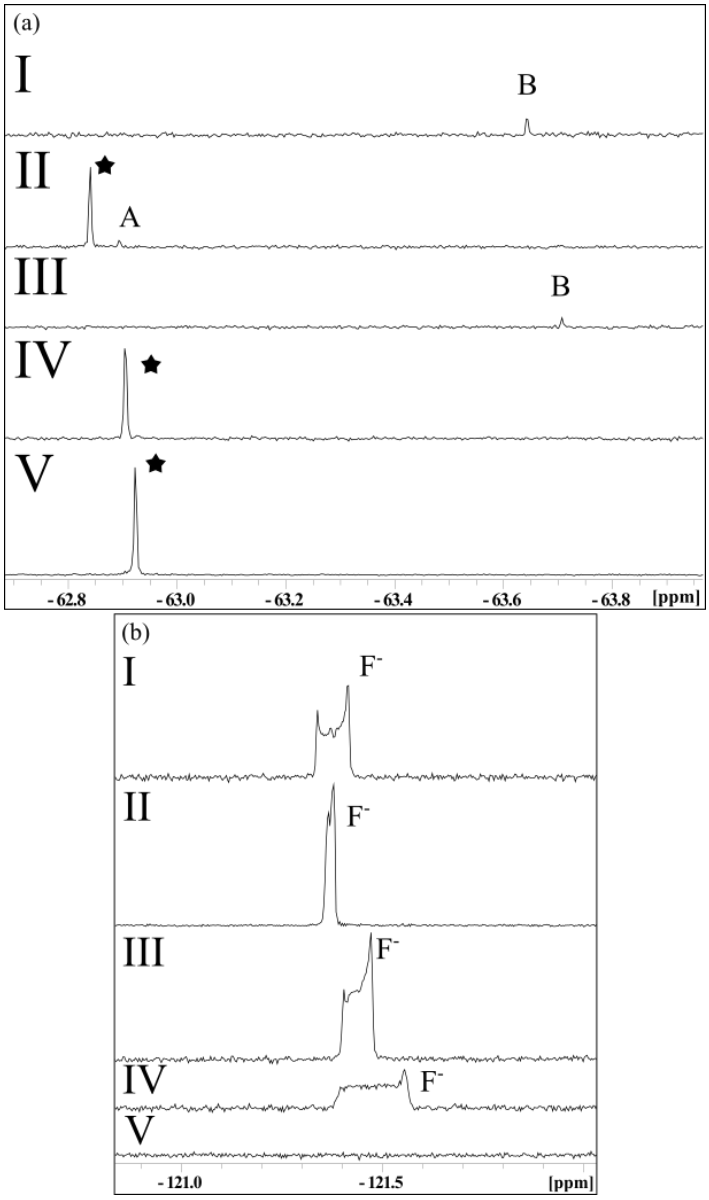

Figure 2-9. ^{19}F-NMR spectra of para-trifluoromethylphenol (4-TFMP) before hydrolysis (V) and after hydrolysis in pH 7 phosphate buffer (IV), pH 10 borate buffer (III), pH 7 buffer with 1 mM H_2O_2 (II), and pH 10 with 0.5 mM SO_3^{2-} (I). The parent, 4-TFMP, (★) and fluorinated photoproducts with similar shifts (A and B) are shown in (a), 4TFMP was completely hydrolyzed in pH 10 and with the addition of sulfite. The unphotolyzed sample was scaled by a factor of 4. Fluoride is shown in (b) and may be either the result of NMR shimming or the overlap with other products, resulting in a broad peak.

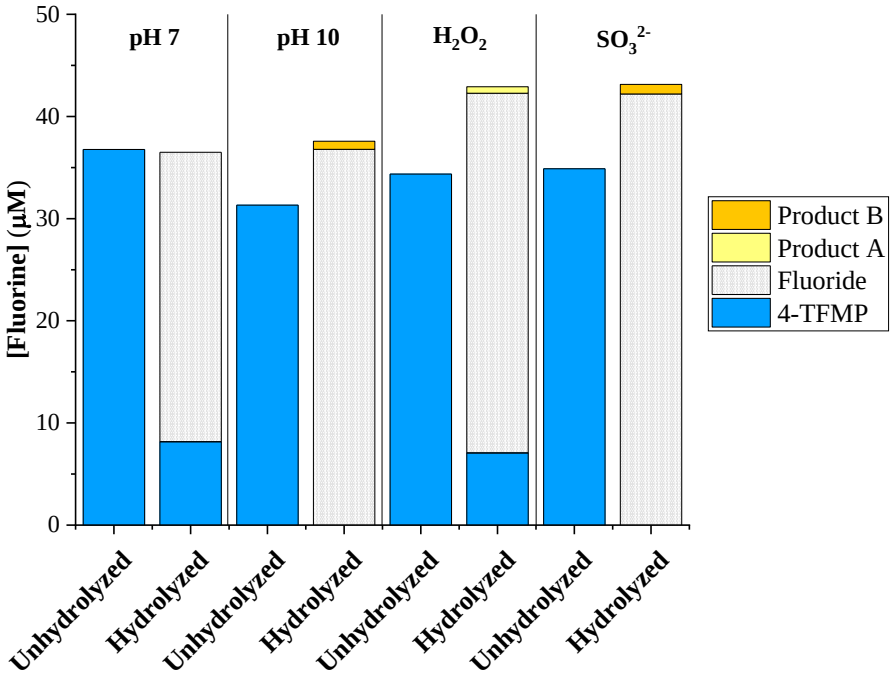

Figure 2-10. Fluorine mass balance as moles of total fluorine for the dark control hydrolysis of meta-trifluoromethylphenol (4-TFMP) at 1 hour for both pH 10 and 0.5 mM SO_3^{2-}, and 6 hours for both pH 7 and 1 mM H_2O_2.

2.3.2 Photolysis of Fluorophenol Model Compounds

Photolysis and fluorinated photoproduct formation of the aryl fluorine motif (Ar-F) were studied with ortho-, meta-, and para-fluorophenol model compounds. For all the compounds, the photolysis rates between pH 5 and 7 were similar. At pH 10, the rate constants increased two orders of magnitude for each fluorophenol. 4-FP had the fastest photodegradation rate of the three isomers (Table 2-7).

Table 2-7. Photolysis rate constants for 2-, 3-, and 4-fluorophenol (FP) using a 450-Watt UV immersion lamp with a 280 nm cutoff value and the corresponding hydrolysis rate constants found with dark control experiments in varying pH buffered waters. The pH values were set by acetate, phosphate, and borate for pH 5, 7, and 10, respectively.

Compound	Matrix	Photolysis k (h^{-1})	Hydrolysis k (h^{-1})
2-FP	pH 5	0.21 ± 0.01[a]	0.01 ± 6.3E-4
	pH 7	0.85 ± 0.03	0.01 ± 2.9E-3
	pH 10	15.99 ± 0.37	0.01 ± 0.13
3-FP	pH 5	$0.17 \pm 2.5\times10^{-3}$	$1.4\times10^{-3} \pm 2.9\times10^{-4}$
	pH 7	0.36 ± 0.01	$3.1\times10^{-3} \pm 1.7\times10^{-3}$
	pH 10	10.15 ± 0.29	0.02 ± 0.10
4-FP	pH 5	4.28 ± 0.10	0.01 ± 0.01
	pH 7	4.17 ± 0.11	9.9E-3 ± 0.02
	pH 10	25.82 ± 1.66	0.01 ± 0.08

[a] Reported errors are 95% confidence intervals determined by a weighted average of triplicate samples.

Fluoride was the only fluorinated product formed from every fluorophenol model compound at pH 5, 7, and 10 (Figures 2-11 to 2-16). All products formed are listed with shift (ppm) and peak geometry (Table 2-8). Sometimes the fluoride peak was broad and had two peaks, this could be due to the shimming of the instrument or presence of an organofluorine photoproduct that is overlapping with the fluoride peak.

Table 2-8. NMR shifts and peak geometry of fluorinated products identified from photolysis of 2-, 3-, and 4-fluorophenol in pH 5, 7, and 10.

Product Name	Shift [ppm]	Peak Geometry
Fluoride	-121.5	s

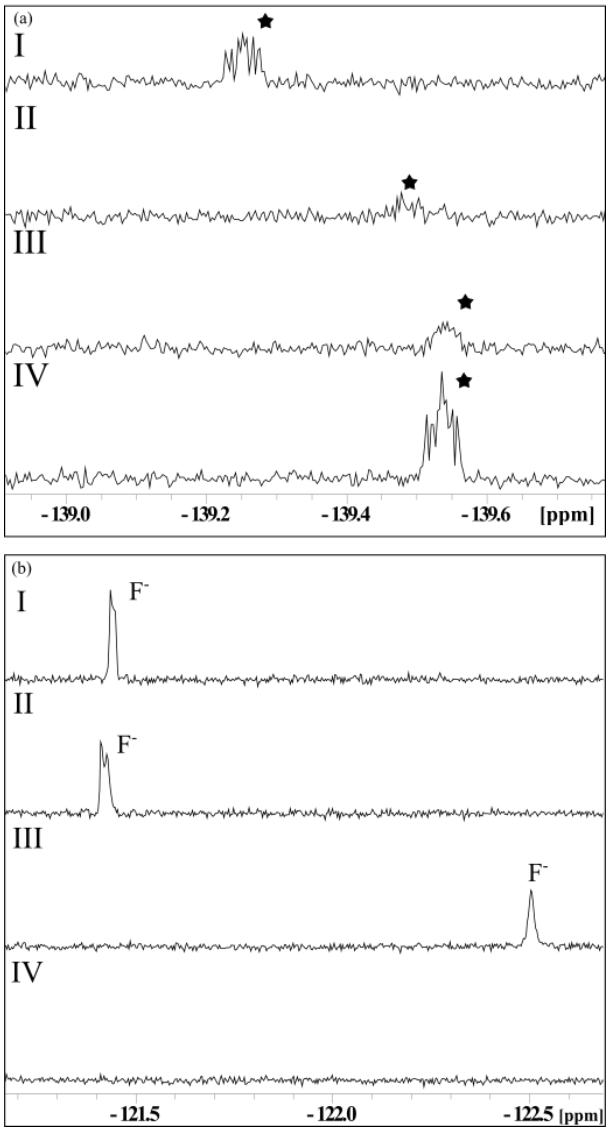

Figure 2-11. ^{19}F-NMR spectra of ortho-fluorophenol (2-FP) before photolysis (IV) and after photolysis in pH 5 acetate buffer (III), pH 7 phosphate buffer (II), and pH 10 borate buffer (I). The parent, 2-FP, (★) is shown in (a), and the fluoride (F^-) production is shown in (b).

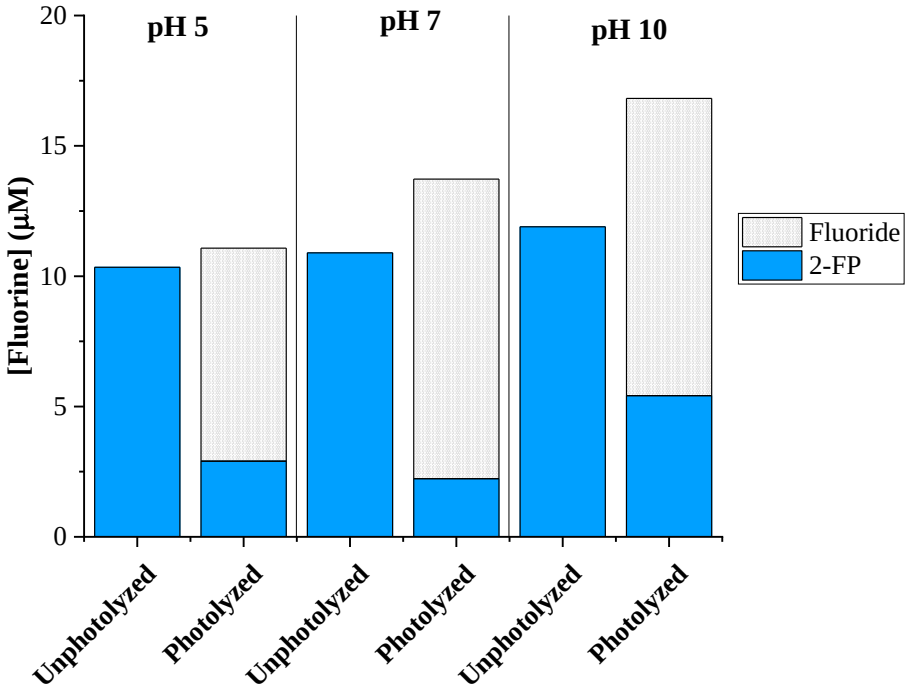

Figure 2-12. Fluorine mass balance as moles of total fluorine for the photolysis of ortho-fluorophenol (2-FP) at 6 hours for pH 5, 2 hours for pH 7, and 5 minutes for pH 10.

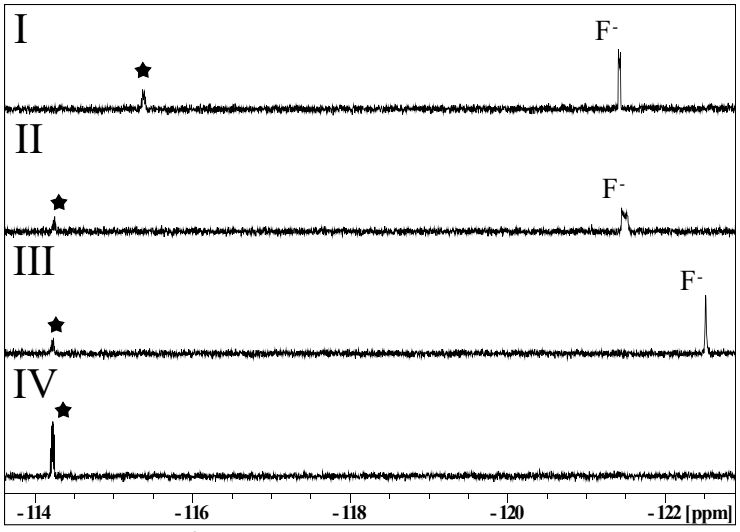

Figure 2-13. ^{19}F-NMR spectra of meta-fluorophenol (3-FP) before photolysis (IV) and after photolysis in pH 5 acetate buffer (III), pH 7 phosphate buffer (II), and pH 10 borate buffer (I). The parent, 3-FP, (★) and fluoride (F^-) production are shown.

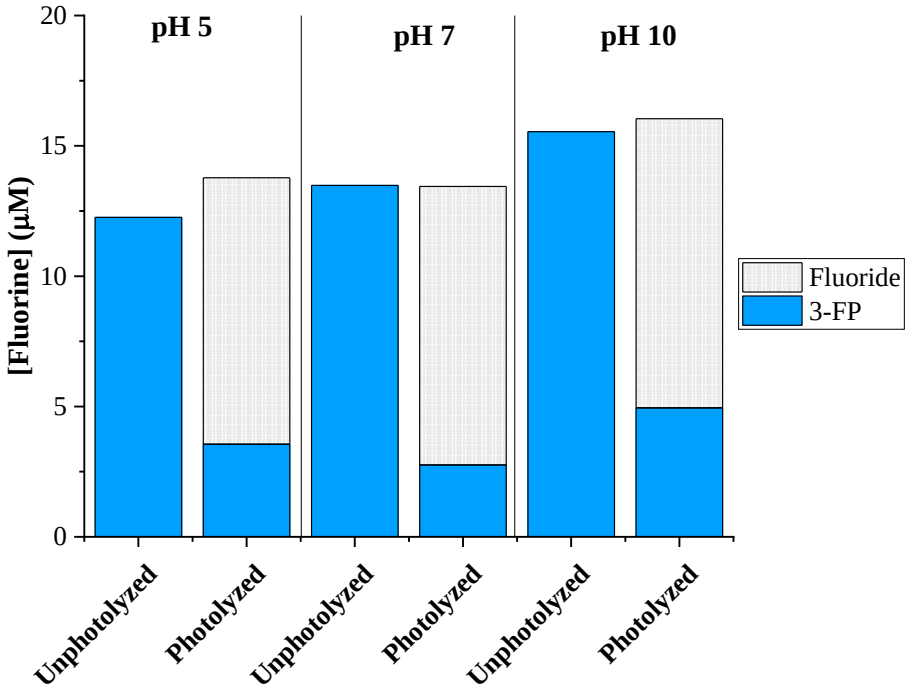

Figure 2-14. Fluorine mass balance as moles of total fluorine for the photolysis of meta-fluorophenol (3-FP) at 4 hours for pH 5, 4 hours for pH 7, and 8 minutes for pH 10.

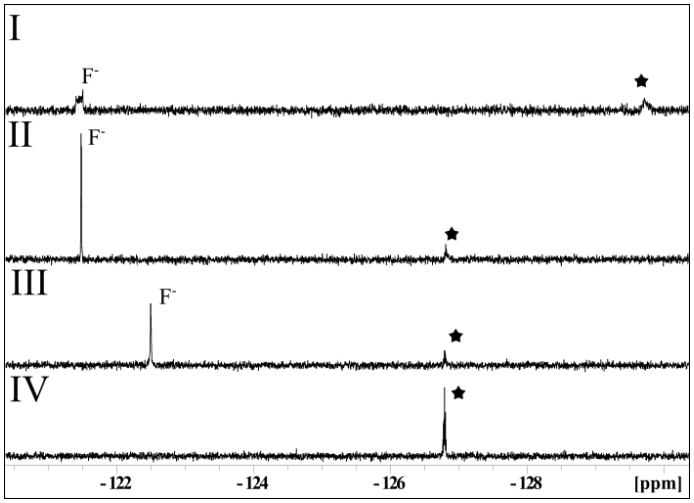

Figure 2-15. ^{19}F-NMR spectra of para-fluorophenol (4-FP) before photolysis (IV) and after photolysis in pH 5 acetate buffer (III), pH 7 phosphate buffer (II), and pH 10 borate buffer (I). The parent ,4-FP, (★) and fluoride (F^-) production are shown in (a).

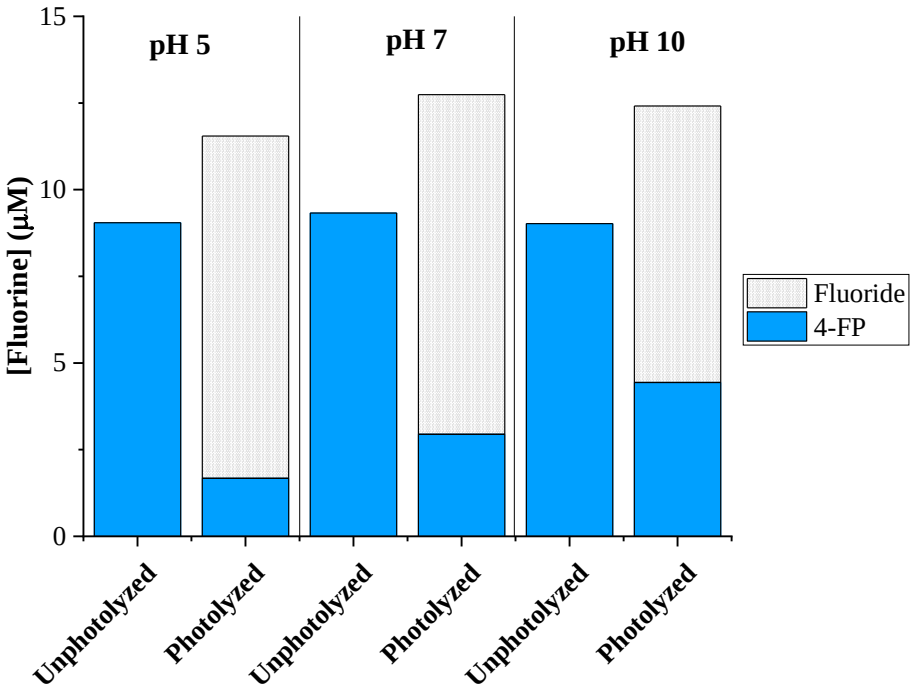

Figure 2-16. Fluorine mass balance as moles of total fluorine for the photolysis of para-fluorophenol (4-FP) at 20 minutes for pH 5, 20 minutes for pH 7, and 3 minutes for pH 10.

2.3.3 Photolysis of Fluoxetine

Photolysis and fluorinated photoproduct formation of fluoxetine was studied and compared to the three Ar-CF_3 model compounds. The photolysis rate was pH dependent. At pH 10, the rate was nearly double that at pH 7. The addition of H_2O_2 and SO_3^{-2} increased the rate roughly 45-fold and 10-fold, respectively (Table 2-9), suggesting that both AOPs and ARPs increase the photolysis rate of fluoxetine.

Table 2-9. Photolysis rate constants for fluoxetine and sitagliptin using a 450-Watt UV immersion lamp with a 280 nm cutoff value and the corresponding hydrolysis rate constants found with dark control experiments in various aqueous matrices. The pH values were set with phosphate and borate for pH 7 and 10, respectively, and the pH of H_2O_2 and SO_3^{-2} were set to 7 and 10, respectively.

Compound	Matrix	Photolysis k (h^{-1})	Hydrolysis k (h^{-1})
Fluoxetine	pH 7	0.27 ± 0.01[a]	0.02 ± 0.01
	pH 10	0.56 ± 0.15	0.01 ± 0.10
	1 mM H_2O_2	12.13 ± 1.54	1.73 ± 1.46
	0.5 mM SO_3^{-2}	5.79 ± 0.95	0.34 ± 0.11

[a] Reported errors are 95% confidence intervals determined by a weighted average of triplicate samples.

Fluorinated photoproduct formation from fluoxetine varied with reaction conditions. Fluoride was the largest product formed, on a mole basis. Four organofluorinated products formed, one being TFA (Figure 2-17 and 2-18). All products formed in every reaction condition are listed with shifts (ppm) and peak geometry (Table 2-10). TFA was only detected at pH 7 and with the addition of H_2O_2, consistent with data for 4-TFMP. The three other products had similar shifts to the parent fluoxetine compound, suggesting that the products retained the Ar-CF_3 motif. Product A was formed at pH 7 with and without the addition of H_2O_2, Product B was only formed with H_2O_2, and Product C was formed at pH 7. No organic fluorine photoproduct was formed via direct photolysis at pH 10, however Product C was also detected with the addition of SO_3^{-2} at pH 10 (Figure 2-17 and 2-18). This suggests that mechanisms for degradation are pH dependent and that e_{aq}^- may be involved in a different degradation mechanism than direct photolysis.

Table 2-10. ^{19}F-NMR shifts of fluorinated products identified from photolysis of fluoxetine in pH 7, pH 10, 1 mM H_2O_2, or 0.5 mM sulfite. All peaks were singlets (s) in their peak geometry.

Product Name	Shift [ppm]	Peak Geometry
A	-62.8	s
B	-63.0	s
C	-63.1	s
TFA	-77.3	s
Fluoride	-121.5	s

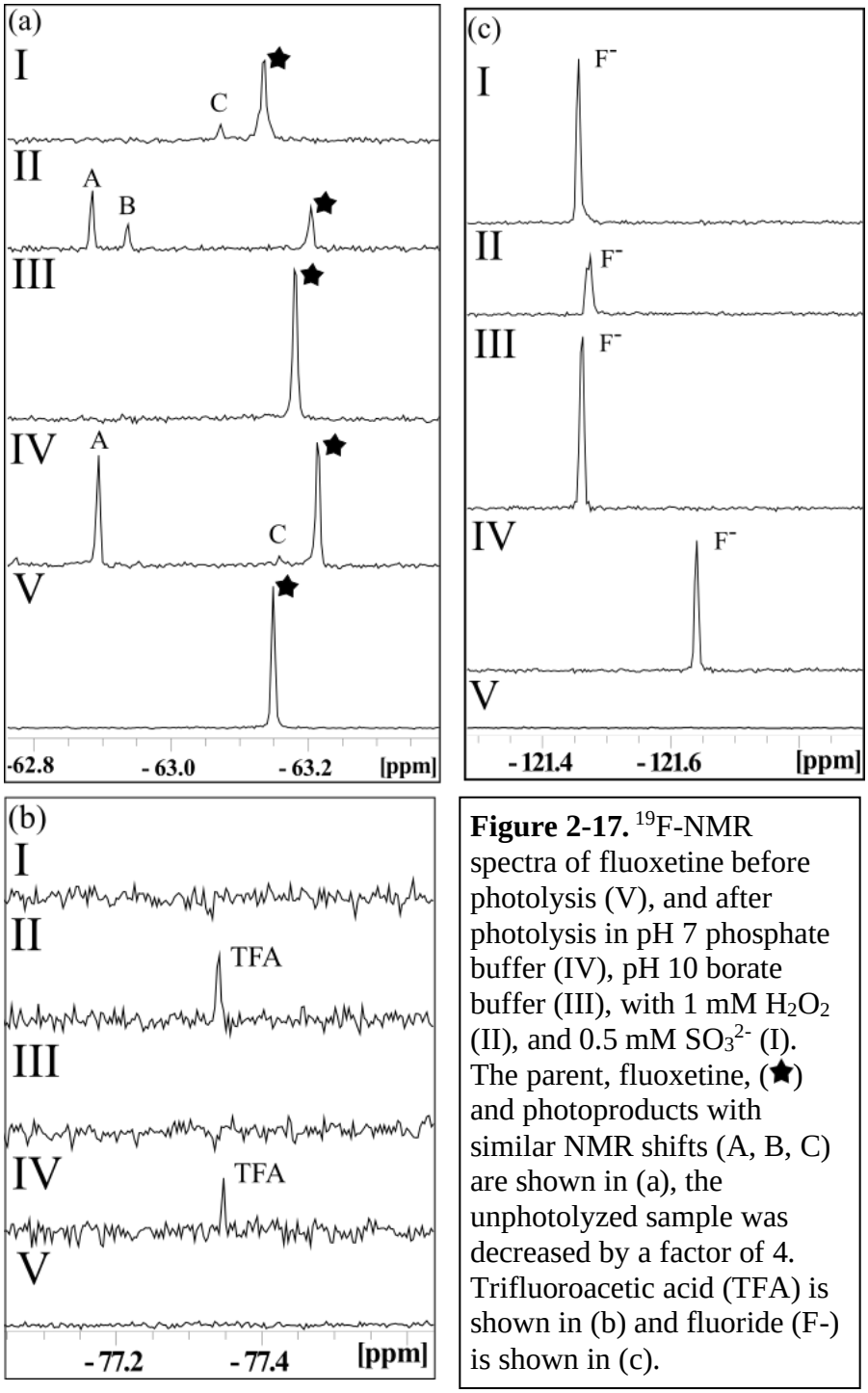

Figure 2-17. ^{19}F-NMR spectra of fluoxetine before photolysis (V), and after photolysis in pH 7 phosphate buffer (IV), pH 10 borate buffer (III), with 1 mM H_2O_2 (II), and 0.5 mM SO_3^{2-} (I). The parent, fluoxetine, (★) and photoproducts with similar NMR shifts (A, B, C) are shown in (a), the unphotolyzed sample was decreased by a factor of 4. Trifluoroacetic acid (TFA) is shown in (b) and fluoride (F-) is shown in (c).

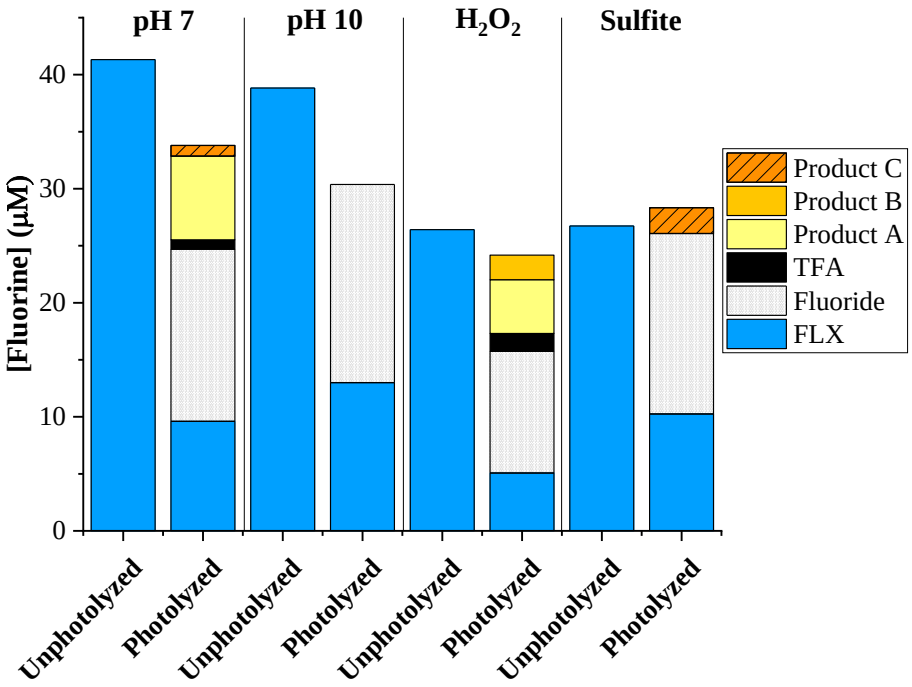

Figure 2-18. Fluorine mass balance as moles of total fluorine for the photolysis of fluoxetine (FLX) at 4 hours for pH 7, 2 hours for pH 10, 10 minutes for 1 mM H_2O_2, and 20 minutes for 0.5 mM SO_3^{2-}.

2.3.4 Photolysis of Sitagliptin

Photolysis and fluorinated photoproduct formation of sitagliptin were studied and comparisons to the Ar-F model compounds were made. The pH dependence of sitagliptin photolysis could not be fully assessed due to a newer lamp apparatus being used for the pH 10 samples. The newer lamp produced faster photolysis rates, thus the increase in rate could be from the lamp or from the increase in pH. The addition of H_2O_2 increased the photolysis rate nearly 145-fold, suggesting that AOPs are effective at increasing photolysis rates of sitagliptin. The addition of SO_3^{-2} in the older lamp apparatus was about 15-fold faster than the direct photolysis rate with the new lamp at pH 10 (Table 2-11), suggesting that ARPs increase the photolysis rate of sitagliptin as well.

Table 2-11. Photolysis rate constants for fluoxetine and sitagliptin using a 450-Watt UV immersion lamp with a 280 nm cutoff value and the corresponding hydrolysis rate constants found with dark control experiments in various aqueous matrices. The pH values were set with phosphate and borate for pH 7 and 10, respectively, and the pH of H_2O_2 and SO_3^{-2} were set to 7 and 10, respectively.

Compound	Matrix	Photolysis k (h^{-1})	Hydrolysis k (h^{-1})
Sitagliptin	pH 7 [b]	$9.6\times10^{-3} \pm 3.8\times10^{-4}$ [a]	1.0E-4 ± 2.1×10^{-4}
	pH 10	$0.03 \pm 1.4\times10^{-3}$	5.7E-4 ± 1.1×10^{-3}
	1 mM H_2O_2 [b]	1.21 ± 0.04	0.02 ± 0.03
	0.5 mM SO_3^{-2} [b]	0.43 ± 0.06	-0.01 ± 0.04

[a] Reported errors are 95% confidence intervals determined by a weighted average of triplicate samples.
[b] Denotes photolysis conducted on an older Hg-vapor lamp

Two NMR signals were found for two of the three Ar-F motifs (-120.5 and -120.6 ppm and -144.8 and -144.9 ppm) as well as the Py-CF_3 motif (-65.3ppm). This could be due to an impurity in the stock solution. Two HPLC peaks were also observed for sitagliptin. Many organic fluorine photoproducts were formed in every matrix. All the fluorinated products were singlets and had shifts close to the parent Py-CF_3 shift (Figure 2-19). All products formed in every reaction condition are listed with shifts (ppm) and peak geometry (Table 2-12). Both NMR peaks for each motif were combined into a single value for a fluorine mass balance (Figure 2-20). Additionally, all the Ar-F NMR peaks were combined, and all the Py-CF_3 NMR peaks were combined (Figure 2-21). This showed the change of concentration for Py-CF_3 and Ar-F motifs while fluoride was forming, ultimately determining what motif was producing the fluoride. The same pattern occurred for each reaction condition except for direct photolysis at pH 10. The Ar-F motifs decreased as the fluoride appeared, the Py-CF_3 motif stayed relatively even throughout photolysis. This suggests that at pH 7, the addition of H_2O_2, and SO_3^{2-}, fluoride is being produced from the Ar-F motifs. Direct photolysis at pH 10, however,

showed something different. The Py-CF_3 motif decreased more than the Ar-F motif, suggesting that the fluoride is also being produced from the Py-CF_3 motif. The difference between the addition of SO_3^{2-} and pH 10 reaction conditions further suggesting that e_{aq}^- provides a different mechanism for degradation than direct photolysis.

Table 2-12. ^{19}F-NMR shifts of fluorinated products identified from photolysis of sitagliptin in pH 7, pH 10, 1 mM H_2O_2, or 0.5 mM sulfite. All peaks were singlets (s) in their peak geometry.

Product Name	Shift [ppm]	Peak Geometry
A	-63.7	s
B	-64.0	s
C	-64.7	s
D	-64.8	s
E	-65.0	s
F	-65.1	s
G	-65.3	s
H	-65.4	s
I	-65.4	s
J	-65.5	s
K	-65.6	s

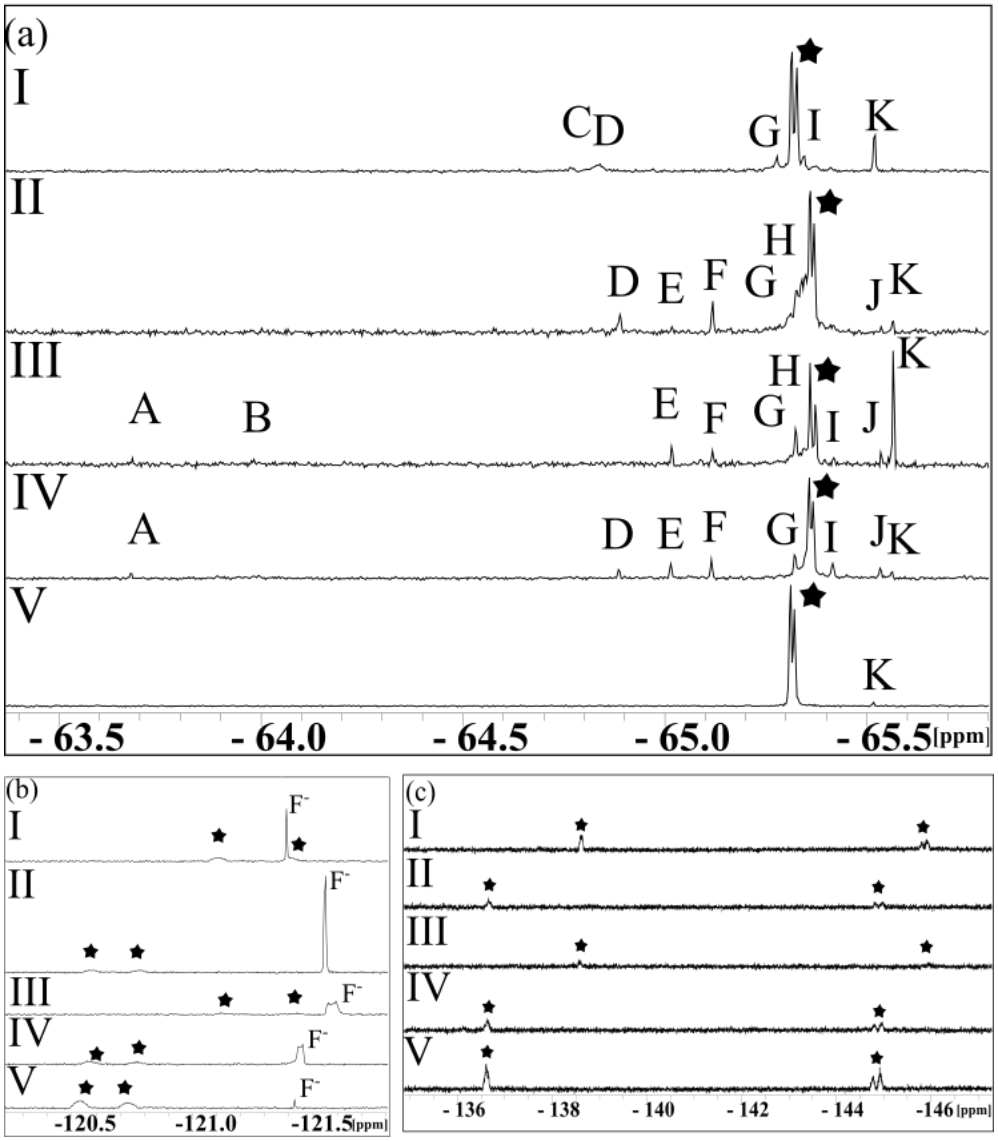

Figure 2-19. ^{19}F-NMR spectra of sitagliptin before photolysis (V) and after photolysis in a pH 7 phosphate buffer (IV), pH 10 borate buffer (III), pH 7 with 2 mM H_2O_2 (II), and pH 10 with 0.5 mM SO_3^{2-} (I). The Py-CF_3 motif from the parent, sitagliptin, (★) is shown in (a) with all of the organofluorined photoproducts (A-K), the unphotolyzed sample was scaled by a factor of 4. Fluoride (F^-) production is shown in (b) along with one of the Ar-F parent compounds signals. The other Ar-F motifs on the parent compounds are shown in (c).

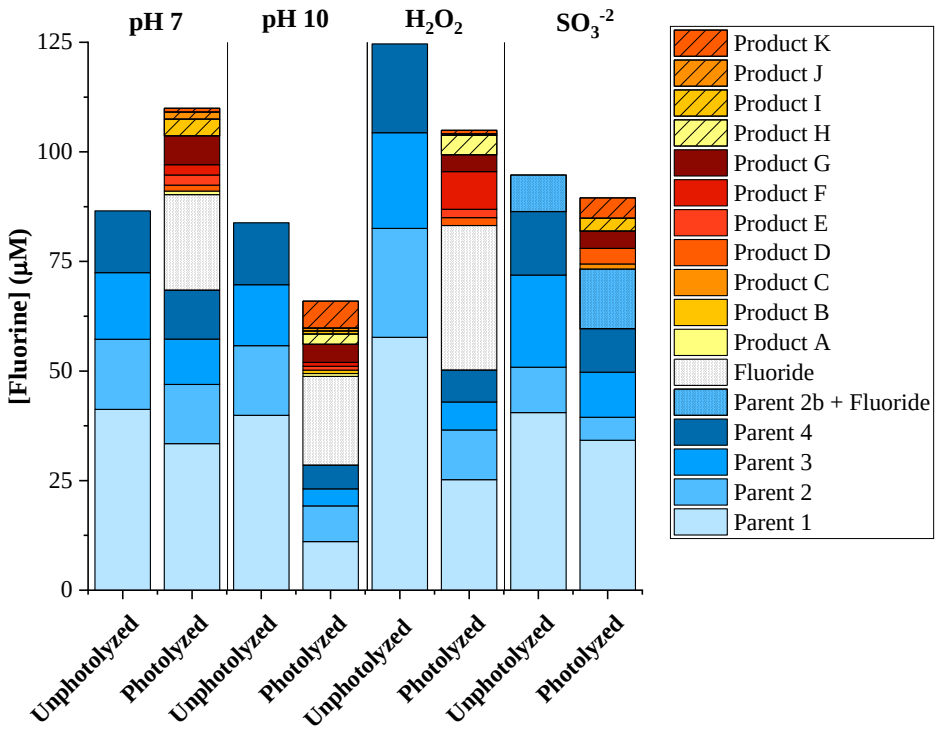

Figure 2-20. Fluorine mass balance as moles of total fluorine for the photolysis of sitagliptin at 96 hours for pH 7, 40 hours for pH 10, 2 hours for 2 mM H_2O_2, and 2 hours for 0.5 mM SO_3^{2-}. Overlap of a parent peak with the fluoride peak occurred in the sulfite sample, thus the total fluorine for both peaks were reported as one.

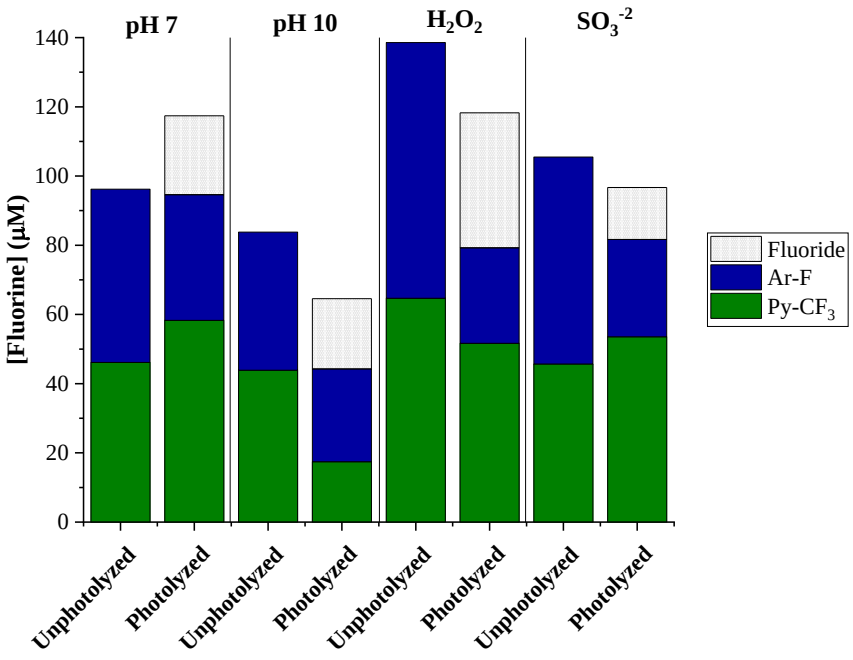

Figure 2-21. Fluorine mass balance as moles of total fluorine for the photolysis of sitagliptin at 96 hours for pH 7, 40 hours for pH 10, 2 hours for 2 mM H_2O_2, and 2 hours for 0.5 mM SO_3^{2-}. Due to the many products formed during photolysis, the shifts were split into either the aryl fluorine (Ar-F) or the trifluoromethyl group on the pyrazole ring (Py-CF_3), including the parent peaks. The fluoride peak for the SO_3^{2-} reaction condition overlapped with an Ar-F parent peak that was relatively small compared to the total moles of fluorine for the fluoride product.

Possible fluorinated photoproducts formed from sitagliptin at pH 7 were identified with LC-MS/MS (Table 2-13). The addition of oxygen occurred in each photoproduct. One photoproduct replaced an Ar-F with a hydroxyl group, providing a route to fluoride mineralization. Others added a hydroxyl group to the ring, replacing a single hydrogen. One product replaced the -NH_2 group with a ketone. Oxidation continued with this product as two more oxygen atoms were added to the aromatic ring as hydroxyl groups, (Figure 2-22). No fluorine was lost from the Py-CF_3 motif, corresponding to what was found via ^{19}F-NMR at pH 7. Due to COVID-19 no additional LC-HRMS analyses could be conducted.

Table 2-13. Sitagliptin fluorinated photoproduct formation in a pH 7 phosphate buffer. Identification of products was done by LC-HRMS and confidence levels were given based on MS isotope ratios and MS/MS fragmentation data (Appendix C).

Elution Time (min)	Name	Structure	Product Confidence
19.7	Parent	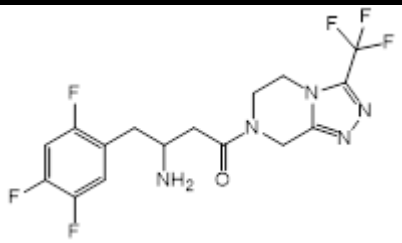	2b
19.4	Product 1	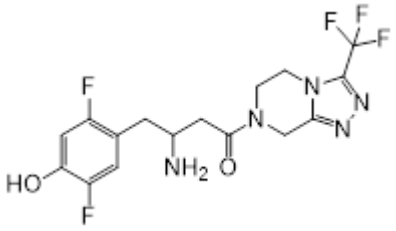	2b
25.5	Product 2	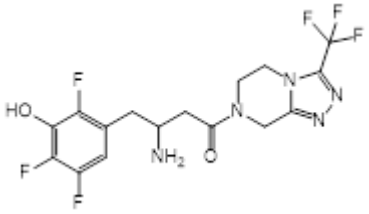	3
27.2	Product 3	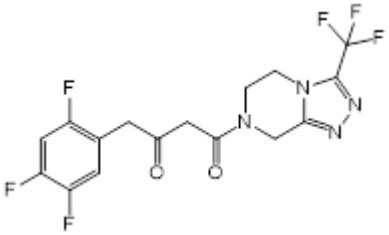	2b
28.5	Product 4	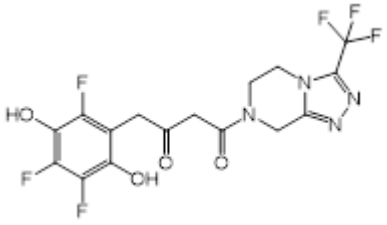	3

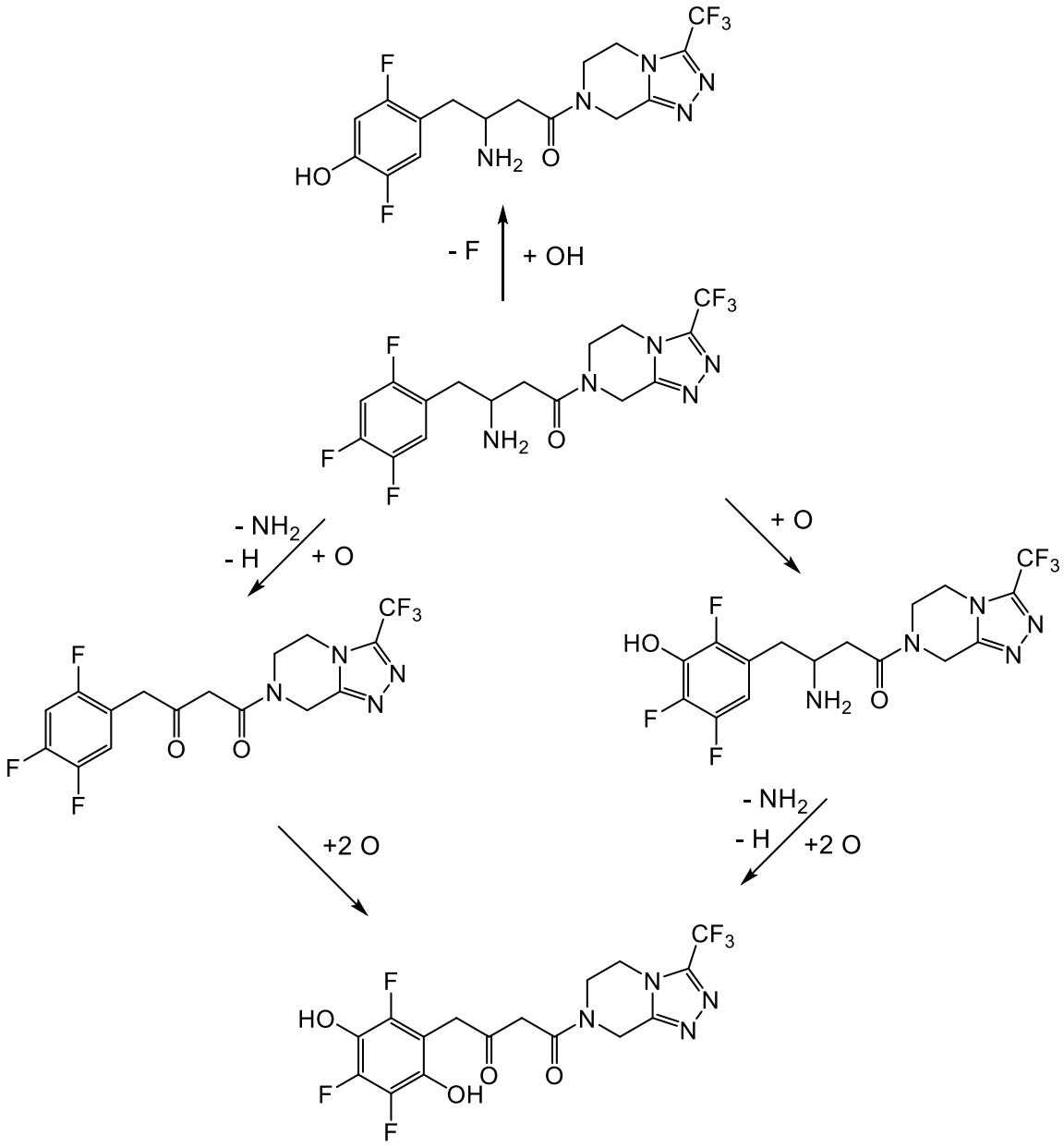

Figure 2-22. Possible scheme for photoproduct formation for sitagliptin at pH 7. The total atoms added and removed are shown next to the arrows.

2.4 Discussion

Photolysis rates of the Ar-CF_3 model compounds varied with the position of the Ar-CF_3 motif relative to the hydroxyl group. There was an observable pH dependence on the photolysis rate for all isomers. Differences in pH dependence are affected by on the position of the motif as well. Under basic conditions, 2- and 3-TFMP degraded rapidly, with the 4-TFMP rate constant being two orders of magnitude slower. At pH 7, 2-TFMP degraded quickest, 3-TFMP was an order of magnitude slower than 2-TFMP, and 4-TFMP was an order of magnitude slower than 3-TFMP. Under acidic conditions, 2- and 3-TFMP had similar rates while 4-TFMP was two orders of magnitude slower than the others. 4-TFMP also had higher hydrolysis rates than the other isomers, as shown in the dark controls. Consistent among the three positions was the increase in rate with the addition of H_2O_2 and no change in rate with the addition of SO_3^{-2}. This indicates that AOPs are effective at increasing the degradation of these motifs but that the Ar-CF_3 motif is resistant to e_{aq}^-.

Although organic fluorine photoproducts are produced by 2- and 4-TFMP, fluoride was the major fluorinated product detected for all three model compounds in every reaction condition. TFA was formed from 4-TFMP at pH 5, 7, and pH 7 with H_2O_2. Products A and C were formed with the addition of H_2O_2 and at pH 5, respectively. These products were close the parent compound and may be an addition of one or more hydroxyl groups onto the aromatic ring. This would explain the additional oxygen required for TFA formation. The pK_a values of 2-, 3, and 4-TFMP are 8.9, 9.0, and 9.4, respectively. This explains the rate constant pH dependence at pH 10. Unique photoproducts are observed when reaction conditions are above the pK_a values of the

TFMPs. Products D and E were observed under basic conditions for 4-TFMP and 2-TFMP, respectively. The hydrolysis of 4-TFMP under basic conditions gave rise to a unique product (Product B). 2-TFMP also formed a product in the Ar-F range (Product F) at pH 5. This product is in the Ar-F range, but Ar-CFH_2 is also in this range and explains the multiplet, or this could also be a fluoride peak as described in Appendix B. 3-TFMP does not show any change in product formation with changes in reaction conditions. The fluorine products formed from the dark controls of 4-TFMP were also pH dependent. At pH 10 with and without the addition of sulfite, fluoride was the main product, but one organofluorine product was produced (Product B). At pH 7, only fluoride formation occurred, while the addition of H_2O_2 produced another organofluorine product (Product A) along with fluoride.

Three conclusions can be made from the Ar-CF_3 motif data. First, for every Ar-CF_3 model compound the addition of SO_3^{2-} did not change the product formation, further suggesting a resistance to e_{aq}^-. Second, unique products were formed under basic, neutral, and acidic conditions, suggesting that pH not only affects the rate, but also the product formation of the Ar-CF_3 motif. Lastly, ortho-, meta-, and para- Ar-CF_3 motifs had different products form under the same reaction conditions, suggesting that product formation is related to position of the motif.

Photolysis rates of the Ar-F model compounds varied with position of the motif relative to the hydroxyl group. There was an observable pH dependence on the photolysis rate for all isomers. The pK_a values of 2-, 3-, and 4-fluorophenol are 8.7, 9.3, and 9.9, respectively. The rate constants were fastest at pH 10 for all isomers. At pH 5 and 7 the

rates were similar for each compound. 4-FP was observably quicker than 2- and 3-FP in all reaction conditions.

Ar-F model compounds formed only fluoride at pH 5, 7, and 10. The fluoride peaks are not clean singlets at pH 7 and 10, which may be due to parameters on the NMR instrument or overlap with an organofluorine photoproduct with a similar NMR shift. The phenolate is abundant when the pH is above the pK_a value of each isomer. It is known that the phenolate can undergo ring condensation as a photodegradation mechanism. Under basic conditions, the Ar-F motif is able to remain on the ring structure.[112] Two degradation mechanisms involving ring-condensation form either fluoride (Figure 2-23) or an organofluorine compound (Figure 2-24). Both mechanisms require formation of the phenolate, either by the fluorine removing the hydroxyl hydrogen, or reaction conditions such that the pH is above the pK_a value. The ^{19}F-NMR spectra of the fluorophenol model compounds only show fluoride formation suggesting that if ring-condensation occurs, it is through the mechanism shown in Figure 2-23.

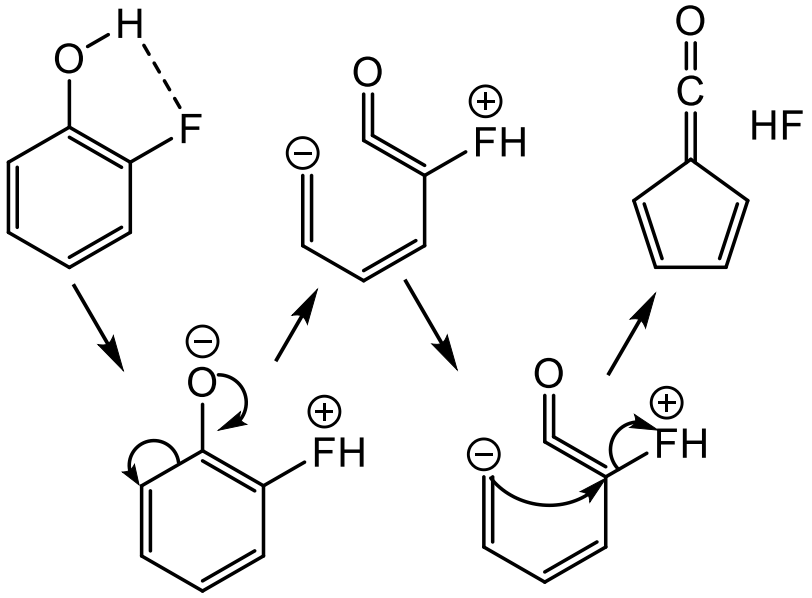

Figure 2-23. Mineralization pathway of 2-FP as proposed by Chatterjee et al. Electron pushing is shown between the transition state.

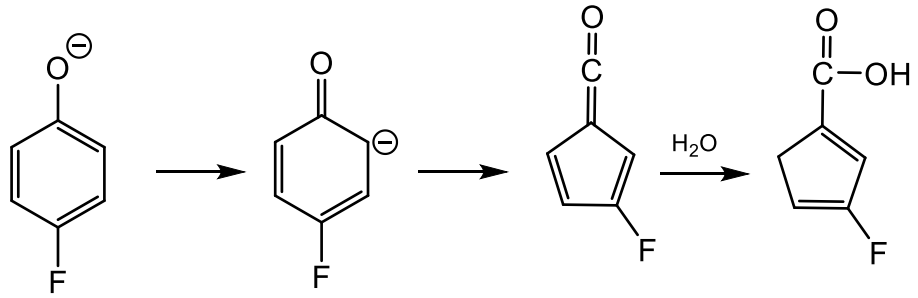

Figure 2-24. Possible photo-contraction of the 6-membered aromatic ring to a 5-memebered ring as proposed by Bole et al.

The *s-cis* conformation of 2-FP is more stable than the *s-trans* conformation by 0.73 kcal/mol due to the hydroxyl hydrogen and fluorine interaction (Figure 2-25).[113] The more stable *s-cis* conformation can be assumed to be more abundant than the *s-trans* conformation. According to the IUPAC standards of bond angle and separation distance, this interaction is a hydrogen bond. Some mechanisms suggest that the hydrogen bond on

the 2-FP molecule creates a pathway for mineralization by creating a 5-memebered ring.[114,115] The fluorine pulls the hydrogen away from the oxygen leading to ring condensation and removal of an HF group (Figure 2-23). This pathway requires an energy input, which photons provide.[114] At a pH value above the pK_a of the fluorophenol, the hydroxyl hydrogen disassociates and is not available for hydrogen bonding with the fluorine.

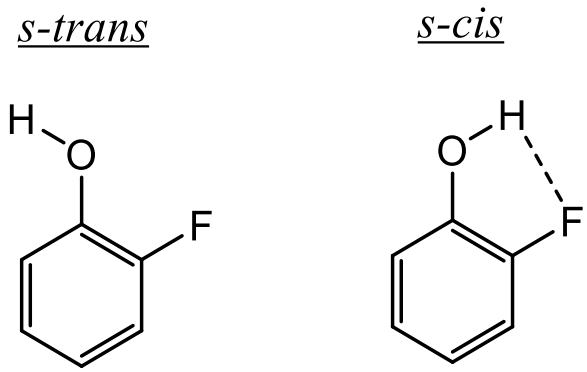

Figure 2-25. Cis and trans conformations of ortho-fluorophenol, showing the hydrogen bond between the alcohol and the fluorine.

The use of Ar-CF_3 motif model compounds to better understand TFA formation allowed insight into the TFA formation from fluoxetine. With 4-TFMP being a proposed intermediate photoproduct for TFA formation, this model compound was subject to photolysis at multiple pH values as well as with H_2O_2 and SO_3^{-2}. TFA was formed at pH 5 and 7, as well as in the presence of H_2O_2, which was added at pH 7. This matches the TFA formation with fluoxetine. No TFA was formed under basic conditions, with and without the addition of SO_3^{2-}. The position of the Ar-CF_3 motif relative to the hydroxyl group was also studied. Ortho- and meta- positions were subject to photolysis in the same reaction conditions as 4-TFMP. No TFA was detected from the photolysis of 2- and 3-TFMP. This suggests that the position of the Ar-CF_3 motif on fluoxetine may be

important for TFA formation. The model compounds are not a perfect representation of fluoxetine. At pH 10, small amounts of organofluorine products are observed from the Ar-CF_3 model compounds, where only fluoride is formed from fluoxetine.

Sitagliptin has a pK_a value of 7.7. At pH 10, the primary amide loses a hydrogen, yielding an overall negative charge. There is no hydroxyl group on the aromatic ring on which the Ar-F motifs reside. Thus, other mineralization mechanisms than what is observed with the fluorophenol model compounds may occur. All reaction conditions shared many of the same products. Only two unique products were identified, Product B at pH 10 and Product C with the addition of H_2O_2. All products were within 2 ppm of each other in the NMR spectrum, suggesting that the unique products formed were similar to the other photoproducts. Direct photolysis at pH 10 showed fluoride formation with the Py-CF_3 motif decreasing. However, at pH 10 with the addition of SO_3^{-2}, the Ar-F motif decreases as fluoride is formed. Suggesting that e_{aq}^- may provide an alternate route of photodegradation at pH 10. All other reaction conditions showed the Ar-F motif decrease as fluoride was formed. Suggesting that fluoride is formed from the Ar-F motif in these reaction conditions.

Chapter 3 Summary and Recommendations

Pharmaceuticals are released into the environment and lead to concerns including toxicity, bioaccumulation, and transformations into other compounds of concern.[28,63,66] The incorporation of fluorinated functional groups in the pharmaceutical industry has consistently increased since its first use in 1955.[10] The change in physiochemical properties of molecules with the addition of fluorine make fluorinated contaminants more resistant to oxidation than their non-fluorinated counterparts, but photolysis is an important degradation pathway of these compounds.[34] Advanced oxidation practices (AOPs) coupled with ultraviolet radiation are used in water treatment facilities for disinfection and are capable of degrading fluorinated compounds as well.[46,57] Advanced reduction practices (ARPs) have been proposed to degrade oxidized contaminants. Although the parent molecule may degrade, the fluorinated photoproducts may also be of concern and required further investigation.

Performing photolysis experiments on every fluorinated pharmaceutical to determine possible harmful photoproducts is challenging. The use of model compounds to study photoproduct formation from fluorine motifs was used to determine possible photoproducts based on the molecular environment surrounding the fluorine atom. 2-, 3-, and 4-TFMP were used to study the Ar-CF_3 motif and 2-,3-, and 4-FP were used to study the Ar-F motif. Photoproduct formation detection by ^{19}F-NMR of fluoxetine (Ar-CF_3) and sitagliptin (Ar-F and Py-CF_3) was performed. TFA is a known photoproduct of fluoxetine and is proposed to form from via a 4-TFMP intermediate.[75] ^{19}F-NMR was able to detect TFA from both fluoxetine and 4-TFMP, confirming that 4-TFMP is the intermediate for TFA production from fluoxetine. TFA was only formed at pH 5 and 7. 2-

and 3-TFMP did not produce TFA as a photoproduct, suggesting that the para position of the Ar-CF_3 motif is important for TFA formation from TFMP.

The three Ar-F model compounds were photolyzed at pH 5, 7, and 10 to better understand product formation of this fluorine motif at varying pH conditions. Fluoride was the only fluorinated photoproduct detected by ^{19}F-NMR at every pH. Even though proposed mechanisms for organic fluorine products exist, only fluoride was observed.[112,114] When pH conditions are above the pK_a of the Ar-F model compounds, the phenolate is abundant. However, no change in fluorinated photoproducts occurred. The Ar-F motifs of sitagliptin also produced fluoride under most reaction conditions, following the trend of the model compounds. At pH 10, however, the Ar-F motifs do not produce fluoride, rather the Py-CF_3 motif does.

Use of ^{19}F-NMR for quantitative determination of fluorinated photoproducts was effective. The large spectral range and 100% abundance of the ^{19}F isotope made it possible to detect all fluorinated photoproducts and parent compounds with good peak separation. The use of an internal standard (HFB) in a capillary tube allowed quantification of ^{19}F-NMR peaks as total moles of fluorine. Mass balance calculations were conducted, and the concentrations of each fluorinated photoproduct were found. Errors were high (~20%), due to the NMR method not being optimized for unknown photoproducts. Due to the nature of NMR, the shift of each peak provided useful information on the structure and motif of the photoproduct. When the product peaks were near the parent peaks, it could be assumed that the products had a similar fluorine motif as the parent. While if the peak shifted dramatically, the assumption that the fluorine motif changed from the parent compound could be made. The majority of the products

had similar shifts to the parent compounds, suggesting that the organofluorine photoproducts retained their fluorine motifs.

Continuing LC-HRMS analyses on the photolyzed samples of the compounds studied need to be done to determine structures of photoproducts. Additionally, more model compounds need to be studied to look at other fluorine motifs, such as Py-CF_3. Computational prediction of NMR shifts for potentioal products would also be valuable information for the identifications of observed products in the NMR spectra. More pharmaceuticals and agrochemicals with various fluorine motifs need to be studied to determine fluorinated photoproduct formation and relate them to model compounds. Highly fluorinated MRI contrast agents also need to be photolyzed in various reaction conditions, especially with ARPs.

Bibliography

(1) Harper, D. B.; O'Hagan, O. The Fluorinated Natural Products. *Nat. Prod. Rep.* **1994**, *11*, 123–133. https://doi.org/10.1039/np9941100123.

(2) Eisenhauer, A.; Geochemie, I. Natural CF4 and SF6 on Earth. *Geophys. Res. Lett.* **1998**, *25* (13), 2401–2404.

(3) Gribble, G. W. Naturally Occurring Organofluorines. *The Handbook of Environmental Chemistry*; 2006; Vol. 3, pp 121–136. https://doi.org/10.1007/10721878_5.

(4) Symonds, R. B.; Rose, W. I.; Reed, M. H. Contibution of Cl- and F-Bearing Gasses to the Atomosphere by Volcanoes. *Nature* **1988**, *334* (4), 415–418.

(5) Stoiber, R.; Leggett, D.; Jenkins, T.; Murrmann, R.; Rose Jr., W. Organic Compounds in Volcanic Gas from Santiaguito Volcano, Guatemala. *Geol. Soc. Am. Bull.* **1971**, *82* (August), 2299–2302.

(6) Marais, J. S. C. Monofluoroacetic Acid, the Toxic Principle of " Gifblaar " Dichapetalum Cymosum. *Ondersterpoort J. Verterinary Sci. Anim. Ind.* **1944**, *20* (1), 67–73.

(7) Saunders, B. *Some Aspects of the Chemistry and Toxic Action of Organic Compounds Containing Phosphorous and Fluorine*; 1957.

(8) Murphy, C. D.; Schaffrath, C.; O'Hagan, D. Fluorinated Natural Products: The Biosynthesis of Fluoroacetate and 4-Fluorothreonine in Streptomyces Cattleya. *Chemosphere* **2003**, *52* (2), 455–461. https://doi.org/10.1016/S0045-6535(03)00191-7.

(9) Mei, H.; Han, J.; Fustero, S.; Medio-simon, M. Fluorine-Containing Drugs Approved by the FDA in 2018. **2019**, 11797–11819. https://doi.org/10.1002/chem.201901840.

(10) Zhou, Y.; Wang, J.; Gu, Z.; Wang, S.; Zhu, W.; Acenã, J. L.; Soloshonok, V. A.; Izawa, K.; Liu, H. Next Generation of Fluorine-Containing Pharmaceuticals, Compounds Currently in Phase II-III Clinical Trials of Major Pharmaceutical Companies: New Structural Trends and Therapeutic Areas. *Chem. Rev.* **2016**, *116* (2), 422–518. https://doi.org/10.1021/acs.chemrev.5b00392.

(11) Müller, K.; Faeh, C.; Diederich, F. Fluorine in Pharmaceuticals: Looking beyond Intuition. *Science.* **2007**, *317* (5846), 1881–1886. https://doi.org/10.1126/science.1131943.

(12) Laise, B. Y. E. The Lipitor Dilemma. *Wall Str. J. Mag. Pers. Bus.* **2003**, No.

NOVEMBER.

(13) Wenthur, C. J.; Bennett, M. R.; Lindsley, C. W. Classics in Chemical Neuroscience: Fluoxetine (Prozac). *ACS Chem. Neurosci.* **2014**, *5*, 14–23.

(14) Braun, M.; Eicher, J. The Fluorine Atom in Health Care and Agrochemical Applications: A Contribution to Life Science. In *Modern Synthesis Processes and Reactivity of Fluorinated Compounds: Progress in Fluorine Science*; Elsevier Inc., 2016; pp 7–25. https://doi.org/10.1016/B978-0-12-803740-9.00002-0.

(15) Jeschke, P. The Unique Role of Fluorine in the Design of Active Ingredients for Modern Crop Protection. *ChemBioChem* **2004**, *5*, 570–589. https://doi.org/10.1002/cbic.200300833.

(16) Maienfisch, P.; Hall, R. G. The Importance of Fluorine in the Life Science Industry. *Fluor. Life Sci. Ind.* **2004**, *58* (3), 93–99.

(17) Park, B. K.; Kitteringham, N. R.; Neill, P. M. O. METABOLISM OF FLUORINE -CONTAINING DRUGS. *Annu. Rev. Pharmacol. Toxicol.* **2001**, *41*, 443–470.

(18) Stabel, A.; Dasaradhi, L.; Hagan, D. O.; Rabe, J. P. Scanning Tunneling Microscopy Imaging of Single Fluorine Atom Substitution in Stearic Acid. *Langmuir* **1995**, *11*, 1427–1430. https://doi.org/10.1021/la00005a003.

(19) Meanwell, N. A. Fluorine and Fluorinated Motifs in the Design and Application of Bioisosteres for Drug Design. *J. Med. Chem.* **2018**, *61*, 5822–5880. https://doi.org/10.1021/acs.jmedchem.7b01788.

(20) Shaughnessy, M. J.; Harsanyi, A.; Li, J.; Bright, T.; Murphy, C. D. Targeted Fluorination of a Nonsteroidal Anti-Inflammatory Drug to Prolong Metabolic Half-Life. *ChemMedChem* **2014**, *9*, 733–736. https://doi.org/10.1002/cmdc.201300490.

(21) Swallow, S. Fluorine in Medicinal Chemistry. In *Progress in Medicinal Chemistry*; Elsevier B.V., 2015; Vol. 54, pp 65–133. https://doi.org/10.1016/bs.pmch.2014.11.001.

(22) Bohm, H.; Banner, D.; Bendels, S.; Kansy, M.; Kuhn, B.; Klaus, M.; Obst-sander, U.; Stahl, M. Fluorine in Medicinal Chemistry. *ChemBioChem* **2004**, *5*, 637–643. https://doi.org/10.1002/cbic.200301023.

(23) Swain, C.; Rupniak, N. M. J. Progress in the Development of Neurokinin Antagonists. *Annu. Rep. Med. Chem.* **1999**, *34*, 51–60.

(24) Niel, M. B. Van; Collins, I.; Beer, M. S.; Broughton, H. B.; Cheng, S. K. F.; Goodacre, S. C.; Heald, A.; Locker, K. L.; Macleod, A. M.; Morrison, D.; Moyes,

C. R.; Connor, D. O.; Pike, A.; Rowley, M.; Russell, M. G. N.; Sohal, B.; Stanton, J. A.; Thomas, S.; Verrier, H.; Watt, A. P. Fluorination of 3-3-(Piperidin-1-Yl)Propyl)Indoles and 3-(3-(Piperazin-1-Yl)Propyl)Indoles Gives Selective Human 5-HT 1D Receptor Ligands with Improved Pharmacokinetic Profiles. *J. Med. Chem.* **1999**, *42*, 2087–2104. https://doi.org/10.1021/jm981133m.

(25) Clayden, J. Fluorine and Amide Groups Together at Last. *Nature* **2019**, *573*, 37–38.

(26) Martin, J.; Smithwick, M.; Braune, B.; Hoekstra, P.; Muir, D.; Mabury, S. Identification of Long-Chain Perfluorinated Acids in Biota from the Canadian Arctic. *Environ. Sci. Technol.* **2004**, *38*, 373–380.

(27) Yeung, L. W. Y.; Silva, A. O. De; Loi, E. I. H.; Marvin, C. H.; Taniyasu, S.; Yamashita, N.; Mabury, S. A.; Muir, D. C. G.; Lam, P. K. S. Perfluoroalkyl Substances and Extractable Organic Fluorine in Surface Sediments and Cores from Lake Ontario. *Environ. Int.* **2013**, *59*, 389–397. https://doi.org/10.1016/j.envint.2013.06.026.

(28) Logarinho, F.; Rosado, T.; Lourenco, C.; Barroso, M.; Araujo, A. R. T. S.; Gallardo, E. Determination of Antipsychotic Drugs in Hospital and Wastewater Treatment Plant Samples by Gas Chromatography / Tandem Mass. *J. Chromatogr. B* **2016**, *1038*, 127–135. https://doi.org/10.1016/j.jchromb.2016.10.031.

(29) Patel, M.; Kumar, R.; Kishor, K.; Mlsna, T.; Pittman, C. U.; Mohan, D. Pharmaceuticals of Emerging Concern in Aquatic Systems: Chemistry, Occurrence, Effects, and Removal Methods. *Chem. Rev.* **2019**, *119*, 3510–3673. https://doi.org/10.1021/acs.chemrev.8b00299.

(30) Azuma, T.; Arima, N.; Tsukada, A.; Hirami, S.; Matsuoka, R.; Moriwake, R.; Ishiuchi, H.; Inoyama, T.; Teranishi, Y.; Yamaoka, M.; Mino, Y.; Hayashi, T.; Fujita, Y.; Masada, M. Science of the Total Environment Detection of Pharmaceuticals and Phytochemicals Together with Their Metabolites in Hospital Effluents in Japan , and Their Contribution to Sewage Treatment Plant in Effluents. *Sci. Total Environ.* **2016**, *548–549*, 189–197. https://doi.org/10.1016/j.scitotenv.2015.12.157.

(31) Lin, A. Y.; Yu, T.; Lin, C. Pharmaceutical Contamination in Residential, Industrial, and Agricultural Waste Streams: Risk to Aqueous Environments in Taiwan. *Chemosphere* **2008**, *74*, 131–141. https://doi.org/10.1016/j.chemosphere.2008.08.027.

(32) Wightwick, A. M.; Duyen Bui, A.; Zhang, P.; Rose, G.; Allinson, M.; Myers, J.;

Richman, S.; Menzies, N.; Pettigrove, V.; Allinson, G. Environmental Fate of Fungicides in Surface Waters of a Horticultural-Production Catchment in Southeastern Australia. *Arch. Environ. Contam. Toxicol.* **2012**, *62*, 380–390. https://doi.org/10.1007/s00244-011-9710-y.

(33) Rice, P.; Rice, P.; Arthur, E.; Barefoot, A. Advances in Pesticide Environmental Fate and Exposure Assessments. *J. Agric. Food Chem.* **2007**, *55*, 5367–5376. https://doi.org/10.1021/jf063764s.

(34) Gimenez, D.; Andreu, C.; del Olmo, M.; Varea, T.; Diaz, D.; Asensio, G. The Introduction of Fluorine Atoms or Trifluoromethyl Groups in Short Cationic Peptides Enhances Their Antimicrobial Activity. *Bioorg. Med. Chem.* **2006**, *14*, 6971–6978. https://doi.org/10.1016/j.bmc.2006.06.027.

(35) Schwarzenbach, R. P.; Gschwend, P. M.; Imboden, D. M. *Environmental Organic Chemistry*, Third edit.; Wiley: Hoboken, New Jersey, 2017.

(36) Litter, M. I. Introduction to Photochemical Advanced Oxidation Processes for Water Treatment. In *Environmental Photochemistry Part II*; 2005; Vol. 2, pp 325–366. https://doi.org/10.1007/b138188.

(37) Rosario-Ortiz, F. L.; Canonica, S. Probe Compounds to Assess the Photochemical Activity of Dissolved Organic Matter. *Environ. Sci. Technol.* **2016**, *50*, 12532–12547. https://doi.org/10.1021/acs.est.6b02776.

(38) McNeill, K.; Canonica, S. Triplet State Dissolved Organic Matter in Aquatic Photochemistry: Reaction Mechanisms, Substrate Scope, and Photophysical Properties. *Environ. Sci. Process. Impacts* **2016**, *18* (11), 1381–1399. https://doi.org/10.1039/C6EM00408C.

(39) Erickson, P. R.; Moor, K. J.; Werner, J.; Latch, D. E.; Arnold, W. A.; Mcneill, K. Singlet Oxygen Phosphorescence as a Probe for Triplet-State Dissolved Organic Matter Reactivity. *Environ. Sci. Technol.* **2018**, *52*, 9170–9178. https://doi.org/10.1021/acs.est.8b02379.

(40) Cote, C. D.; Schneider, S. R.; Lyu, M.; Gao, S.; Gan, L.; Holod, A. J.; Chou, T. H. H.; Styler, S. A. Photochemical Production of Singlet Oxygen by Urban Road Dust. *Environ. Sci. Technol. Lett.* **2018**, *5*, 92–97. https://doi.org/10.1021/acs.estlett.7b00533.

(41) Allen, J. M.; Gossett, C. J.; Allen, S. K. Photochemical Formation of Singlet Molecular Oxygen in Illuminated Aqueous Solutions of Several Commercially Available Sunscreen Active Ingredients. *Chem. Reseach Toxicol.* **1996**, *9*, 605–609. https://doi.org/10.1021/tx950197m.

(42) Haag, W. R.; Hoigné, J. Singlet Oxygen in Surface Waters. 3. Photochemical Formation and Steady-State Concentrations in Various Types of Waters. *Environ. Sci. Technol.* **1986**, *20*, 341–348. https://doi.org/10.1021/es00146a005.

(43) Buxton, G. V; Greenstock, C. L.; Helman, W. P.; Ross, A. B.; Buxton, G. V; Greenstock, C. L.; Helman, P.; Ross, A. B. Critical Review of Rate Constants for Reactions of Hydrated Electrons , Hydrogen Atoms and Hydroxyl Radicals (· OH / · O − in Aqueous Solution. **2011**, *513* (1988).

(44) Zepp, R. G.; Faust, B. C.; Hoigné, J. Hydroxyl Radical Formation in Aqueous Reactions (PH 3-8) of Hydrogen Peroxide: The Photo-Fenton Reaction Iron (II) with Hydrogen Peroxide: The Photo-Fenton Reaction. *Environ. Sci. Technol.* **1992**, *26*, 313–319. https://doi.org/10.1021/es00026a011.

(45) France, J. L.; King, M. D.; Lee-Taylor, J. Hydroxyl (OH) Radical Production Rates in Snowpacks from Photolysis of Hydrogen Peroxide (H2O2) and Nitrate (NO3-). *Atmos. Environ.* **2007**, *41*, 5502–5509. https://doi.org/10.1016/j.atmosenv.2007.03.056.

(46) Barbusi, K.; Filipek, K. Use of Fenton's Reagent for Removal of Pesticides from Industrial Wastewater. *Polish J. Environ. Stud.* **2001**, *10* (4), 207–212.

(47) Cui, J.; Gao, P.; Deng, Y. Destruction of Per- and Polyfluoroalkyl Substances (PFAS) with Advanced Reduction Processes (ARPs): A Critical Review. **2020**. https://doi.org/10.1021/acs.est.9b05565.

(48) Vellanki, B. P.; Abdel-wahab, A.; Batchelor, B. Advanced Reduction Processes: A New Class of Treatment Processes. *Environ. Eng. Sci.* **2013**, *30* (5), 264–271. https://doi.org/10.1089/ees.2012.0273.

(49) Hart, E. J.; Gordon, S.; Thomas, J. K. Rate Constants of Hydrated Electron Reactions with Organic Compounds. *J. Phys. Chem.* **1964**, *68* (6), 1271–1274. https://doi.org/10.1021/j100788a001.

(50) Chawla, O. P.; Arthur, N. L.; Fessenden, R. W. An Electron Spin Resonance Study of the Photolysis of Aqueous Sulfite Solutions1. **1973**, *1245* (1), 772–776. https://doi.org/10.1021/j100625a008.

(51) Deister, U.; Warneck, P.; Otto-hahn-instituí, M. C.; May, F. R. G. R. Photooxidation of S032- in Aqueous Solution. **1990**, No. 17, 2191–2198. https://doi.org/10.1021/j100368a084.

(52) Dogliotti, L.; Hayon, E. Flash Photolysis Study of Sulfite, Thiocyanate, and Thiosulfate Ions in Solution. **1967**, *1074* (1951), 1800–1807. https://doi.org/10.1021/j100851a073.

(53) Fischer, M.; Warneck, P. Photodecomposition and Photooxidation of Hydrogen Sulfite in Aqueous Solution. **1996**, *3654* (95), 15111–15117. https://doi.org/10.1021/jp953236b.

(54) Wilf, E. H. A. T. J. Electronic Spectra, Photochemistry, and Autoxidation Mechanism of the Sulfite-Bisulfite-Pyrosulfite Systems. SO2-, SO3-, SO4-, and SO5- Radicals. **1968**, *4* (5), 47–57. https://doi.org/10.1021/ja00756a009.

(55) Buxton, G. V.; Greenstock, C. L.; Helman, W. P.; Ross, A. B. Critical Review of Rate Constants for Reactions of Hydrated Electrons, Hydrogen Atoms and Hydroxyl Radicals (•OH/•O^-) In Aqueous Solution. *J. Phys. Chem. Ref. Data* **1988**, *17* (2), 513–886. https://doi.org/10.1063/1.555805.

(56) Schymanski, E. L.; Jeon, J.; Gulde, R.; Fenner, K.; Ruff, M.; Singer, H. P.; Hollender, J. Identifying Small Molecules via High Resolution Mass Spectrometry: Communicating Confidence. *Environ. Sci. Technol.* **2014**, *48* (4), 2097–2098. https://doi.org/10.1021/es5002105.

(57) Cui, J.; Gao, P.; Deng, Y. Destruction of Per- and Polyfluoroalkyl Substances (PFAS) with Advanced Reduction Processes (ARPs): A Critical Review. *Environ. Sci. Technol.* **2020**, *54* (7), 3752–3766. https://doi.org/10.1021/acs.est.9b05565.

(58) Loge, F. J.; Emerick, R. W.; Heath, M.; Jacangelo, J.; Tchobanoglous, G.; Darby, J. L. Ultraviolet Disinfection of Secondary Wastewater Effluents: Prediction of Performance and Design. *Water Environ. Res.* **1996**, *68* (5), 900–916. https://doi.org/10.2175/106143096X127910.

(59) Hallmich, C.; Gehr, R. Effect of Pre- and Post-UV Disinfection Conditions on Photoreactivation of Fecal Coliforms in Wastewater Effluents. *Water Res.* **2010**, *44* (9), 2885–2893. https://doi.org/10.1016/j.watres.2010.02.003.

(60) Deng, Y.; Zhao, R. Advanced Oxidation Processes (AOPs) in Wastewater Treatment. *Curr. Pollut. Reports* **2015**, *1*, 167–176. https://doi.org/10.1007/s40726-015-0015-z.

(61) Wallace, D.; Hand, L.; Oliver, R. THE ROLE OF INDIRECT PHOTOLYSIS IN LIMITING THE PERSISTENCE OF CROP PROTECTION PRODUCTS IN SURFACE WATERS. *Environ. Toxicol. Chem.* **2010**, *29* (3), 575–581. https://doi.org/10.1002/etc.65.

(62) Kümmerer, K. Resistance in the Environment. *J. Antimicrob. Chemother.* **2004**, *54* (2), 311–320. https://doi.org/10.1093/jac/dkh325.

(63) Schwartz, T.; Kohnen, W.; Jansen, B.; Obst, U. Detection of Antibiotic-Resistant Bacteria and Their Resistance Genes in Wastewater, Surface Water, and Drinking

Water Biofilms. *FEMS Microbiol. Ecol.* **2003**, *43* (3), 325–335. https://doi.org/10.1016/S0168-6496(02)00444-0.

(64) Walker, R. D. The Use of Fluoroquinolones for Companion Animal Antimicrobial Therapy. *Aust. Vet. J.* **2000**, *78* (2), 84–90.

(65) Howard, P. H.; Muir, D. C. G. Identifying New Persistent and Bioaccumulative Organics among Chemicals in Commerce II: Pharmaceuticals. *Environ. Sci. Technol.* **2011**, *45* (16), 6938–6946. https://doi.org/10.1021/es201196x.

(66) Muir, D.; Simmons, D.; Wang, X.; Peart, T.; Villella, M.; Miller, J.; Sherry, J. Bioaccumulation of Pharmaceuticals and Personal Care Product Chemicals in Fish Exposed to Wastewater Effluent in an Urban Wetland. *Sci. Rep.* **2017**, *7* (1), 1–11. https://doi.org/10.1038/s41598-017-15462-x.

(67) Xie, Z.; Lu, G.; Yan, Z.; Liu, J.; Wang, P.; Wang, Y. Bioaccumulation and Trophic Transfer of Pharmaceuticals in Food Webs from a Large Freshwater Lake. *Environ. Pollut.* **2017**, *222*, 356–366. https://doi.org/10.1016/j.envpol.2016.12.026.

(68) Konwick, B. J.; Garrison, A. W.; Black, M. C.; Avants, J. K.; Fisk, A. T. Bioaccumulation, Biotransformation, and Metabolite Formation of Fipronil and Chiral Legacy Pesticides in Rainbow Trout. *Environ. Sci. Technol.* **2006**, *40* (9), 2930–2936. https://doi.org/10.1021/es0600678.

(69) Kinney, C. A.; Furlong, E. T.; Kolpin, D. W.; Burkhardt, M. R.; Zaugg, S. D.; Werner, S. L.; Bossio, J. P.; Benotti, M. J. Bioaccumulation of Pharmaceuticals and Other Anthropogenic Waste Indicators in Earthworms from Agricultural Soil Amended with Biosolid or Swine Manure. *Environ. Sci. Technol.* **2008**, *42* (6), 1863–1870. https://doi.org/10.1021/es702304c.

(70) Reinhold, D. M.; Saunders, F. M. Phytoremediation of Fluorinated Agrochemicals by Duckweed. *Am. Soc. Agric. Biol. Eng.* **2006**, *49* (6), 2077–2084.

(71) Herrera, S.; Santiago-morales, J. Oxidative and Photochemical Processes for the Removal of Galaxolide and Tonalide from Wastewater. **2012**, *6*. https://doi.org/10.1016/j.watres.2012.05.051.

(72) Scheurer, M.; Nodler, K.; Freeling, F.; Janda, J.; Happel, O.; Riegel, M.; Muller, U.; Storck, F.; Fleif, M.; Lange, F.; Brunsch, A.; Brauch, H.-J. Small, Mobile, Persistent: Trifluoroacetate in the Water Cyclee- Overlooked Sources, Pathways, and Consequences for Drinking Water Supply. *Water Res.* **2017**, *126*, 460–471. https://doi.org/10.1016/j.watres.2017.09.045.

(73) Boutonnet, J. C.; Bingham, P.; Calamari, D.; Rooij, C. de; Franklin, J.; Kawano,

T.; Libre, J.-M.; McCul-loch, A.; Malinverno, G.; Odom, J. M.; Rusch, G. M.; Smythe, K.; Sobolev, I.; Thompson, R.; Tiedje, J. M. Environmental Risk Assessment of Trifluoroacetic Acid. *Hum. Ecol. Risk Assess. An Int. J.* **1999**, *5* (1), 59–124. https://doi.org/10.1080/10807039991289644.

(74) Kim, B. R.; Suidan, M. T.; Wallington, T. J.; Du, X. Biodegradability of Trifluoroacetic Acid. *Environ. Eng. Sci.* **2000**, *17* (6), 337–342.

(75) Tisler, S.; Zindler, F.; Freeling, F.; Nödler, K.; Toelgyesi, L.; Braunbeck, T.; Zwiener, C. Transformation Products of Fluoxetine Formed by Photodegradation in Water and Biodegradation in Zebrafish Embryos (Danio Rerio). *Environ. Sci. Technol.* **2019**, *53* (13), 7400–7409. https://doi.org/10.1021/acs.est.9b00789.

(76) Lam, M. W.; Young, C. J.; Mabury, S. A. Aqueous Photochemical Reaction Kinetics and Transformations of Fluoxetine. *Environ. Sci. Technol.* **2005**, *39* (2), 513–522. https://doi.org/10.1021/es0494757.

(77) Razavi, B.; Ben Abdelmelek, S.; Song, W.; O'Shea, K. E.; Cooper, W. J. Photochemical Fate of Atorvastatin (Lipitor) in Simulated Natural Waters. *Water Res.* **2011**, *45* (2), 625–631. https://doi.org/10.1016/j.watres.2010.08.012.

(78) Adachi, F.; Yamamoto, A.; Takakura, K. I.; Kawahara, R. Occurrence of Fluoroquinolones and Fluoroquinolone-Resistance Genes in the Aquatic Environment. *Sci. Total Environ.* **2013**, *444*, 508–514. https://doi.org/10.1016/j.scitotenv.2012.11.077.

(79) Yuan, F.; Hu, C.; Hu, X.; Wei, D.; Chen, Y.; Qu, J. Photodegradation and Toxicity Changes of Antibiotics in UV and UV/H2O2 Process. *J. Hazard. Mater.* **2011**, *185* (2), 1256–1263. https://doi.org/https://doi.org/10.1016/j.jhazmat.2010.10.040.

(80) Sayed, M.; Ismail, M.; Khan, S.; Tabassum, S.; Khan, H. M. Degradation of Ciprofloxacin in Water by Advanced Oxidation Process: Kinetics Study, Influencing Parameters and Degradation Pathways. *Environ. Technol. (United Kingdom)* **2016**, *37* (5), 590–602. https://doi.org/10.1080/09593330.2015.1075597.

(81) Paul, T.; Dodd, M. C.; Strathmann, T. J. Photolytic and Photocatalytic Decomposition of Aqueous Ciprofloxacin: Transformation Products and Residual Antibacterial Activity. *Water Res.* **2010**, *44* (10), 3121–3132. https://doi.org/10.1016/j.watres.2010.03.002.

(82) Golet, E.; Xifra, I.; Siegrist, H.; Alder, A.; Giger, W. Environmental Exposure Assessment of Fluoroquinolone Antibacterial Agents from Sewage to Soil. *Environ. Sci. Technol.* **2003**, *37* (15), 3243–3249.

https://doi.org/10.1021/es0264448.

(83) Holland, G. N.; Bottomley, P. A.; Hinshaw, W. S. 19F Magnetic Resonance Imaging. *J. Magn. Reson.* **1977**, *28*, 133–136.

(84) Tirotta, I.; Dichiarante, V.; Pigliacelli, C.; Cavallo, G.; Terraneo, G.; Bombelli, F. B.; Metrangolo, P.; Resnati, G. F Magnetic Resonance Imaging (MRI): From Design of Materials to Clinical Applications. *Chem. Rev.* **2015**, *115*, 1106–1129. https://doi.org/10.1021/cr500286d.

(85) Díaz-López, R.; Tsapis, N.; Fattal, E. Liquid Perfluorocarbons as Contrast Agents for Ultrasonography and 19F-MRI. *Pharm. Res.* **2010**, *27* (1), 1–16. https://doi.org/10.1007/s11095-009-0001-5.

(86) Neubauer, A. M.; Caruthers, S. D.; Hockett, F. D.; Cyrus, T.; Robertson, J. D.; Allen, J. S.; Williams, T. D.; Fuhrhop, R. W.; Lanza, G. M.; Wickline, S. A. Fluorine Cardiovascular Magnetic Resonance Angiography in Vivo at 1.5 T with Perfluorocarbon Nanoparticle Contrast Agents. *J. Cardiovasc. Magn. Reson.* **2007**, *9* (3), 565–573. https://doi.org/10.1080/10976640600945481.

(87) Bloembergen, N.; Purcell, E. M.; Pound, R. V. Relaxation Effects in Nuclear Magnetic Resonance Absorption. *Phys. Rev.* **1947**, *73* (7), 679–712.

(88) Meier, B. H.; Bachmann, P.; Ernst, R. R. Investigation of Exchange Processes by Two-Dimensional NMR Spectroscopy. *J. Chem. Phys.* **1979**, *71*, 4546–4553.

(89) Bax, A.; Ferretti, J. A.; Nashed, N. Complete Proton and Carbon-13 NMR Assignment of Complex Polycyclic Aromatic Hydrocarbons. *J. Org. Chem.* **1985**, *50* (17), 3029–3034. https://doi.org/10.1021/jo00217a001.

(90) Vulpetti, A.; Dalvit, C. Fluorine Local Environment: From Screening to Drug Design. *Drug Discov. Today* **2012**, *17* (15–16), 739–746. https://doi.org/10.1016/j.drudis.2012.03.014.

(91) Okaru, A. O.; Brunner, T. S.; Ackermann, S. M.; Kuballa, T.; Walch, S. G.; Kohl-Himmelseher, M.; Lachenmeier, D. W. Application of ^{19} F NMR Spectroscopy for Content Determination of Fluorinated Pharmaceuticals. *J. Anal. Methods Chem.* **2017**, *2017*, 1–7. https://doi.org/10.1155/2017/9206297.

(92) Bhattacharyya, R.; Kumar, A. A Fast Method for the Measurement of Long Spin–Lattice Relaxation Times by Single Scan Inversion Recovery Experiment. *Chem. Phys. Lett.* **2004**, *383*, 99–103. https://doi.org/10.1016/j.cplett.2003.10.133.

(93) Murgia, S.; Mele, S.; Monduzzi, M. Quantitative Characterization of Phospholipids in Milk Fat via 31P NMR Using a Monophasic Solvent Mixture.

Lipids **2003**, *38* (5), 585–591. https://doi.org/10.1007/s11745-003-1500-3.

(94) Koch, K. R. Quantitative Determination of Aluminium in Tea by Means of Aluminium-27 Nuclear Magnetic Resonance Spectroscopy. **1990**, *115*, 823–825.

(95) Ycas, P. D.; Wagner, N.; Olsen, N. M.; Fu, R.; Pomerantz, W. C. K. 2 - Fluorotyrosine Is a Valuable but Understudied Amino Acid for Protein - Observed 19 F NMR. *J. Biomol. NMR* **2020**, *74* (1), 61–69. https://doi.org/10.1007/s10858-019-00290-0.

(96) Simpson, A. J.; Simpson, M. J.; Soong, R. Environmental Nuclear Magnetic Resonance Spectroscopy: An Overview and a Primer. *Anal. Chem.* **2018**, *90*, 628–639. https://doi.org/10.1021/acs.analchem.7b03241.

(97) Rosenau, C. P.; Jelier, B. J.; Gossert, A. D.; Togni, A. Exposing the Origins of Irreproducibility in Fluorine NMR Spectroscopy Angewandte. *Angew. Chemie Int. Ed.* **2018**, *57*, 9528–9533. https://doi.org/10.1002/anie.201802620.

(98) Longstaffe, J.; Konzuk, J. NMR in the Environmental Industry. *Magn. Reson. Chem.* **2015**, No. 53, 691–693. https://doi.org/10.1002/mrc.4177.

(99) Smernik, R. J.; Oades, J. M. The Use of Spin Counting for Determining Quantitation in Solid State 13 C NMR Spectra of Natural Organic Matter 2. HF-Treated Soil Fractions. *Geoderma* **2000**, *96*, 159–171.

(100) Masoom, H.; Courtier-murias, D.; Farooq, H.; Soong, R.; Kelleher, B. P.; Zhang, C.; Maas, W. E.; Fey, M.; Kumar, R.; Monette, M.; Stronks, H. J.; Simpson, M. J.; Simpson, A. J. Soil Organic Matter in Its Native State: Unravelling the Most Complex Biomaterial on Earth. *Environ. Sci. Technol.* **2016**, *50*, 1670–1680. https://doi.org/10.1021/acs.est.5b03410.

(101) Young, I. M.; Crawford, J. W. Interactions and Self-Organization in the Soil-Microbe Complex. *Science* **2004**, *304*, 1634–1638.

(102) Giraudeau, P.; Silvestre, V.; Akoka, S. Optimizing Water Suppression for Quantitative NMR-Based Metabolomics: A Tutorial Review. *Metabolomics* **2015**, No. 11, 1041–1055. https://doi.org/10.1007/s11306-015-0794-7.

(103) Strynar, M.; Dec, J.; Bensei, A.; Jones, A. D.; Fry, R. A.; Bollag, J.-M. Using 19 F NMR Spectroscopy to Determine Trifluralin Binding to Soil. *Environ. Sci. Technol.* **2004**, *38* (24), 6645–6655. https://doi.org/10.1021/es0403110.

(104) Achtnich, C.; Fernandes, E.; Bollag, J.-M.; Knackmuss, H.-J.; Lenke, H. Covalent Binding of Reduced Metabolites of [15N3] TNT to Soil Organic Matter during a Bioremediation Process Analyzed by N NMR Spectroscopy. *Environ. Sci.*

Technol. **1999**, *33* (24), 4448–4456.

(105) Cochiara, S. G.; Phillips, B. L. NMR SPECTROSCOPY OF NATURALLY OCCURRING SURFACE-ADSORBED FLUORIDE ON GEORGIA KAOLINITE. *Clay Clay Miner.* **2008**, *56* (1), 90–99. https://doi.org/10.1346/CCMN.2008.0560108.

(106) Liu, Y.; Tossell, J. Possible Al - F Bonding Environment in Fluorine-Bearing Sodium Aluminosilicate Glasses: From Calculation of 19 F NMR Shifts. *J. Phys. Chem. Biochem.* **2003**, *107*, 11280–11289. https://doi.org/10.1021/jp0350417.

(107) Moody, C. A.; Kwan, W. C.; Martin, J. W.; Muir, D. C. G.; Mabury, S. A. Determination of Perfluorinated Surfactants in Surface Water Samples by Two Independent Analytical Techniques: Liquid Chromatography / Tandem Mass Spectrometry and 19 F NMR. *Anal. Chem.* **2001**, *73* (10), 2200–2206. https://doi.org/10.1021/ac0100648.

(108) Ellis, D. A.; Martin, J. W.; Muir, D. C. G.; Mabury, S. A. Development of an 19 F NMR Method for the Analysis of Fluorinated Acids in Environmental Water Samples. *Anal. Chem.* **2000**, *72* (4), 726–731. https://doi.org/10.1021/ac9910280.

(109) Malz, F.; Jancke, H. Validation of Quantitative NMR. *J. Pharm. Biomed. Anal.* **2005**, *38*, 813–823. https://doi.org/10.1016/j.jpba.2005.01.043.

(110) Mattes, A. O.; Russell, D.; Tishchenko, E.; Liu, Y.; Cichewicz, R. H.; Robinson, S. J. Application of 19F Quantitative NMR to Pharmaceutical Analysis. *Concepts Magn. Reson. Part A Bridg. Educ. Res.* **2018**, *45A* (5), 1–8. https://doi.org/10.1002/cmr.a.21422.

(111) Meek, S. J.; Pitman, C. L.; Miller, A. J. M. Deducing Reaction Mechanism: A Guide for Students, Researchers, and Instructors. **2016**. https://doi.org/10.1021/acs.jchemed.5b00160.

(112) Latch, D. E.; Packer, J. L.; Stender, B. L.; VanOverbeke, J.; Arnold, W. A.; McNeill, K. AQUEOUS PHOTOCHEMISTRY OF TRICLOSAN: FORMATION OF 2-4 DICHLOROPHENOL, 2,8-DICHLORODIBENZO-p-DIOXIN, AND OLIGOMERIZATION PRODUCTS. *Environ. Toxicol. Chem.* **2005**, *24* (3), 517–525.

(113) Bole, P.; Guyon, C.; LeMaire, J. Photochemistry and the Environment. VIII. Photochemical Behavior Of dichlorophenols in a Dilute Aqueous Solution. *Chemosphere* **1984**, *13* (5), 603–612.

(114) Bell, A.; Singer, J.; Desmond, D.; Mahassneh, O.; van Wijngaarden, J. Rotational Spectra and Conformer Geometries of 2-Fluorophenol and 3-Fluorophenol. *J. Mol.*

Spectrosc. **2017**, *331*, 53–59. https://doi.org/10.1016/j.jms.2016.11.007.

(115) Chatterjee, P.; Ghosh, A. K.; Chakraborty, T. Hydrogen Bond Induced HF Elimination from Photoionized Fluorophenol Dimers in the Gas Phase. *J. Chem. Phys.* **2017**, *146* (084310). https://doi.org/10.1063/1.4976988.

Appendix A Additional Data

A.1 UV-Spectrum of Compounds of Interest

The spectrophotometer was used to obtain the absorbance spectra of each compound of interest. The concentration of each compound of interest was at 100 µM so that a large absorbance could be obtained. They were all taken in MilliQ water with the blank sample being the pure MilliQ water. The total sweep width of the instrument was from 600 to 200 λ.

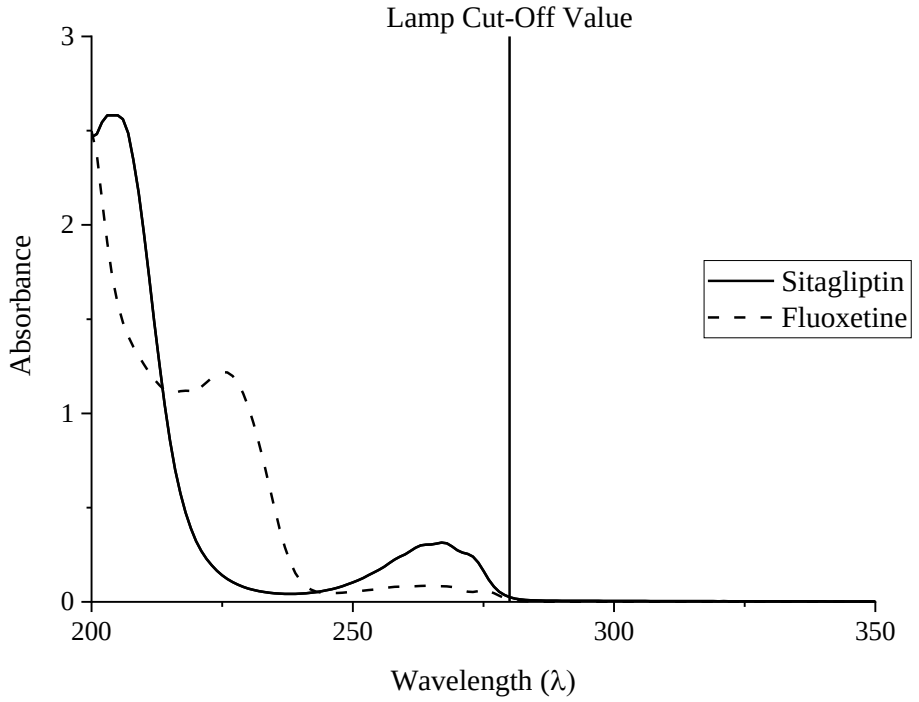

Figure A-1. Ultraviolet absorbance spectra of sitagliptin and fluoxetine in MilliQ water (pH 7). The vertical line represents the minimum wavelength emitted from the Hg-vapor lamp apparatus, as controlled by a cut-off sleeve.

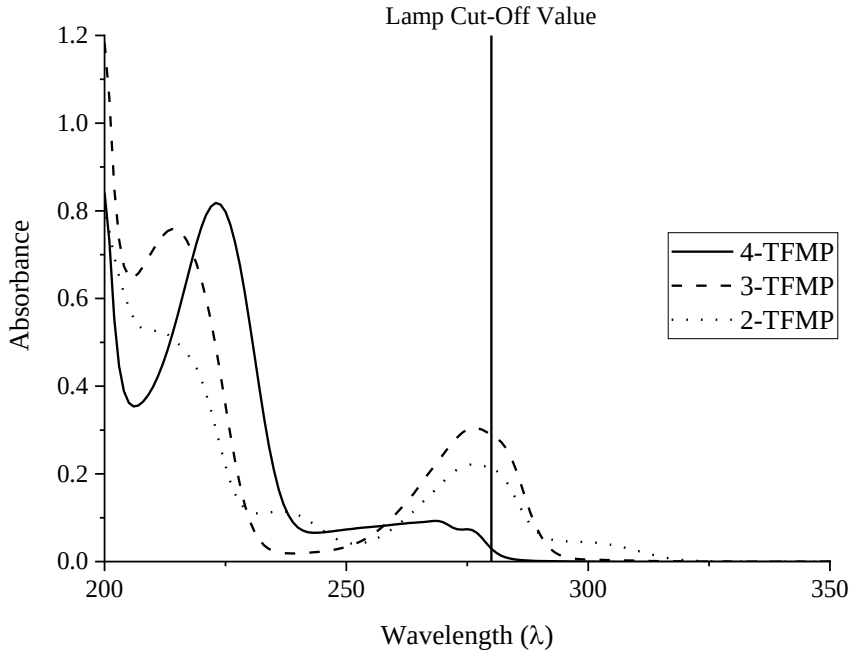

Figure A-2. Ultraviolet absorbance spectra of 4-, 3-, and 2-trifluoromethylphenol (TFMP) in MilliQ water (pH 7). The vertical line represents the minimum wavelength emitted from the Hg-vapor lamp apparatus, as controlled by a cut-off sleeve.

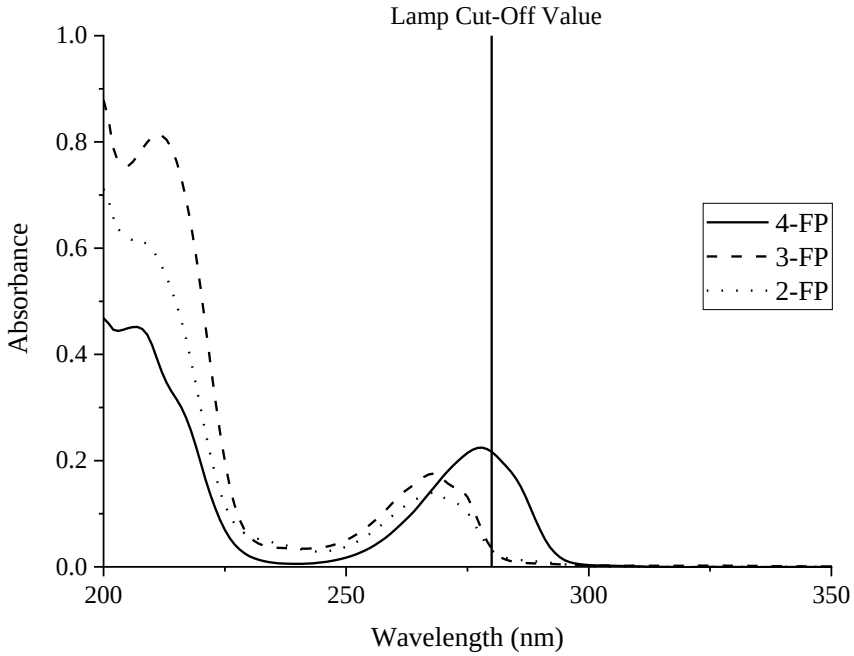

Figure A-3. Ultraviolet absorbance spectra of 4-, 3-, and 2-fluorophenol (FP) in MilliQ water (pH 7). The vertical line represents the minimum wavelength emitted from the Hg-vapor lamp apparatus, as controlled by a cut-off sleeve.

A.2 Photolysis Reaction Kinetics

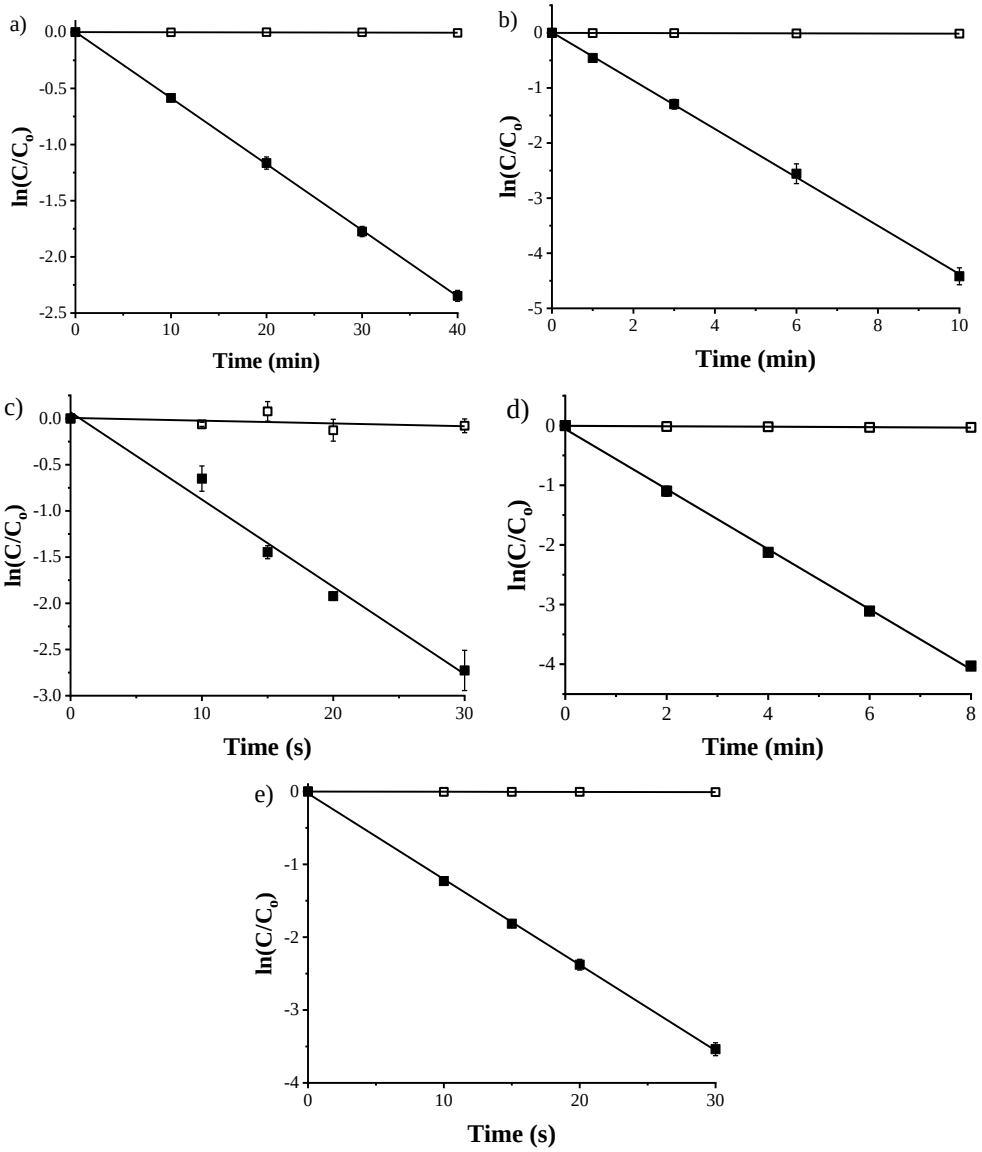

Figure A-4. Photochemical degradation plots of ortho-trifluoromethylphenol (2-TFMP) with hydrolysis (□) and photolysis (■) rate constants of 0.01 ± 0.01 h^{-1} and 3.52 ± 0.07 h^{-1} in a 10 mM pH 5 acetate buffer (a), 0.08 ± 0.03 h^{-1} and 26.37 ± 0.64 h^{-1} in a 10 mM pH 7 phosphate buffer (b), 10.78 ± 28.57 h^{-1} and 334.09 ± 93.45 h^{-1} in a 10 mM pH 10 borate buffer (c), 0.22 ± 0.10 h^{-1} and 29.99 ± 1.47 h^{-1} in a 10 mM pH 7 phosphate buffer with 1 mM H_2O_2 (d), and 0.99 ± 1.62 h^{-1} and 422.43 ± 9.38 h^{-1} in a 10 mM pH 10 borate buffer with 0.5 mM SO_3^{-2} (e). Error bars represent the standard deviation between triplicate samples taken on HPLC. Reported rate constant errors represent the average 95% confidence interval determined by regression statistics.

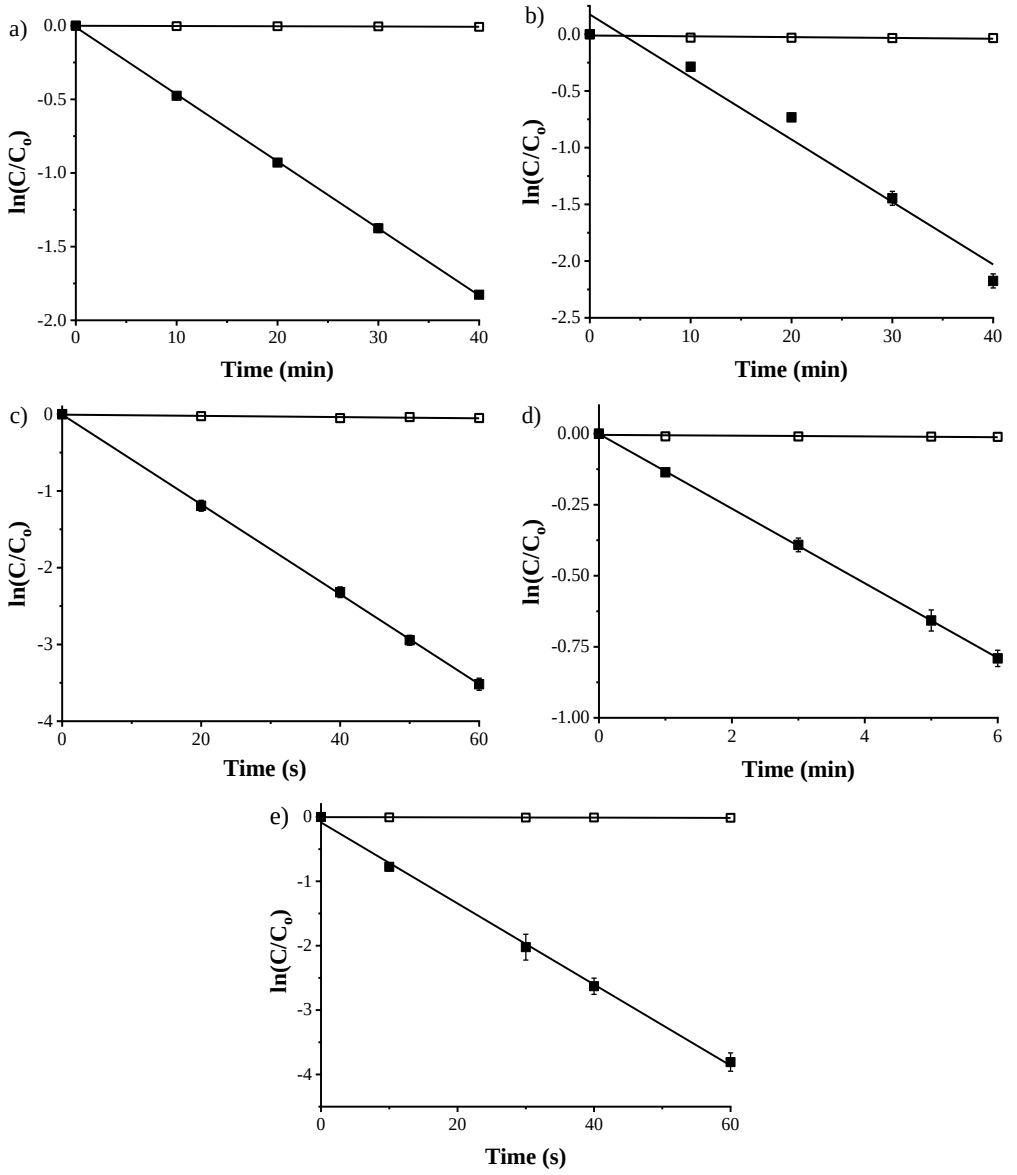

Figure A-5. Photochemical degradation plots of meta-trifluoromethylphenol (3-TFMP) with hydrolysis (□) and photolysis (■) rate constants of 0.01 ± 0.01 h^{-1} and 2.72 ± 0.06 h^{-1} in a 10 mM pH 5 acetate buffer (a), 0.04 ± 0.04 h^{-1} and 3.27 ± 0.63 h^{-1} in a 10 mM pH 7 phosphate buffer (b), 2.84 ± 2.08 h^{-1} and 207.90 ± 7.51 h^{-1} in a 10 mM pH 10 borate buffer (c), 0.08 ± 0.08 h^{-1} and 7.80 ± 0.20 h^{-1} in a 10 mM pH 7 phosphate buffer with 1 mM H_2O_2 (d), and 0.72 ± 0.41 h^{-1} and 225.83 ± 13.60 h^{-1} in a 10 mM pH 10 borate buffer with 0.5 mM SO_3^{-2} (e). Error bars represent the standard deviation between triplicate samples taken on HPLC. Reported rate constant errors represent the average 95% confidence interval determined by regression statistics. Note the change in units along the x-axis.

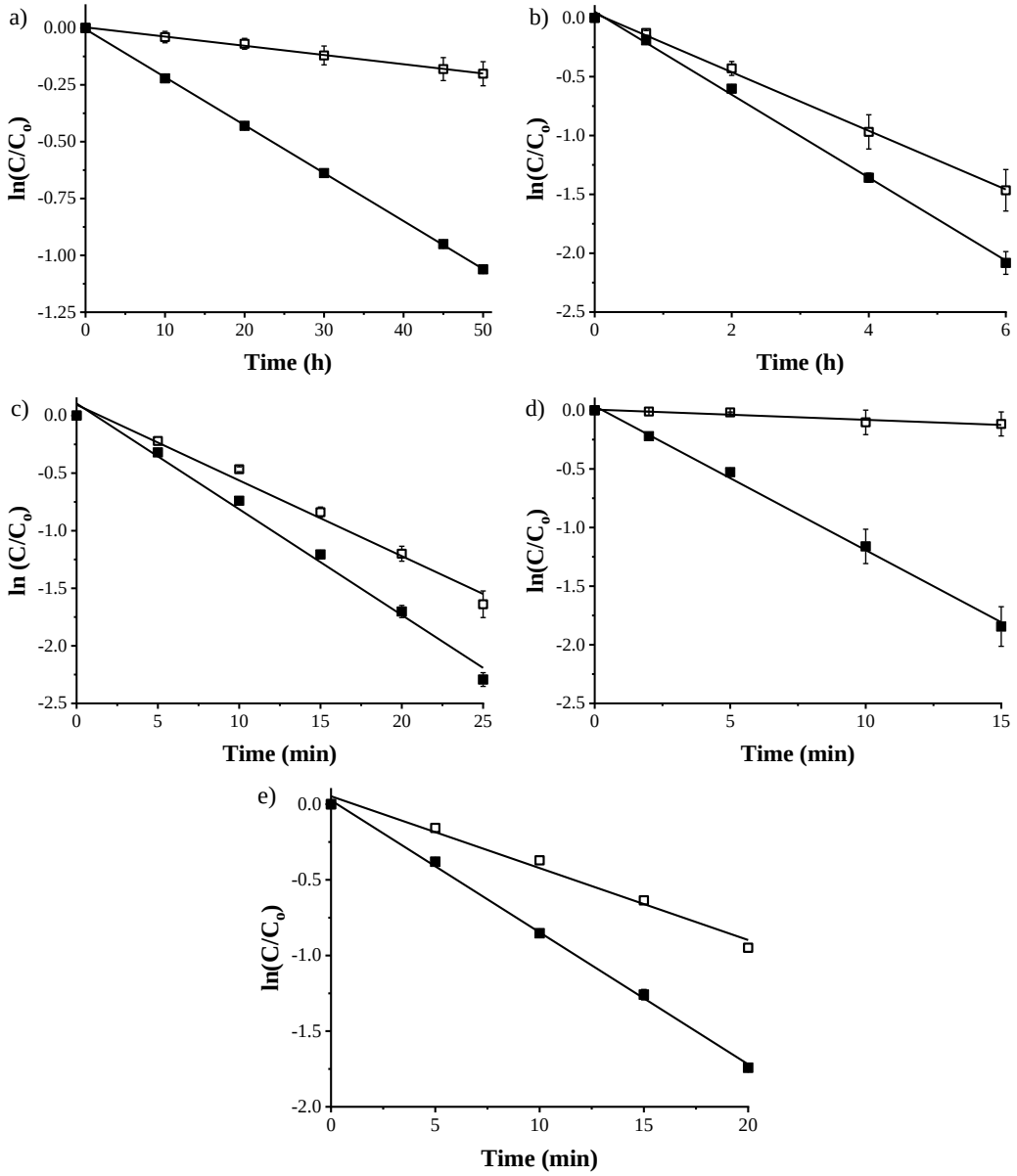

Figure A-6. Photochemical degradation plots of para-trifluoromethylphenol (4-TFMP) with hydrolysis (□) and photolysis (■) rate constants of 4.1×10^{-3} ± 3.6×10^{-4} h^{-1} and 0.02 ± 5.5×10^{-4} h^{-1} in a 10 mM pH 5 acetate buffer (a), 0.25 ± 0.01 h^{-1} and 0.10 ± 0.02 h^{-1} in a 10 mM pH 7 phosphate buffer (b), 3.93 ± 0.57 h^{-1} and 1.58 ± 0.71 h^{-1} in a 10 mM pH 10 borate buffer (c), 0.52 ± 0.18 h^{-1} and 6.85 ± 0.93 h^{-1} in a 10 mM pH 7 phosphate buffer with 1 mM H_2O_2 (d), and 2.85 ± 0.39 h^{-1} and 2.38 ± 0.45 h^{-1} in a 10 mM pH 10 borate buffer with 0.5 mM SO_3^{-2} (e). Note the change in time units on the x-axis. Error bars represent the standard deviation between triplicate samples taken on HPLC. Reported rate constant errors represent the average 95% confidence interval determined by regression statistics.

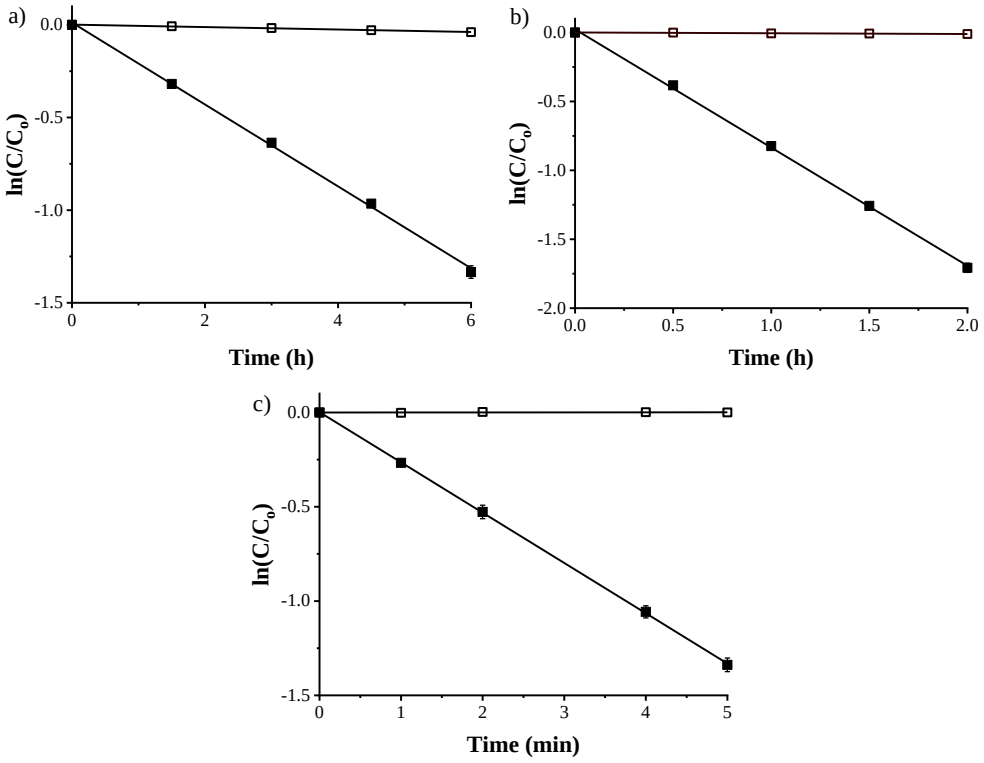

Figure A-7. Photochemical degradation plots of ortho-fluorophenol (2-FP) with hydrolysis (□) and photolysis (■) rate constants of 0.01 ± 6.3×10^{-4} h^{-1} and 0.21 ± 0.01 h^{-1} in a 10 mM pH 5 acetate buffer (a), 0.01 ± 2.9×10^{-3} h^{-1} and 0.85 ± 0.03 h^{-1} in a 10 mM pH 7phosphate buffer (b), and 0.01 ± 0.13 h^{-1} and 15.99 ± 0.37 h^{-1} in a 10 mM pH 10 borate buffer (c). Note the change in time units on the x-axis. Error bars represent the standard deviation between triplicate samples taken on HPLC. Reported rate constant errors represent the average 95% confidence interval determined by regression statistics.

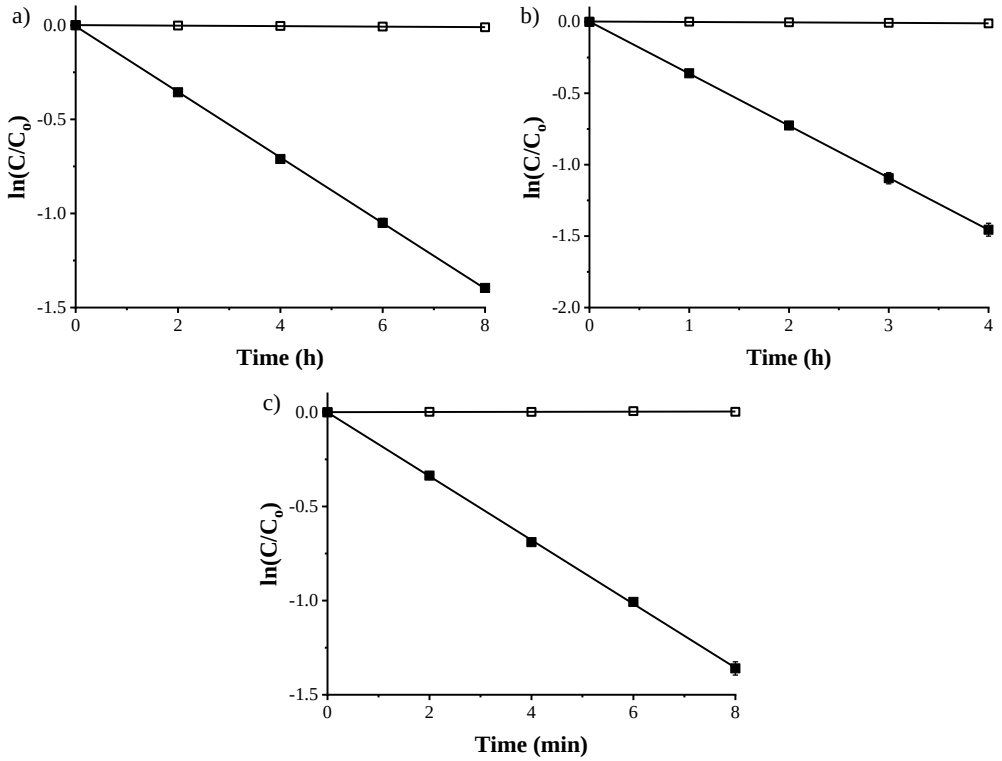

Figure A-8. Photochemical degradation plots of meta-fluorophenol (3-FP) with hydrolysis (□) and photolysis (■) rate constants of $1.4\times10^{-3} \pm 2.9\times10^{-4}$ h^{-1} and $0.17 \pm 2.5\times10^{-3}$ h^{-1} in a 10 mM pH 5 acetate buffer (a), $3.1\times10^{-3} \pm 1.7\times10^{-3}$ h^{-1} and 0.36 ± 0.01 h^{-1} in a 10 mM pH 7phosphate buffer (b), and 0.02 ± 0.10 h^{-1} and 10.15 ± 0.29 h^{-1} in a 10 mM pH 10 borate buffer (c). Note the change in time units on the x-axis. Error bars represent the standard deviation between triplicate samples taken on HPLC. Reported rate constant errors represent the average 95% confidence interval determined by regression statistics.

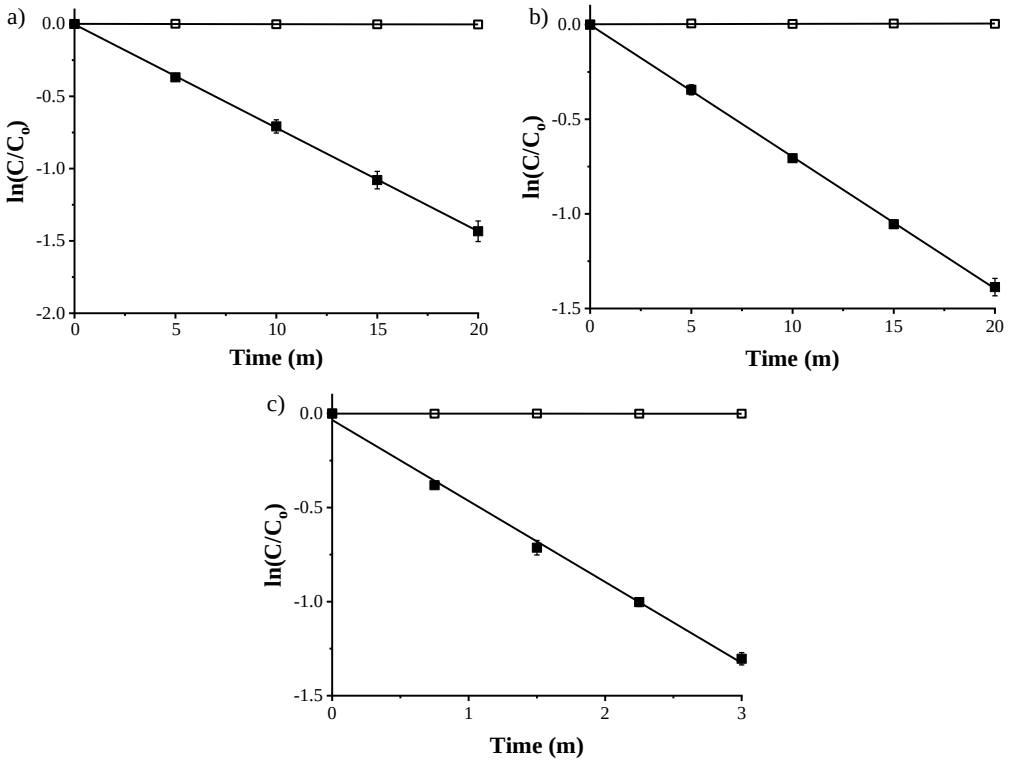

Figure A-9. Photochemical degradation plots of para-fluorophenol (4-FP) with hydrolysis (□) and photolysis (■) rate constants of 0.01 ± 0.01 h^{-1} and 4.28 ± 0.10 h^{-1} in a 10 mM pH 5 acetate buffer (a), 9.9×10^{-3} ± 0.02 h^{-1} and 4.17 ± 0.11 h^{-1} in a 10 mM pH 7phosphate buffer (b), and 0.01 ± 0.08 h^{-1} and 25.82 ± 1.66 h^{-1} in a 10 mM pH 10 borate buffer (c). Error bars represent the standard deviation between triplicate samples taken on HPLC. Reported rate constant errors represent the average 95% confidence interval determined by regression statistics.

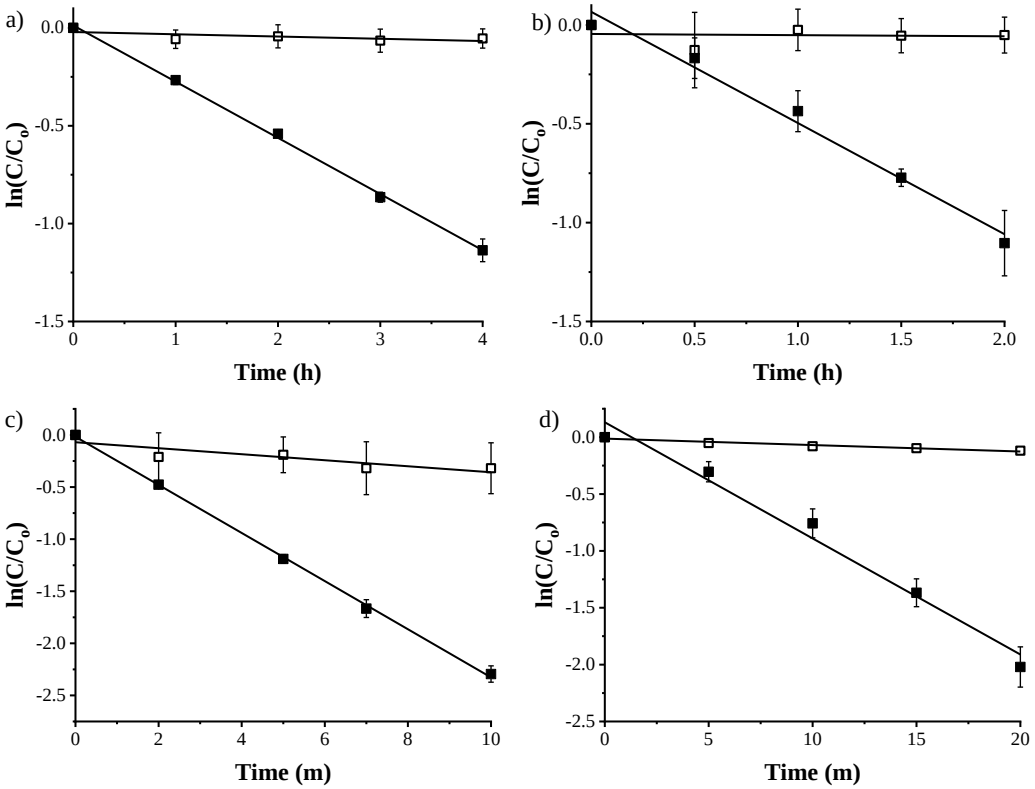

Figure A-10. Photochemical degradation plots of fluoxetine with hydrolysis (□) and photolysis (■) rate constants of 0.02 ± 0.01 h^{-1} and 0.27 ± 0.01 h^{-1} in a 10 mM pH 7 phosphate buffer (a), 0.01 ± 0.10 h^{-1} and 0.56 ± 0.15 h^{-1} in a 10 mM pH 10 borate buffer (b), 1.73 ± 1.46 h^{-1} and 12.13 ± 1.54 h^{-1} in a 10 mM pH 7 phosphate buffer with 1 mM H_2O_2 (c), and 0.34 ± 0.11 h^{-1} and 5.79 ± 0.95 h^{-1} in a 10 mM pH 10 borate buffer with 0.5 mM SO_3^{-2}. Note the change in time units on the x-axis. Error bars represent the standard deviation between triplicate samples taken on HPLC. Reported rate constant errors represent the average 95% confidence interval determined by regression statistics.

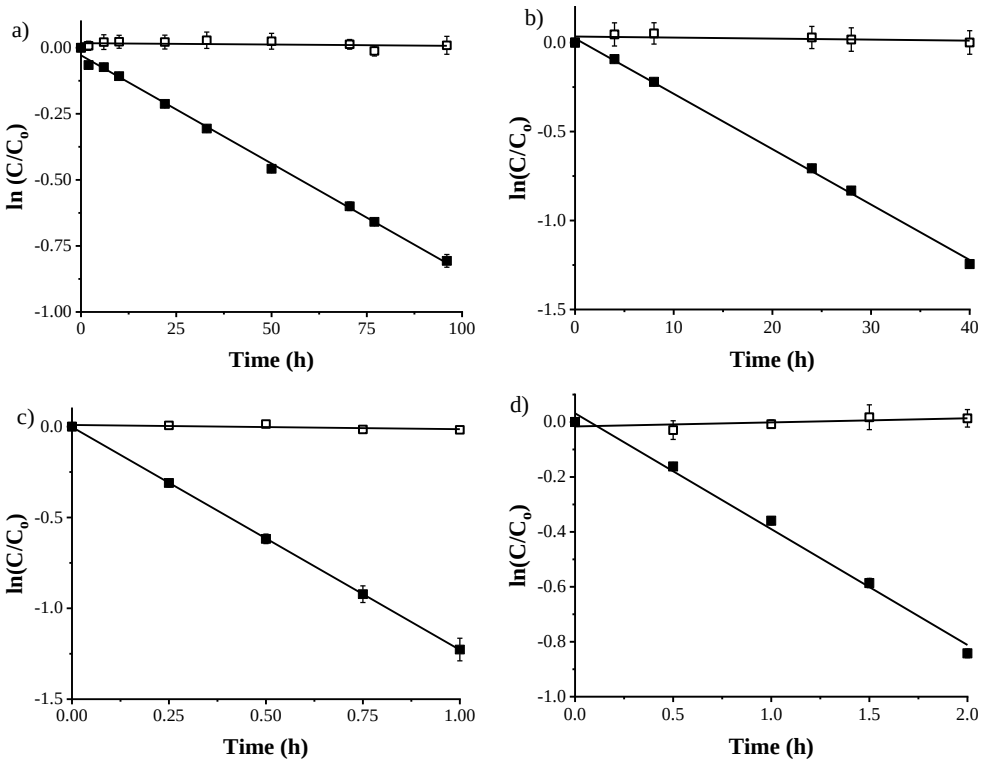

Figure A-11. Photochemical degradation plot of sitagliptin with hydrolysis (□) and photolysis (■) rate constants of $1.0\times10^{-4} \pm 2.1\times10^{-4}$ h^{-1} and $9.6\times10^{-3} \pm 3.8\times10^{-4}$ h^{-1} in a 10 mM pH 7 phosphate buffer (a), $5.7\times10^{-4} \pm 1.1\times10^{-3}$ h^{-1} and $0.03 \pm 1.4\times10^{-3}$ h^{-1} in a 10 mM pH 10 borate buffer (b), 0.02 ± 0.03 h^{-1} and 1.21 ± 0.04 h^{-1} in a 10 mM pH 7 phosphate buffer with 2 mM H_2O_2 (c), and -0.01 ± 0.04 h^{-1} and 0.43 ± 0.06 h^{-1} in a 10 mM pH 10 borate buffer with 0.5 mM SO_3^{-2} (d). Error bars represent the standard deviation between triplicate samples taken on HPLC. Reported rate constant errors represent the average 95% confidence interval determined by regression statistics.

Appendix B Detailed NMR Protocols and Additional Data

B.1 NMR Experimental Set-Up

NMR experiments were chosen from the dropdown menu in the autosampler software in TopSpin. In the corresponding row numbered with the sample location, a unique experiment number was automated for the experiment. The solvent chosen was D_2O and the experiment chosen was named "N 19 F no decoupling." After the experiment and solvent were chosen, in the top-menu, "parameters" then "edit all parameters" were chosen. The editable parameters are described in detail below, after they were changed to the desired values, the "return to ICON" button was selected to save the parameters and return to the NMR sequence run.

B.2 NMR Parameters

The receiver gain, (RG), was initially automated and determined an optimal value of 101. All subsequent NMR experiments used this value. The acquisition time, (AQ), was found by visually inspecting the FID and choosing a cut-off time which captures minimal noise and maximum signal based on the signal decay. This value was found to be 0.3 seconds. The fluorine resonances observed in these experiments fell within the values of -60 ppm to -170 ppm, thus the sweep width (SW) was set to be 201 ppm. The center frequency (O1p) was set to -100 ppm, such that the spectral range was from 0 to -200 ppm, allowing for all the fluorine signals to be observed. The delay time (D1) was incrementally increased from 3 to 6 seconds using 1 second intervals on an NMR sample containing 10 µM of fluoxetine, hexafluorobenzene, fluoride, lansoprazole, and TFA. The signal to noise of each compound's peak was taken for each D1 time. D1 times that are too short do not provide enough time for the ^{19}F nuclei to relax leading to an

underreporting of the fluorine concentrations. Increasing the D1 time also increases the experiment time, so a trade-off for time was made, while still maintaining a high enough signal-to-noise for analysis. The results of this test can be found in Table B-1. Most compounds did not have a large change in signal-to-noise along this range of times. A time of 4 seconds was chosen, giving sufficient signal to noise for each fluorine motif, while not having an extensively long method time. The D1 time of 4 seconds did not show maximum S/N for fluoride, consequently, the quantification of fluoride may be underrepresented. The number of scans (NS) can be changed to increase the signal-to-noise as a function of the square of the NS. An NS value of 1024 led to good signal-to-noise (>10) for the fluorinated products within a reasonable experiment time (75 min). The number of dummy scans (DS) were kept at the automatic setting of 4, this is the number of scans taken before data is collected. Other values were kept at the initial value or whatever they changed to be once the AQ, NS, SW, and D1 values were adjusted.

Table B-1. Change in S/N due to change in D1 times.

Compound	D1: 3 sec.	D1: 4 sec.	D1: 5 sec.	D1: 6 sec.
Fluoride	53.71	55.85	61.53	64.31
Fluoxetine	17.79	19.73	13.61	19.27
HFB	97.05	104.39	122.44	110.71
Lansoprazole	35.1	32.04	30.46	34.06
TFA	35.51	38.58	29.82	37.77

B.3 NMR Sample Set-Up

The HFB standards are fragile, and one technique proved to be adequate at inserting and removing the standard from the NMR tube without breaking either. This process should be done after the NMR tube has been filled with D_2O and the sample of interest.

1. Wipe the HFB standard tube with a chemwipe.
2. Make sure all of the liquid standard is at the bottom of the capillary tube.
3. Gently place the HFB standard tube in the NMR tube with the flame sealed tip facing up.
4. If the standard tube doesn't fall to the bottom of the NMR tube, carefully tap the bottom of the NMR tube on a notebook or other hard surface. The standard tube will slowly fall down the NMR tube until it reaches the bottom.
5. Cap and label the NMR tube.

Each NMR tube should be clearly labeled so that you can remember what standard tube corresponds to which NMR tube because every IS_{ratio} is unique. When this is completed, wipe down the outside of the NMR tube with a chemwipe and place it in a spinner. Use the depth gauge to check that the volume is within the range that the instrument can accurately analyze the sample. Place the NMR tubes in the corresponding holders in the autosampler. To run the samples on the NMR, highlight all the lines that you want to run and click the "submit" button. The term "queued" should appear by each sample that was highlighted. Click the "start" button, a pop-up will appear asking where to start, type in the first location number that you have submitted, then press "OK."

B.4 NMR Spectrum Processing

Baseline corrections were needed to obtain a usable baseline for spectral integration. To flatten the baseline across the NMR spectra, processing parameters must be edited. Under the 'Process Parameters" tab, a 7-step protocol can be followed.

1. Scroll down to the “ME_mod” tab and select “LPbr” from the dropdown menu.
2. In the NCOEF window, type in “32”.
3. In the LPBIN window, type in “16”.
4. In the TDoff window, type in “16”.
5. In the command window, located in the bottom left-hand corner, type in “CONVDTA”.
6. In the pop-up window type in an experiment number that is different from the other experiment numbers in the file that you are working in. This saves it as a new file instead of overwriting an existing file.
7. Once you saved it as a new file, give it a new title and adjust the phase so that every peak in the desired range is in phase.

B.5 Calculations of Error

Errors for every ^{19}F-NMR peak were propogated from the error found of each HFB IS_{ratio}. Calibration of the IS_{ratio} of each HFB standard with TFA was run in triplicate. The average integration and standard deviation of each the HFB and the TFA peaks were determined. The mathematical operations to calculate the IS_{ratio} were multiplication and/or division. Equation B-1 was used to propagate the error. An example of the calculations in Microsoft Excel is shown in Figure B-1.

$$\%\ Error = \sqrt{\left(\frac{STDV_{HFB}}{Area_{HFB}}\right)^2 + \left(\frac{STDV_{TFA}}{Area_{TFA}}\right)^2} \qquad \text{Equation B-1}$$

This % error was then used to calculate the variability of the quantification of the moles of fluorine. This calculation multiplies the calculated moles of fluorine by the % error of

the corresponding HFB standard. This calculation includes the assumption that the calculated moles of fluorine from the HFB standard was an exact number. When the total moles of fluorine are added together, a new error calculation was made using Equation B-2, where *n* is the number of values being added or subtracted together.

$$Total\ Error = \sqrt{(Error_1)^2 + (Error_2)^2 + \cdots (Error_n)^2} \qquad \text{Equation B-2}$$

Run #	HFB Area	TFA Area	AVG. HFB Area	STDV. HFB	AVG. TFA Area	STDV. TFA	Ratio	% Error
1	1.81E+12	9.83E+12	1.80E+12	9.45E+09	9.78E+12	3.6115E+10	10.89	0.6428
2	1.79E+12	9.75E+12						
3	1.79E+12	9.76E+12						

Figure B-1. Example of IS_{ratio} calculations in Microsoft Excel.

B.6 Fluorine Mass Balance

Table B-2. 2-Trifluoromethylphenol (2-TFMP) parent and photoproduct mass balance as total moles of fluorine before and after 40 minutes of photolysis in a pH 5 acetate buffer.

Sample	Name	[Fluorine] (moles)	Error ±
Unphotolyzed	2-TFMP	30.85	0.22
	Total	**30.85**	**0.22**
Photolyzed	2-TFMP	3.22	0.02
	Product F	8.33	0.06
	Fluoride	20.37	0.15
	Total	**31.93**	**0.16**

Table B-3. 2-Trifluoromethylphenol (2-TFMP) parent and photoproduct mass balance as total moles of fluorine before and after 6 minutes of photolysis in a pH 7 phosphate buffer.

Sample	Name	[Fluorine] (moles)	Error ±
Unphotolyzed	2-TFMP	33.77	0.30
	Total	**33.77**	**0.30**
Photolyzed	2-TFMP	3.58	0.03
	Fluoride	29.65	0.22
	Total	**33.22**	**0.22**

Table B-4. 2-Trifluoromethylphenol (2-TFMP) parent and photoproduct mass balance as total moles of fluorine before and after 0.5 minutes of photolysis in a pH 10 borate buffer.

Sample	Name	[Fluorine] (moles)	Error ±
Unphotolyzed	2-TFMP	33.87	0.25
	Total	**33.87**	**0.25**
Photolyzed	2-TFMP	1.02	3.3×10^{-3}
	Product E	0.68	2.2×10^{-3}
	Fluoride	35.28	0.11
	Total	**36.99**	**0.11**

Table B-5. 2-Trifluoromethylphenol (2-TFMP) parent and photoproduct mass balance as total moles of fluorine before and after 4 minutes of photolysis in a pH 7 phosphate buffer with 1 mM H_2O_2.

Sample	Name	[Fluorine] (moles)	Error ±
Unphotolyzed	2-TFMP	39.53	0.31
	Total	**39.53**	**0.31**
Photolyzed	2-TFMP	8.65	0.06
	Fluoride	26.10	0.19
	Total	**34.74**	**0.20**

Table B-6. 2-Trifluoromethylphenol (2-TFMP) parent and photoproduct mass balance as total moles of fluorine before and after 0.5 minutes of photolysis in a pH 10 borate buffer with 0.5 mM SO_3^{-2}.

Sample	Name	[Fluorine] (moles)	Error ±
Unphotolyzed	2-TFMP	34.34	0.15
	Total	**34.34**	**0.15**
Photolyzed	2-TFMP	0.82	3.6×10^{-3}
	Product E	1.02	4.4×10^{-3}
	Fluoride	37.74	0.16
	Total	**39.58**	**0.16**

Table B-7. 3-Trifluoromethylphenol (3-TFMP) parent and photoproduct mass balance as total moles of fluorine before and after 40 minutes of photolysis in a pH 5 acetate buffer.

Sample	Name	[Fluorine] (moles)	Error ±
Unphotolyzed	3-TFMP	56.08	0.18
	Total	**56.08**	**0.18**
Photolyzed	3-TFMP	9.28	0.07
	Fluoride	50.35	0.40
	Total	**59.63**	**0.41**

Table B-8. 3-Trifluoromethylphenol (3-TFMP) parent and photoproduct mass balance as total moles of fluorine before and after 40 minutes of photolysis in a pH 7 phosphate buffer.

Sample	Name	[Fluorine] (moles)	Error ±
Unphotolyzed	3-TFMP	59.45	0.38
	Total	**59.45**	**0.38**
Photolyzed	3-TFMP	1.03	4.5×10^{-3}
	Fluoride	55.01	0.24
	Total	**56.04**	**0.24**

Table B- 9. 3-Trifluoromethylphenol (3-TFMP) parent and photoproduct mass balance as total moles of fluorine before and after 1 minute of photolysis in a pH 10 borate buffer.

Sample	Name	[Fluorine] (moles)	Error ±
Unphotolyzed	3-TFMP	64.34	0.54
	Total	**64.34**	**0.54**
Photolyzed	3-TFMP	5,68	0.05
	Fluoride	64.32	0.54
	Total	**70.00**	**0.54**

Table B- 10. 3-Trifluoromethylphenol (3-TFMP) parent and photoproduct mass balance as total moles of fluorine before and after 6 minutes of photolysis in a pH 7 phosphate buffer.

Sample	Name	[Fluorine] (moles)	Error ±
Unphotolyzed	3-TFMP	57.43	0.46
	Total	**57.43**	**0.46**
Photolyzed	3-TFMP	23.84	0.18
	Fluoride	29.16	0.22
	Total	**53.00**	**0.28**

Table B-11. 3-Trifluoromethylphenol (3-TFMP) parent and photoproduct mass balance as total moles of fluorine before and after 1 minute of photolysis in a pH 10 borate buffer with 0.5 mM SO_3^{-2}.

Sample	Name	[Fluorine] (moles)	Error ±
Unphotolyzed	3-TFMP	50.62	0.37
	Total	**50.62**	**0.37**
Photolyzed	3-TFMP	4.55	0.03
	Fluoride	50.07	0.37
	Total	**54.62**	**0.37**

Table B-12. 4-Trifluoromethylphenol (4-TFMP) parent and photoproduct mass balance as total moles of fluorine before and after 40 hours of photolysis in a pH 5 acetate buffer.

Sample	Name	[Fluorine] (moles)	Error ±
Unphotolyzed	4-TFMP	30.53	0.13
	Total	**30.53**	**0.13**
Photolyzed	4-TFMP	10.89	0.05
	Product C	6.82	0.03
	TFA	1.67	7.3×10^{-3}
	Fluoride	14.19	0.06
	Total	**33.57**	**0.08**

Table B-13. 4-Trifluoromethylphenol (4-TFMP) parent and photoproduct mass balance as total moles of fluorine before and after 6 hours of photolysis in a pH 7 phosphate buffer.

Sample	Name	[Fluorine] (moles)	Error ±
Unphotolyzed	4-TFMP	33.75	0.15
	Total	**33.75**	**0.15**
Photolyzed	4-TFMP	7.13	0.02
	Fluoride	26.47	0.09
	Total	**33.60**	**0.09**

Table B-14. 4-Trifluoromethylphenol (4-TFMP) parent and photoproduct mass balance as total moles of fluorine before and after 25 minutes of photolysis in a pH 10 borate buffer.

Sample	Name	[Fluorine] (moles)	Error ±
Unphotolyzed	4-TFMP	32.76	0.11
	Total	**32.76**	**0.11**
Photolyzed	4-TFMP	3.84	0.03
	Product D	0.91	7.6×10^{-3}
	Fluoride	38.30	0.32
	Total	**43.05**	**0.32**

Table B-15. 4-Trifluoromethylphenol (4-TFMP) parent and photoproduct mass balance as total moles of fluorine before and after 20 minutes of photolysis in a pH 7 phosphate buffer with 1 mM H_2O_2.

Sample	Name	[Fluorine] (moles)	Error ±
Unphotolyzed	4-TFMP	34.45	0.22
	Total	**34.45**	**0.22**
Photolyzed	4-TFMP	7.08	0.03
	Product A	7.11	0.03
	TFA	0.86	3.7×10^{-3}
	Fluoride	13.58	0.06
	Total	**28.63**	**0.07**

Table B-16. 4-Trifluoromethylphenol (4-TFMP) parent and photoproduct mass balance as total moles of fluorine before and after 20 minutes of photolysis in a pH 10 borate buffer with 0.5 mM SO_3^{-2}.

Sample	Name	[Fluorine] (moles)	Error ±
Unphotolyzed	4-TFMP	36.05	0.26
	Total	**36.05**	**0.26**
Photolyzed	4-TFMP	1.42	0.01
	Product D	1.19	0.01
	Fluoride	38.46	0.32
	Total	**41.06**	**0.32**

Table B-17. 4-Trifluoromethylphenol (4-TFMP) parent and product mass balance as total moles of fluorine before and after 6 hours of hydrolysis in a pH 7 phosphate buffer.

Sample	Name	[Fluorine] (moles)	Error ±
Unhydrolyzed	4-TFMP	36.77	0.24
	Total	**36.77**	**0.24**
Hydrolyzed	4-TFMP	8.16	0.04
	Fluoride	28.34	0.12
	Total	**36.50**	**0.13**

Table B-18. 4-Trifluoromethylphenol (4-TFMP) parent and product mass balance as total moles of fluorine before and after 1 hour of hydrolysis in a pH 10 borate buffer.

Sample	Name	[Fluorine] (moles)	Error ±
Unhydrolyzed	4-TFMP	31.32	0.14
	Total	**31.32**	**0.14**
Hydrolyzed	4-TFMP	0	0
	Product B	0.80	3.4×10^{-3}
	Fluoride	36.78	0.16
	Total	**37.58**	**0.16**

Table B-19. 4-Trifluoromethylphenol (4-TFMP) parent and product mass balance as total moles of fluorine before and after 1 hour of hydrolysis in a pH 7 phosphate buffer with 1 mM H_2O_2.

Sample	Name	[Fluorine] (moles)	Error ±
Unhydrolyzed	4-TFMP	34.36	0.15
	Total	**34.36**	**0.15**
Hydrolyzed	4-TFMP	7.05	0.05
	Product A	0.64	4.6×10^{-3}
	Fluoride	35.22	0.26
	Total	**42.91**	**0.26**

Table B-20. 4-Trifluoromethylphenol (4-TFMP) parent and product mass balance as total moles of fluorine before and after 1 hour of hydrolysis in a pH 10 borate buffer with 0.5 mM sulfite.

Sample	Name	[Fluorine] (moles)	Error ±
Unhydrolyzed	4-TFMP	34.87	0.11
	Total	**34.87**	**0.11**
Hydrolyzed	4-TFMP	0	0
	Product B	0.94	6.8×10^{-3}
	Fluoride	42.20	0.31
	Total	**43.14**	**0.31**

Table B-21. 2-Fluorophenol (2-FP) parent and photoproduct mass balance as total moles of fluorine before and after 6 hours of photolysis in a pH 5 acetate buffer.

Sample	Name	[Fluorine] (moles)	Error ±
Unphotolyzed	2-FP	10.34	0.03
	Total	**10.34**	**0.03**
Photolyzed	2-FP	2.90	0.02
	Fluoride	8.18	0.05
	Total	**11.08**	**0.06**

Table B-22. 2-Fluorophenol (2-FP) parent and photoproduct mass balance as total moles of fluorine before and after 2 hours of photolysis in a pH 7 phosphate buffer.

Sample	Name	[Fluorine] (moles)	Error ±
Unphotolyzed	2-FP	10.89	0.05
	Total	**10.89**	**0.05**
Photolyzed	2-FP	2.23	0.02
	Fluoride	11.49	0.08
	Total	**23.73**	**0.08**

Table B-23. 2-Fluorophenol (2-FP) parent and photoproduct mass balance as total moles of fluorine before and after 5 minutes of photolysis in a pH 10 borate buffer.

Sample	Name	[Fluorine] (moles)	Error ±
Unphotolyzed	2-FP	11.89	0.10
	Total	**11.89**	**0.10**
Photolyzed	2-FP	5.42	0.04
	Fluoride	11.40	0.10
	Total	**16.82**	**0.11**

Table B-24. 3-Fluorophenol (3-FP) parent and photoproduct mass balance as total moles of fluorine before and after 4 hours of photolysis in a pH 5 acetate buffer.

Sample	Name	[Fluorine] (moles)	Error ±
Unphotolyzed	3-FP	12.26	0.10
	Total	**12.26**	**0.10**
Photolyzed	3-FP	3.55	0.10
	Fluoride	10.22	0.03
	Total	**13.78**	**0.04**

Table B-25. 3-Fluorophenol (3-FP) parent and photoproduct mass balance as total moles of fluorine before and after 4 hours of photolysis in a pH 7 phosphate buffer.

Sample	Name	[Fluorine] (moles)	Error ±
Unphotolyzed	3-FP	13.48	0.09
	Total	**13.48**	**0.09**
Photolyzed	3-FP	2.75	0.01
	Fluoride	10.69	0.05
	Total	**13.44**	**0.05**

Table B-26. 3-Fluorophenol (3-FP) parent and photoproduct mass balance as total moles of fluorine before and after 8 minutes of photolysis in a pH 10 borate buffer.

Sample	Name	[Fluorine] (moles)	Error ±
Unphotolyzed	3-FP	15.55	0.13
	Total	**15.55**	**0.13**
Photolyzed	3-FP	4.95	0.04
	Fluoride	11.10	0.08
	Total	**16.04**	**0.09**

Table B-27. 4-Fluorophenol (4-FP) parent and photoproduct mass balance as total moles of fluorine before and after 20 minutes of photolysis in a pH 5 acetate buffer.

Sample	Name	[Fluorine] (moles)	Error ±
Unphotolyzed	4-FP	9.05	0.03
	Total	**9.05**	**0.03**
Photolyzed	4-FP	1.67	0.03
	Fluoride	9.87	0.04
	Total	**11.55**	**0.08**

Table B-28. 4-Fluorophenol (4-FP) parent and photoproduct mass balance as total moles of fluorine before and after 20 minutes of photolysis in a pH 7 phosphate buffer.

Sample	Name	[Fluorine] (moles)	Error ±
Unphotolyzed	4-FP	9.33	0.06
	Total	**9.33**	**0.06**
Photolyzed	4-FP	2.94	0.01
	Fluoride	9.80	0.04
	Total	**12.74**	**0.04**

Table B-29. 4-Fluorophenol (4-FP) parent and photoproduct mass balance as total moles of fluorine before and after 3 minutes of photolysis in a pH 10 borate buffer.

Sample	Name	[Fluorine] (moles)	Error ±
Unphotolyzed	4-FP	9.02	0.04
	Total	**9.02**	**0.04**
Photolyzed	4-FP	4.44	0.02
	Fluoride	7.97	0.03
	Total	**12.41**	**0.04**

Table B-30. Fluoxetine parent and photoproduct mass balance as total moles of fluorine before and after 4 hours of photolysis in a pH 7 phosphate buffer.

Sample	Name	[Fluorine] (moles)	Error ±
Unphotolyzed	FLX	41.32	0.12
	Total	**41.32**	**0.12**
Photolyzed	FLX	9.60	0.04
	Product A	7.35	0.03
	Product C	0.92	4.0×10^{-3}
	TFA	0.82	3.6×10^{-3}
	Fluoride	15.10	0.07
	Total	**33.79**	**0.08**

Table B-31. Fluoxetine parent and photoproduct mass balance as total moles of fluorine before and after 2 hours of photolysis in a pH 10 borate buffer.

Sample	Name	[Fluorine] (moles)	Error ±
Unphotolyzed	FLX	38.83	0.31
	Total	**38.83**	**0.31**
Photolyzed	FLX	13.0	0.10
	Fluoride	17.37	0.13
	Total	**30.37**	**0.16**

Table B-32. Fluoxetine parent and photoproduct mass balance as total moles of fluorine before and after 10 minutes of photolysis in a pH 7 phosphate buffer with 1 mM H_2O_2.

Sample	Name	[Fluorine] (moles)	Error ±
Unphotolyzed	FLX	25.22	0.11
	Total	**25.22**	**0.11**
Photolyzed	FLX	5.08	0.04
	Product A	4.71	0.04
	Product B	2.16	0.02
	TFA	1.57	0.01
	Fluoride	10.66	0.08
	Total	**24.18**	**0.10**

Table B-33. Fluoxetine parent and photoproduct mass balance as total moles of fluorine before and after 20 minutes of photolysis in a pH 10 borate buffer with 0.5 mM SO_3^{-2}.

Sample	Name	[Fluorine] (moles)	Error ±
Unphotolyzed	FLX	26.22	0.19
	Total	**26.22**	**0.19**
Photolyzed	FLX	10.25	0.07
	Product C	2.26	0.02
	Fluoride	15.83	0.11
	Total	**28.34**	**0.14**

Table B-34. Sitagliptin parent and photoproduct mass balance as total moles of fluorine before and after 96 hours of photolysis in a pH 7 phosphate buffer.

Sample	Name	[Fluorine] (moles)	Error ±
Unphotolyzed	Parent 1a	21.09	2.61
	Parent 1b	20.16	2.49
	Parent 2a	9.20	1.14
	Parent 2b	6.82	0.84
	Parent 3	15.17	1.88
	Parent 4a	6.46	0.80
	Parent 4b	7.65	0.95
	Total	**86.55**	**4.48**
Photolyzed	Parent 1a	17.12	0.16
	Parent 1b	16.30	0.15
	Parent 2a	7.71	0.07
	Parent 2b	5.82	0.05
	Parent 3	10.34	0.01
	Parent 4a	4.86	0.04
	Parent 4b	6.30	0.06
	Product A	0.80	7.4×10^{-3}
	Product D	1.36	0.01
	Product E	2.29	0.02
	Product F	2.34	0.02
	Product G	6.61	0.06
	Product I	3.82	0.04
	Product J	1.62	0.01
	Product K	0.86	7.9×10^{-3}
	Fluoride	21.81	0.20
	Total	**109.97**	**0.34**

Table B-35. Sitagliptin parent and photoproduct mass balance as total moles of fluorine before and after 40 hours of photolysis in a pH 10 borate buffer.

Sample	Name	[Fluorine] (moles)	Error ±
Unphotolyzed	Parent 1a	22.63	0.18
	Parent 1b	17.28	0.14
	Parent 2a	8.84	0.07
	Parent 2b	7.04	0.06
	Parent 3	13.92	0.11
	Parent 4a	5.29	0.04
	Parent 4b	8.81	0.07
	Total	**83.81**	**0.28**
Photolyzed	Parent 1a	6.09	0.03
	Parent 1b	4.98	0.02
	Parent 2a	4.25	0.02
	Parent 2b	3.89	0.02
	Parent 3	3.91	0.02
	Parent 4a	2.44	0.01
	Parent 4b	2.95	0.01
	Product A	0.65	2.8×10^{-3}
	Product B	0.76	3.3×10^{-3}
	Product E	0.88	3.8×10^{-3}
	Product F	0.90	3.9×10^{-3}
	Product G	4.15	0.02
	Product H	2.36	0.01
	Product I	0.68	3.0×10^{-3}
	Product J	0.66	2.9×10^{-3}
	Product K	6.12	0.03
	Fluoride	20.27	0.09
	Total	**65.94**	**0.11**

Table B-36. Sitagliptin parent and photoproduct mass balance as total moles of fluorine before and after 2 hours of photolysis in a pH 7 phosphate buffer with 2 mM H_2O_2.

Sample	Name	[Fluorine] (moles)	Error ±
Unphotolyzed	Parent 1a	31.88	0.29
	Parent 1b	25.80	0.24
	Parent 2a	13.91	0.13
	Parent 2b	10.95	0.10
	Parent 3	21.85	0.20
	Parent 4a	8.38	0.08
	Parent 4b	11.88	0.11
	Total	**124.65**	**0.48**
Photolyzed	Parent 1a	11.32	0.08
	Parent 1b	13.87	0.10
	Parent 2a	6.49	0.05
	Parent 2b	4.86	0.05
	Parent 3	6.39	0.05
	Parent 4a	3.17	0.02
	Parent 4b	4.12	0.03
	Product D	1.82	0.01
	Product E	1.88	0.01
	Product F	8.59	0.06
	Product G	3.87	0.03
	Product H	4.44	0.03
	Product J	0.32	2.4×10^{-3}
	Product K	0.83	6.1×10^{-3}
	Fluoride	32.96	0.24
	Total	**104.94**	**0.30**

Table B-37. Sitagliptin parent and photoproduct mass balance as total moles of fluorine before and after 2 hours of photolysis in a pH 10 borate buffer with 0.5 mM SO_3^{-2}.

Sample	Name	[Fluorine] (moles)	Error ±
Unphotolyzed	Parent 1a	24.07	2.98
	Parent 1b	16.45	2.04
	Parent 2a	10.33	1.28
	Parent 2b + Fluoride	8.32	1.03
	Parent 3	21.05	2.60
	Parent 4a	6.49	0.80
	Parent 4b	8.00	0.99
	Total	**94.71**	**4.91**
Photolyzed	Parent 1a	29.56	0.21
	Parent 1b	4.63	0.03
	Parent 2a	5.26	0.04
	Parent 2b + Fluoride	13.62	0.10
	Parent 3	10.26	0.07
	Parent 4a	4.20	0.03
	Parent 4b	5.77	0.04
	Product C	1.14	8.0×10^{-3}
	Product D	3.56	0.02
	Product G	3.94	0.03
	Product I	2.93	0.02
	Product K	4.63	0.03
	Total	**89.50**	**0.25**

B.7 Fluoride NMR Spectra

To quench hydrolysis reactions, addition of 6 μL of 1 M HCl to each NMR tube was done. This lowered the pH to a value where HF formed. NMR peaks appeared in the Ar-F range and were thought to be organofluorine photoproducts. Upon further investigation it was determined that these peaks were products of HF and the boron from the boric acid buffer (Figure B-2 and B-3). This reaction only occurred when the pH was below the pK_a of HF, above the pK_a, the fluoride ion cannot undergo these reactions. Only the HF peak was present when acid was added to the phosphate buffer, further

suggesting reactions with the boric acid matrix. The multiple peaks could be due to the presence of both ^{10}B and ^{11}B isotopes.[116] For this reason, quenching the hydrolysis reaction after photolysis with acid was not implemented for NMR analysis. It was however, used for quenching the hydrolysis of the time-zero point because no fluorine was formed at that point.

$$H3BO_3 + 3\ HF \rightarrow\ HBF_3(OH) + 2\ H_2O$$

$$HBF_3(OH) + HF \rightarrow HBF_4 + H_2O$$

Figure B-2. Reaction mechanism of boric acid with HF to form BF containing molecules.[117]

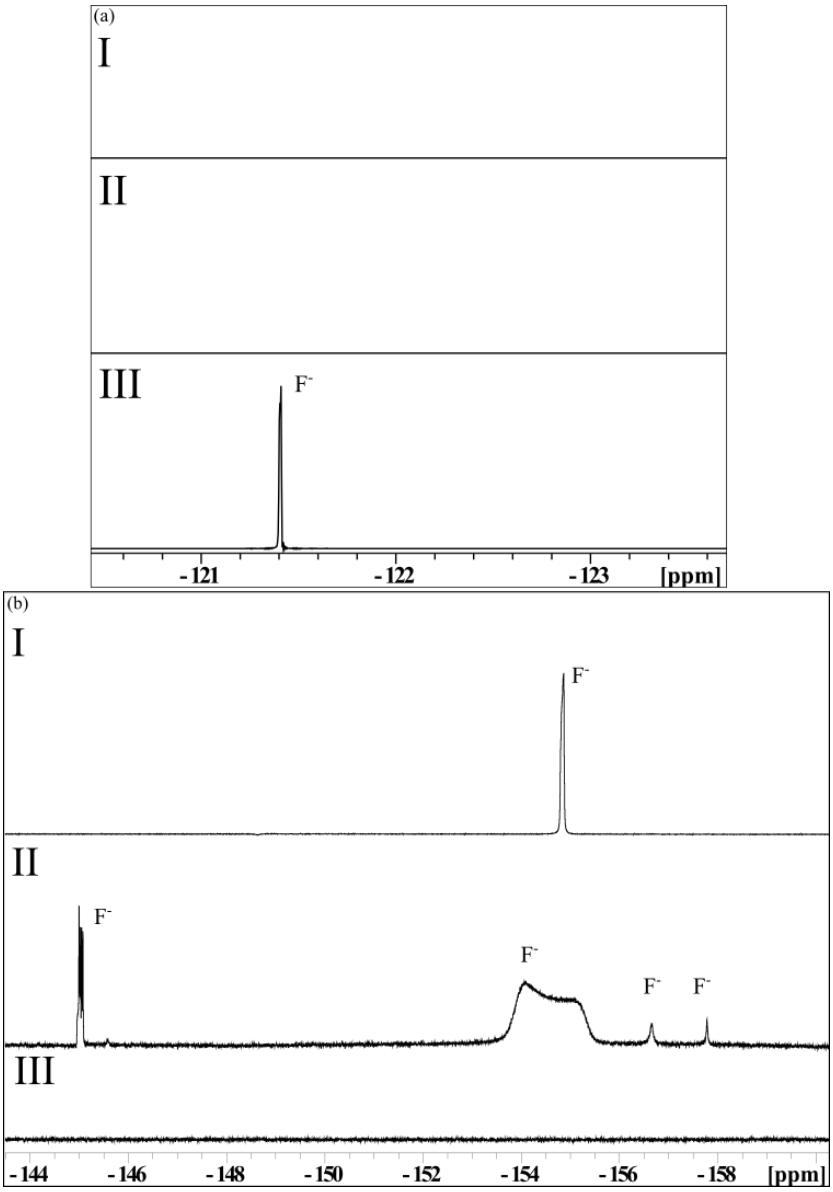

Figure B-3. ^{19}F-NMR spectra of 1 mM fluoride in a pH 7 phosphate buffer with the addition of 6 μL of 1 M HCl (I) and in a pH 10 boric acid buffer with the addition of 6 μL 1 M HCl (II) and without (III). With no acid added, the fluoride peak (F^-) is a singlet in the range of -121.5 ppm, as shown in (a), this is the typical fluoride peak observed in other NMR spectra. With the addition of the acid in the phosphate buffer the fluoride NMR peak shifts downfield, and in the boric acid buffer the fluoride peak shifts downfield and forms many different peaks, as shown in (b).

Appendix C Additional Mass Spectrometry Data

Sitagliptin MS and MS/MS ion spectra of the parent and possible products formed during photolysis in a 10 mM pH 7 phosphate buffer. Possible product MS data were taken from the final photolyzed sample at 96 hours.

Table C-1. Sitagliptin photoproduct identification by LC-HRMS. All products were derived from the parent compound, with oxygen being the only atom allowed to be added to the structure.

Elution Time (min)	Structure	Area	[M+H]
19.7 [a]	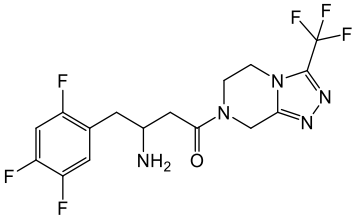	5.08×10^9	408.12482
19.4	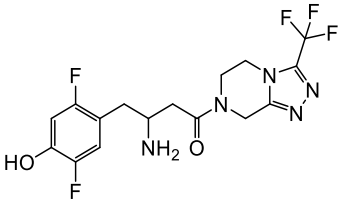	2.18×10^7	406.12965
25.5	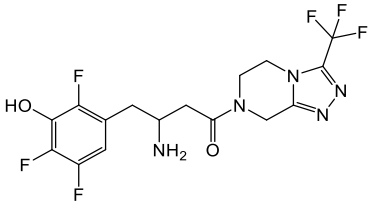	1.82×10^7	424.12027
27.2	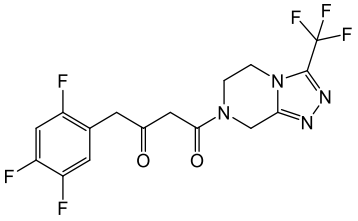	4.26×10^7	407.09378
28.5	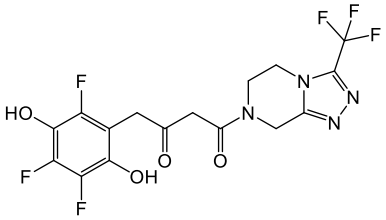	1.73×10^8	439.08332

[a] Denotes parent molecule

Table C-2. MS/MS fragmentation data for identified photoproducts of sitagliptin with masses and possible chemical formulas. If a reasonable structure was able to be made, it is shown.

Elution Time (min)	MS/MS [M]	[+ ion]	Possible Chemical Formula	Possible Structure
[a]19.7	174.05257	+H	$C_8H_7NF_3$	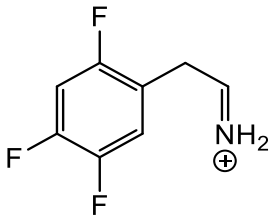
19.4	329.08212	+H	$C_{14}H_9F_5N_4$	
25.5	242.07870	+H	$C_{12}H_{10}F_3NO$	
27.2	254.07827	+H	$C_8H_9F_4N_4O$	
28.5	395.09362	+Na	$C_{15}H_{15}F_3N_4O_4$	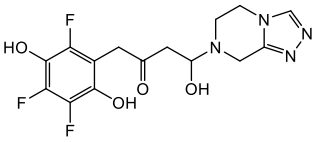

[a] Denotes the parent compound.

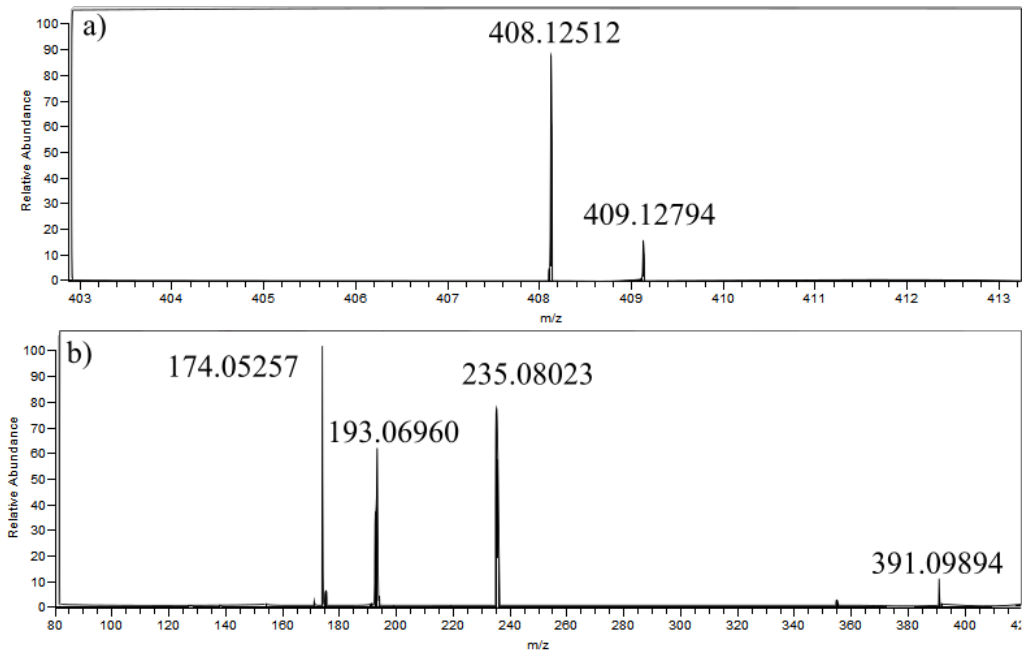

Figure C-1. Parent Sitagliptin MS (a) and MS/MS fragmentation (b) spectra.

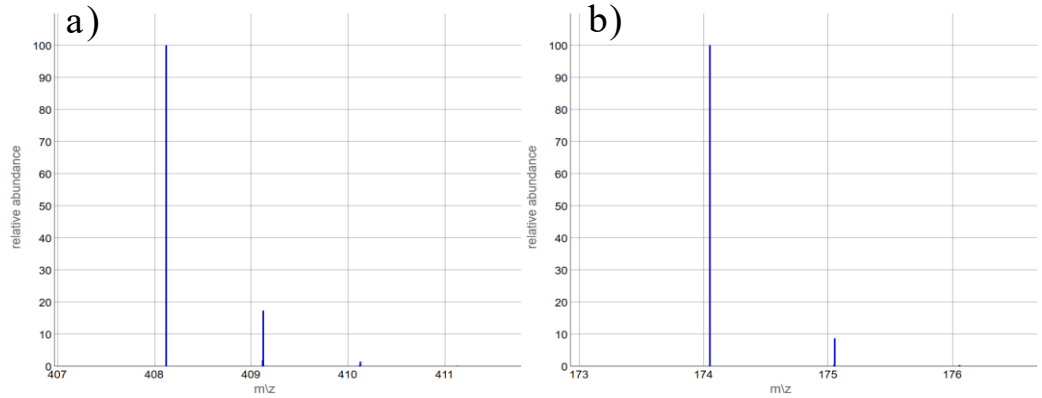

Figure C-2. Predicted MS isotope ratio, based on chemical formula of $C_{16}H_{16}F_6N_5O^+$, which matches the spectra for the parent sitagliptin molecule (a) and MS/MS isotope ratio based on chemical formula of $C_8H_7F_3N^+$, which matches the actual spectra (b).

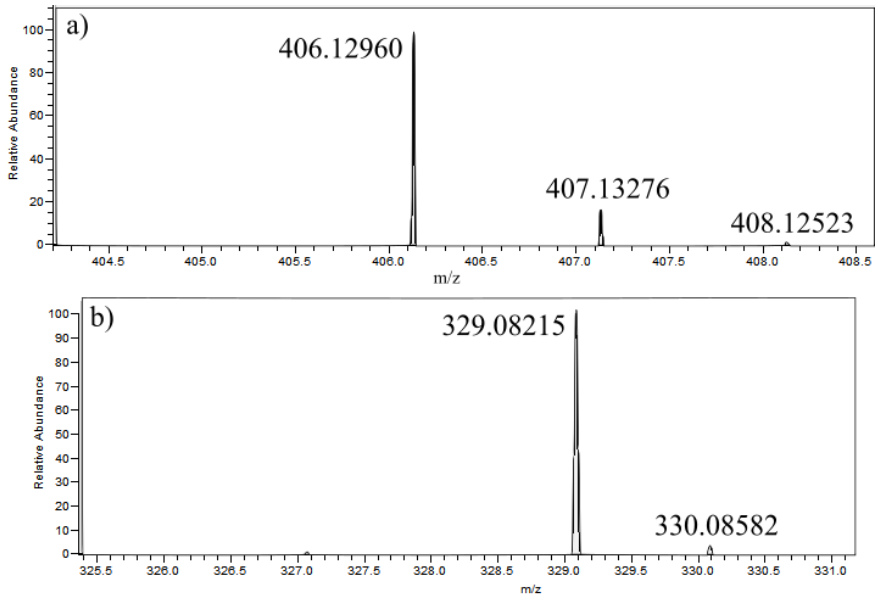

Figure C-3. Possible photoproduct MS (a) and fragmentation (b) data. The possible photoproduct had a retention time of 19.4 minutes.

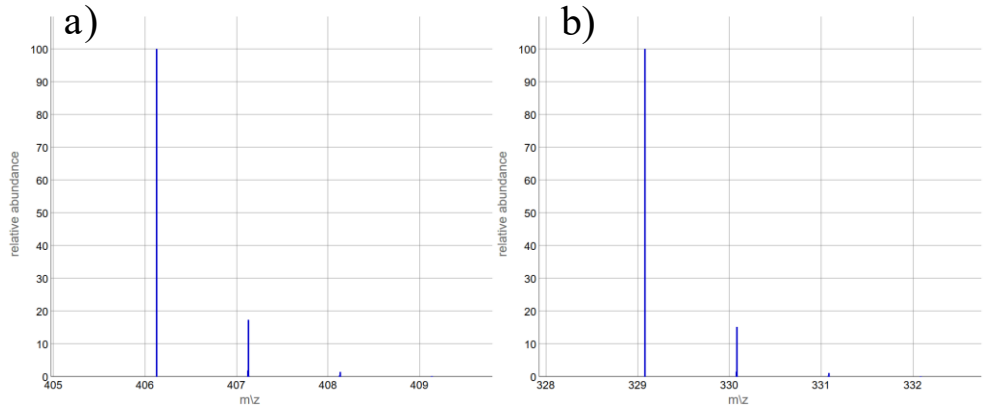

Figure C-4. Predicted MS isotope ratio, based on chemical formula of $C_{16}H_{17}F_5N_5O_2^+$, which matches the spectra for the proposed chemical formula for the possible photoproduct (a) and MS/MS isotope ratio based on the chemical formula of $C_{14}H_{10}F_5N_4^+$, which matches the actual spectra (b).

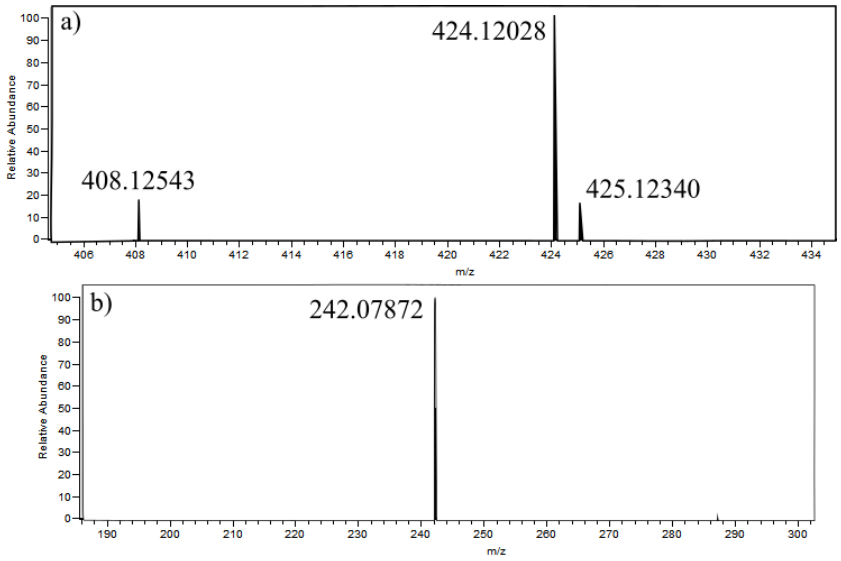

Figure C-5. Possible photoproduct with a retention time of 25.5 minutes MS (a) and MS/MS fragmentation (b) data.

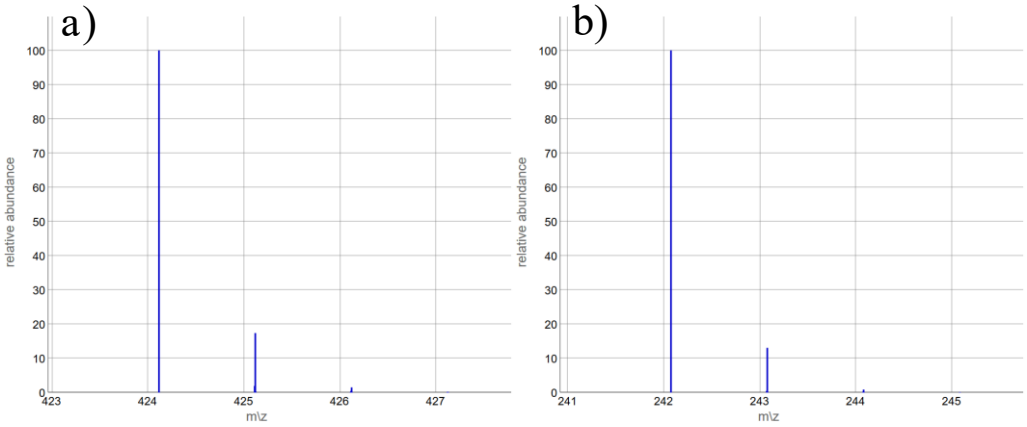

Figure C-6. Predicted MS isotope ratio, based on chemical formula of $C_{16}H_{16}F_6N_5O_2^+$, which matches the spectra for the proposed chemical formula for the possible photoproduct (a) and MS/MS isotope ratio based on the chemical formula of $C_{12}H_{11}F_3NO^+$, this isotope ratio is not observed in the actual spectra (b).

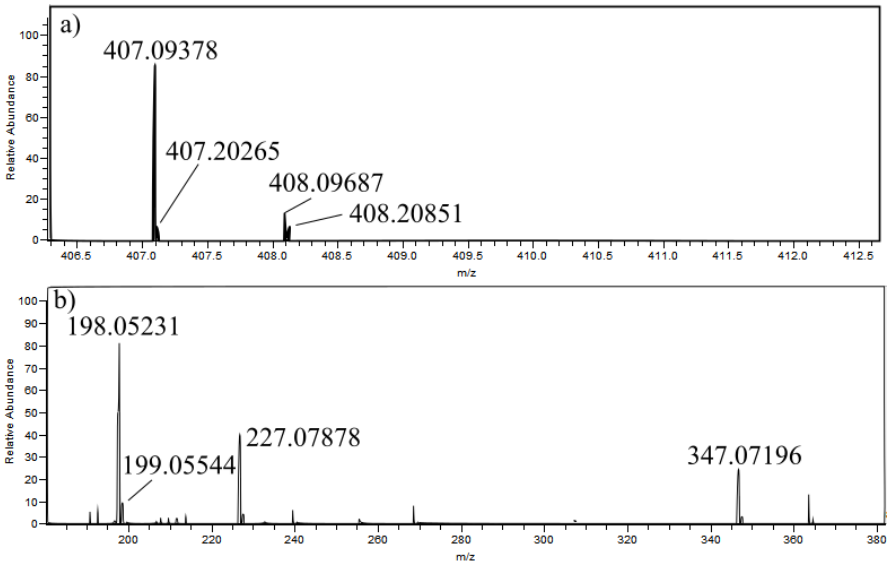

Figure C-7. Possible photoproduct with a retention time of 27.3 minutes MS (a) and MS/MS fragmentation (b) data.

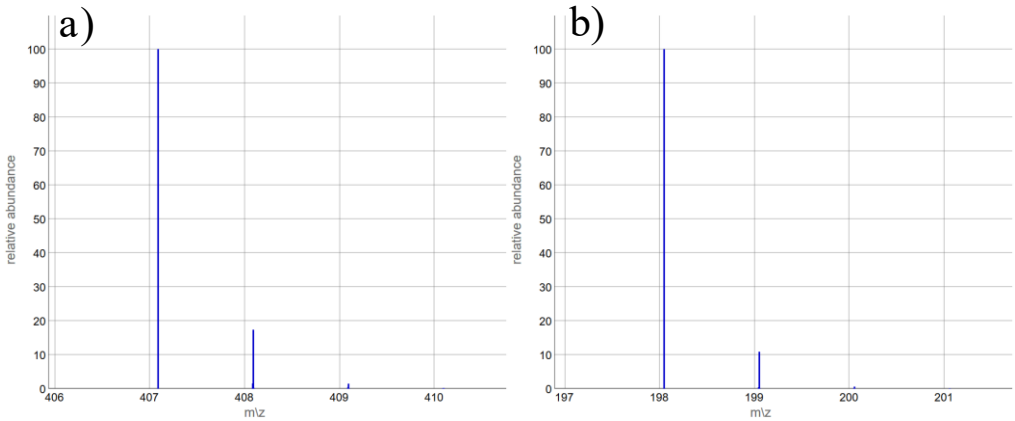

Figure C-8. Predicted MS isotope ratio based on chemical formula of $C_{16}H_{13}F_6N_4O_2^+$, which matches the spectra for the proposed chemical formula for the possible photoproduct (a) and the MS/isotope ratio based on the chemical formula of $C_{10}H_7F_3N^+$, which matches the actual spectra.

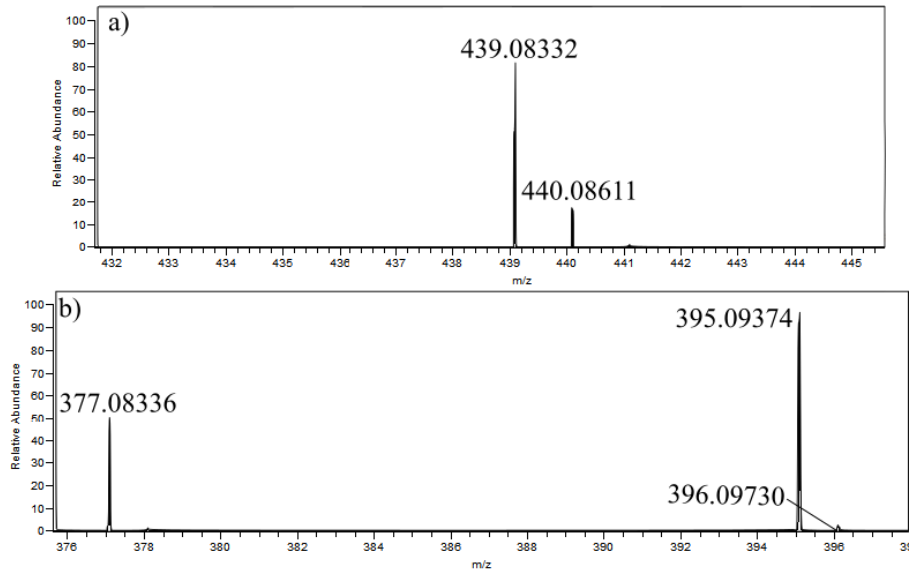

Figure C-9. Possible photoproduct with a retention time of 28.5 minutes MS (a) and MS/MS fragmentation (b) data.

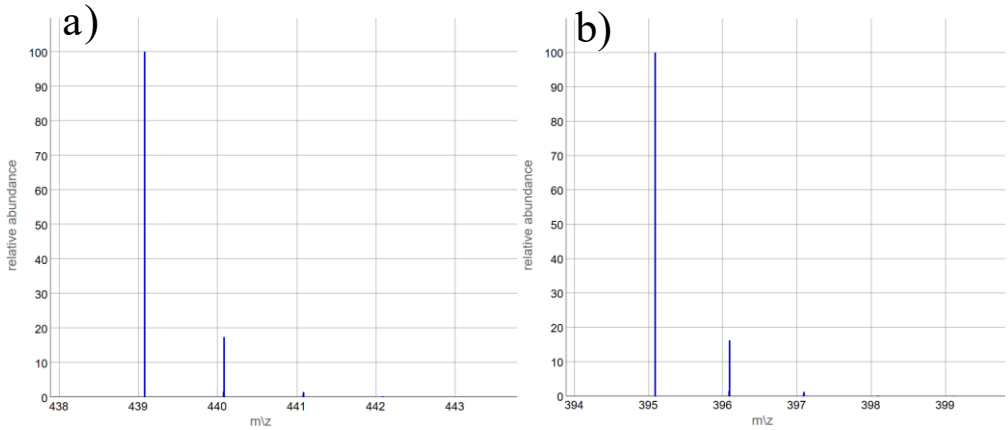

Figure C-10. Predicted MS isotope ratio based on chemical formula of $C_{16}H_{13}F_6N_4O_4^+$, which matches the spectra for the proposed chemical formula for the possible photoproduct (a) and MS/MS isotope ratio based on the chemical formula of $C_{15}H_{15}F_3N_4O_4Na^+$, which have the same m/z values but differ in ratio (b).